Two-loop corrections to the muon magnetic moment from fermion/sfermion loops in the MSSM: detailed results

Helvecio Fargnoli,[a,b] **Christoph Gnendiger,**[a] **Sebastian Paßehr,**[c] **Dominik Stöckinger**[a] **and Hyejung Stöckinger-Kim**[a]

[a]*Institut für Kern- und Teilchenphysik,TU Dresden, Dresden, Germany*

[b]*Universidade Federal de Lavras, Lavras, Brazil*

[c]*Max-Planck Institut für Physik, München, Germany*

E-mail: hfargnoli@yahoo.com.br, Christoph.Gnendiger@tu-dresden.de, passehr@mpp.mpg.de, Dominik.Stoeckinger@tu-dresden.de, Hyejung.Stoeckinger-Kim@tu-dresden.de

ABSTRACT: Recently, first results were presented for two-loop corrections to the muon $(g-2)$ from fermion/sfermion loops in the MSSM. These corrections were shown to be generally large and even logarithmically enhanced for heavy sfermions. Here, full details of the calculation and analytical results are presented. Also, a very compact formula is provided which can be easily implemented and serves as a good approximation of the full result as a function of the fourteen most important input parameters. Finally, a thorough discussion of the numerical behaviour of the fermion/sfermion-loop corrections to $(g-2)_\mu$ is given. The discussion includes the case of very heavy SUSY masses as well as experimentally allowed scenarios with very light SUSY masses.

Contents

1 Introduction

1.1 Current status and motivation

The measurement of the anomalous magnetic moment of the muon, $a_\mu = (g-2)_\mu/2$, by the Brookhaven National Laboratory has reached an accuracy of better than one part per million, corresponding to an experimental uncertainty of 6.3×10^{-10} [1]. With this accuracy, a_μ is sensitive to quantum effects from all Standard Model (SM) interactions — electromagnetic, strong, and weak.

The theory evaluation of the SM prediction has improved very recently on all fronts. In ref. [2], the full calculation of the QED contributions up to the 5-loop level has been reported, completing the effort of several decades. The hadronic vacuum polarization contributions evaluated in refs. [3–5] make use of a large set of recent, complementary experimental data on the $e^+e^- \rightarrow$ hadrons cross section. An earlier discrepancy to analyses based on τ-decays has been resolved [5, 6]. The latest results of hadronic light-by-light calculations using established methods [7, 8] agree within the quoted errors. New approaches [9–12] provide important cross-checks and promise further progress. The electroweak contributions benefit from the Higgs-mass determination at the LHC [13, 14]. Ref. [15] gives an update of previous calculations of refs. [16–20], where the exact two-loop result for the Higgs-dependent contributions is obtained and all known electroweak contributions up to the leading three-loop level are consistently combined. For more details on the SM prediction and expected further progress see the recent reviews [7, 21].

With this progress the theory prediction has reached an even higher accuracy than the experiment. The current deviation between the Brookhaven measurement and the most recent SM theory evaluations, see ref. [15], is as follows (the hadronic evaluation is taken either from ref. [3] or [4] as indicated and does not include the evaluations of refs. [5, 6]):

$$\Delta a_\mu(\text{E821} - \text{SM}) = \begin{cases} (28.7 \pm 8.0) \times 10^{-10}[3], \\ (26.1 \pm 8.0) \times 10^{-10}[4]. \end{cases} \tag{1.1}$$

The importance of this result, which corresponds to a 3–4σ deviation, has motivated two new experiments. First, the successor of the BNL experiment is already under construction at Fermilab [22, 23]. It uses the same technique as at Brookhaven: high-energy muons are inserted into a storage ring at the "magic relativistic γ", for which electric focusing fields do not perturb the muon precession. A second experiment is planned at J-PARC [24], which uses ultra-cold muons with smaller γ, but no electric focusing field. Both of these complementary experiments aim to reduce the uncertainty by more than a factor four.

The exciting prospect of such improved measurements motivates all efforts to further improve the theory prediction for a_μ, both within the SM and beyond. The present paper focusses on supersymmetry (SUSY) and the prediction for a_μ in the Minimal Supersymmetric Standard Model (MSSM). Two-loop diagrams with a closed fermion/sfermion loop inserted into a SUSY one-loop diagram (see figure 1) are computed, together with the associated counterterm diagrams. First results of the calculation have been presented already in ref. [25].
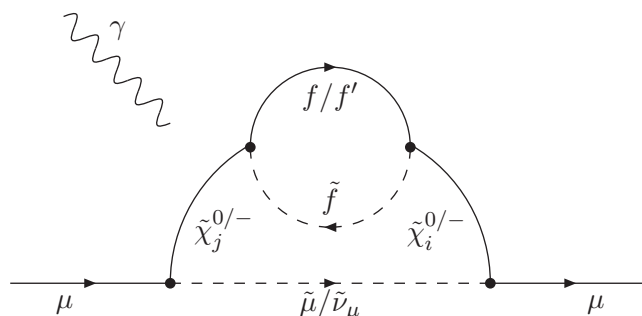
Figure 1. Prototype Feynman diagram with fermion/sfermion-loop insertion. The outer loop is a generalized SUSY one-loop a_μ diagram and contains either neutralinos $\tilde{\chi}^0_{i,j}$ and a smuon $\tilde{\mu}$ or charginos $\tilde{\chi}^-_{i,j}$ and a sneutrino $\tilde{\nu}_\mu$. The generic fermion/sfermion pair in the inner loop is denoted by $(f, \tilde{f})$ and $(f', \tilde{f})$ for neutralinos and charginos, respectively. The photon can couple to each charged particle.

It is well-known that the MSSM could easily account for the deviation (1.1), see e. g. [26] and [27] for reviews. Even the recent LHC results, including the Higgs-mass determination and negative results from SUSY particle searches, can be simultaneously accommodated in the MSSM [28, 29]. In fact, combining LHC data with a_μ motivates MSSM scenarios which are quite distinct from the more traditionally favoured ones [30–38]. Conversely, e. g. in the Constrained MSSM, the LHC results already rule out the possibility to explain the deviation (1.1) [39–41], further highlighting the complementarity between LHC and low-energy observables such as a_μ. Ref. [42] stresses the complementarity between a_μ and a future linear collider. Ref. [21, 43] also demonstrates that the future more precise a_μ determination will help in measuring MSSM parameters such as $\tan\beta$, and in solving the LHC inverse problem [44], i. e. in discriminating between discrete choices of MSSM parameters that fit equally well to LHC data.

For realizing the full potential of the future a_μ experiments, the theory uncertainty of the MSSM should be reduced. In ref. [27], it is estimated to 3×10^{-10} due to unknown two-loop corrections — twice as large as the future experimental uncertainty. The current status of the MSSM prediction for a_μ is as follows: the MSSM one-loop contributions to a_μ have been computed and extensively documented in refs. [27, 45–47]. The two-loop corrections have been classified in ref. [27] into two classes. In class 2L(a) a pure SUSY loop of either charginos, neutralinos or sfermions is inserted into a SM-like diagram. For reference, figure 2 shows a sample diagram of this class. Diagrams like this have been computed in ref. [48], after approximate calculations in refs. [49, 50], and the full calculation of all class 2L(a) contributions has been completed in ref. [19]. Diagrams of class 2L(b) correspond to two-loop corrections to SUSY one-loop diagrams. This class of contributions has not been computed fully yet. The fermion/sfermion-loop corrections of figure 1 belong to this class. Up to now, the full QED corrections [51], including the leading QED logarithms of ref. [52], and the $(\tan\beta)^2$-enhanced corrections [53] have been evaluated. Further computations of selected diagrams of classes 2L(a) and 2L(b) have been carried out in refs. [54–57].
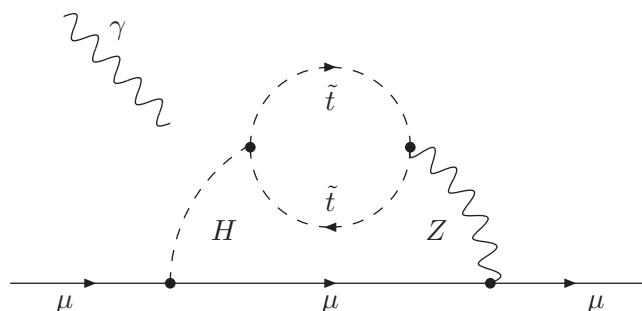
Figure 2. Sample Feynman diagram with closed stop loop inserted into a SM-like one-loop diagram with Higgs- and Z-boson exchange, computed in refs. [48–50]. The photon can couple to each charged particle.

For a full two-loop calculation of a_μ in the MSSM it remains to exactly compute all non-QED diagrams of class 2L(b), i.e. all two-loop diagrams which contain at least one chargino or neutralino, one smuon or sneutrino, and potentially further SM or SUSY particles. These remaining diagrams can be subdivided into diagrams with and diagrams without a closed fermion/sfermion loop.

Numerically, all the known contributions of class 2L(b) can be as large as the future experimental uncertainty or even larger. Hence, these are relevant corrections, and it is motivated to continue the evaluation of the two-loop contributions to a_μ in the MSSM.

1.2 Fermion/sfermion-loop contributions

The fermion/sfermion-loop contributions discussed in the present work correspond to the diagrams of figure 1 and the associated counterterm diagrams. Obviously these diagrams can be regarded as SUSY partners to the diagrams of the type in figure 2. Like the latter, these fermion/sfermion-loop contributions form a gauge independent and finite class of contributions.

This class of two-loop contributions is interesting for several reasons. Of course, its computation represents a significant step towards the full two-loop computation of a_μ in the MSSM, and it reduces the theory uncertainty. The present paper provides full details of the calculation and analytical and numerical results. It also provides a very compact approximation formula for the full result, which can be easily implemented.

Further, this diagram class introduces a dependence of a_μ on squarks and sleptons of all generations, which is phenomenologically interesting. Most notably, if the squark masses (or slepton masses of the first or third generation) become large, the contributions to a_μ do not decouple, instead they are even logarithmically enhanced. This is a striking contrast to the Feynman diagrams considered in the past and illustrated in figure 2. Generally, top/stop loops or top/sbottom loops can have a significant influence and non-trivial parameter dependence owing to the large top-Yukawa coupling and the potentially large stop mixing. The present paper thoroughly discusses the numerical behaviour of the fermion/sfermion-loop contributions as a function of all relevant input parameters.

Finally, the fermion/sfermion-loop contributions involve a set of interesting counterterm contributions which are finite and do not correspond to genuine two-loop diagrams.

These are counterterm contributions to the muon-neutralino-smuon or muon-chargino-sneutrino vertex from counterterm insertions with a fermion/sfermion loop. These counterterms contain in particular the large, universal $\Delta\rho$ corrections from top (and stop) loops to the SUSY one-loop diagrams. The influence of $\Delta\rho$ and the non-decoupling behaviour have already been stressed and discussed in ref. [25].

Technically, the computation of the diagrams of figure 1 is significantly more complicated than all previously considered a_μ two-loop diagrams in the MSSM. This is mainly because of the higher number of different mass scales. Therefore, the diagrams have been computed in two different ways — once by appropriately extending the standard techniques developed for refs. [19, 48], and once using an iterated one-loop calculation similar to the simpler cases of ref. [58]. A similar class of diagrams with neutralino or gluino exchange and non-decoupling behaviour has been considered for electric dipole moments in ref. [59, 60] in an approximation where higgsino-gaugino mixing is neglected. In refs. [58–60] all two-loop diagrams were ultraviolet finite, while in the present case diagrams involve subdivergences and need to be renormalized.

1.3 Outline

Our paper is organized as follows: in section 2 a systematic notation for all appearing MSSM coupling constants is introduced, and it is shown that the one-loop contributions can be elegantly expressed in terms of these. Section 3 is devoted to the renormalization of the two-loop results. Analytic results for the one-loop counterterm diagrams are provided, and in particular the difference between the standard one-loop diagrams and the counterterm diagrams with mixing between two different charginos or neutralinos is highlighted. In section 4 the full analytic results for all two-loop diagrams are given. Also intermediate results for the one-loop subdiagrams are expressed in a form useful for the Barr-Zee technique. The numerical and phenomenological discussion is prepared in section 5 with an overview of the input parameters. In section 6 a very compact approximation formula for the full result is provided which can be easily implemented. Finally, in section 7 a thorough analysis of the numerical behaviour of the fermion/sfermion-loop contributions in a variety of parameter scenarios is presented.

2 Preparations

As a preliminary step, a useful and compact notation for the MSSM coupling constants and vertices is introduced. It generalizes the notation used in the literature and is appropriate for all diagrams considered in the present paper. Then, the known MSSM one-loop results for a_μ are expressed in this simplified notation.

2.1 Coupling structures

All one- and two-loop a_μ diagrams considered in the present paper have the structure represented by the prototypes of figure 1. Apart from the interaction with the external

photon, only vertices of the type fermion-sfermion-chargino/neutralino appear. The relevant interaction Lagrangian is written as

$$
\begin{aligned}
\mathcal{L}_{\text{int}} = {}& \overline{\tilde{\chi}_i^-} \Big(c_{i\tilde{\nu}}^L P_L + c_{i\tilde{\nu}}^R P_R \Big) l\, \tilde{\nu}^\dagger + \overline{\tilde{\chi}_i^+} \Big(c_{i\tilde{l}_k^\dagger}^{R*} P_L + c_{i\tilde{l}_k^\dagger}^{L*} P_R \Big) \nu\, \tilde{l}_k^\dagger \\
& + \overline{\tilde{\chi}_i^-} \Big(c_{i\tilde{u}_k}^L P_L + c_{i\tilde{u}_k}^R P_R \Big) d\, \tilde{u}_k^\dagger + \overline{\tilde{\chi}_i^+} \Big(c_{i\tilde{d}_k^\dagger}^{R*} P_L + c_{i\tilde{d}_k^\dagger}^{L*} P_R \Big) u\, \tilde{d}_k^\dagger \\
& + \sum_{(f,\tilde{f})} \overline{\tilde{\chi}_i^0} \Big(n_{i\tilde{f}_k}^L P_L + n_{i\tilde{f}_k}^R P_R \Big) f\, \tilde{f}_k^\dagger + \text{h.c.}
\end{aligned}
\tag{2.1}
$$

In this formula, family indices have been suppressed and ν, l, u, d denote neutrino, charged lepton, up-type and down-type quarks of any family, respectively. The sum in the last line extends over all these fermions and the corresponding sfermions.

The down-type sfermions in eq. (2.1) couple to the positively charged charginos. For the purposes of the muon $(g-2)$ computation it is more appropriate to rewrite these couplings in terms of negatively charged charginos and anti-up-type fermions. This can be achieved by using flipping rules [61] like

$$
\overline{\tilde{\chi}_i^+} \left(c_{i\tilde{d}_k^\dagger}^{R*} P_L + c_{i\tilde{d}_k^\dagger}^{L*} P_R \right) u\, \tilde{d}_k^\dagger = \overline{u^c} \left(c_{i\tilde{d}_k^\dagger}^{R*} P_L + c_{i\tilde{d}_k^\dagger}^{L*} P_R \right) \tilde{\chi}_i^-\, \tilde{d}_k^\dagger .
\tag{2.2}
$$

Then, it is possible to rewrite the interaction Lagrangian in a compact and unified form as

$$
\begin{aligned}
\mathcal{L}_{\text{int}} = {}& \sum_{(f',\tilde{f})} \overline{\tilde{\chi}_i^-} \left(c_{i\tilde{f}_k}^L P_L + c_{i\tilde{f}_k}^R P_R \right) f'\, \tilde{f}_k^\dagger \\
& + \sum_{(f,\tilde{f})} \overline{\tilde{\chi}_i^0} \left(n_{i\tilde{f}_k}^L P_L + n_{i\tilde{f}_k}^R P_R \right) f\, \tilde{f}_k^\dagger + \text{h.c.},
\end{aligned}
\tag{2.3}
$$

where the sums extend over the following fermion/sfermion pairs:

$$
(f',\tilde{f}) = (l,\tilde{\nu}),\, \big(\nu^c,\tilde{l}^\dagger\big),\, (d,\tilde{u}),\, \big(u^c,\tilde{d}^\dagger\big),
\tag{2.4a}
$$

$$
(f,,\tilde{f}) = (\nu,\tilde{\nu}),\, (l,\tilde{l}),\, (u,\tilde{u}),\, (d,\tilde{d}).
\tag{2.4b}
$$

In this notation the coupling coefficients in eq. (2.3) are all systematically indexed by the outgoing sfermion and the chirality of the incoming fermion.[1]

The relevant coupling coefficients in the MSSM are given by

$$
c_{i\tilde{\nu}_l}^L = -g_2 V_{i1}^* ,
\tag{2.5a}
$$

$$
c_{i\tilde{\nu}_l}^R = y_l U_{i2} ,
\tag{2.5b}
$$

$$
c_{i\tilde{l}_k^\dagger}^{R*} = -g_2 U_{i1}^* U_{k1}^{\tilde{l}} + y_l U_{i2}^* U_{k2}^{\tilde{l}} ,
\tag{2.5c}
$$

$$
c_{i\tilde{l}_k^\dagger}^{L*} = 0 ,
\tag{2.5d}
$$

---

[1]Compared to refs. [46, 51] the notation has been streamlined by removing relative signs and complex conjugations in $n^{L,R}$ and $c^{L,R}$.

$$c^L_{i\tilde{u}_k} = -g_2 V^*_{i1} U^{\tilde{u}}_{k1} + y_u V^*_{i2} U^{\tilde{u}}_{k2}, \tag{2.5e}$$

$$c^R_{i\tilde{u}_k} = y_d U_{i2} U^{\tilde{u}}_{k1}, \tag{2.5f}$$

$$c^{R*}_{i\tilde{d}^\dagger_k} = -g_2 U^*_{i1} U^{\tilde{d}}_{k1} + y_d U^*_{i2} U^{\tilde{d}}_{k2}, \tag{2.5g}$$

$$c^{L*}_{i\tilde{d}^\dagger_k} = y_u V_{i2} U^{\tilde{d}}_{k1}, \tag{2.5h}$$

$$n^L_{i\tilde{u}_k} = \frac{1}{\sqrt{2}} \left(-\frac{1}{3} g_1 N^*_{i1} - g_2 N^*_{i2} \right) U^{\tilde{u}}_{k1} - y_u N^*_{i4} U^{\tilde{u}}_{k2}, \tag{2.5i}$$

$$n^R_{i\tilde{u}_k} = +\frac{2}{3}\sqrt{2} g_1 N_{i1} U^{\tilde{u}}_{k2} - y_u N_{i4} U^{\tilde{u}}_{k1}, \tag{2.5j}$$

$$n^L_{i\tilde{d}_k} = \frac{1}{\sqrt{2}} \left(-\frac{1}{3} g_1 N^*_{i1} + g_2 N^*_{i2} \right) U^{\tilde{d}}_{k1} - y_d N^*_{i3} U^{\tilde{d}}_{k2}, \tag{2.5k}$$

$$n^R_{i\tilde{d}_k} = -\frac{1}{3}\sqrt{2} g_1 N_{i1} U^{\tilde{d}}_{k2} - y_d N_{i3} U^{\tilde{d}}_{k1}, \tag{2.5l}$$

$$n^L_{i\tilde{\nu}_l} = \frac{1}{\sqrt{2}} \left(g_1 N^*_{i1} - g_2 N^*_{i2} \right), \tag{2.5m}$$

$$n^R_{i\tilde{\nu}_l} = 0, \tag{2.5n}$$

$$n^L_{i\tilde{l}_k} = \frac{1}{\sqrt{2}} \left(g_1 N^*_{i1} + g_2 N^*_{i2} \right) U^{\tilde{l}}_{k1} - y_l N^*_{i3} U^{\tilde{l}}_{k2}, \tag{2.5o}$$

$$n^R_{i\tilde{l}_k} = -\sqrt{2} g_1 N_{i1} U^{\tilde{l}}_{k2} - y_l N_{i3} U^{\tilde{l}}_{k1}, \tag{2.5p}$$

with gauge and Yukawa couplings defined as

$$g_1 = \frac{e}{c_W}, \qquad g_2 = \frac{e}{s_W}, \qquad y_{d,l} = \frac{m_{d,l} g_2}{\sqrt{2} M_W \cos\beta}, \qquad y_u = \frac{m_u g_2}{\sqrt{2} M_W \sin\beta}. \tag{2.6}$$

The weak mixing angle is defined via the W and Z pole masses: $s^2_W = 1 - c^2_W = 1 - M^2_W/M^2_Z$. The unitary matrices $U^{\tilde{f}}$ diagonalize the sfermion-mass matrices, while the unitary matrices U/V and N are needed for a Singular Value Decomposition of the chargino- and a Takagi factorization [62] of the neutralino-mass matrices, respectively. For these matrices the same notation as in refs. [25, 27] is used; similarly for the underlying SUSY parameters: μ is the higgsino mass parameter, $\tan\beta = t_\beta = v_u/v_d$ is the ratio of the Higgs doublet vacuum expectation values, $M_{1,2}$ are the gaugino masses, and the soft mass parameters for the squark and slepton doublets and singlets are denoted by M_{Qi}, M_{Ui}, M_{Di}, M_{Li}, M_{Ei} for each generation $i \in \{1, 2, 3\}$. For simplicity, we choose generation-independent masses for the first two generations, $M_{Q1} = M_{Q2} \equiv M_Q$, etc.

A common feature of all a_μ diagrams considered in the present paper, see figure 1, is that the above couplings always appear in pairs, associated with the exchange of a sfermion — either of a smuon/sneutrino from the outer loop or of the generic sfermion from the inner loop. The structure of these coupling pairs is illustrated in figure 3. For the following it is useful to abbreviate the appearing coupling combinations as

$$\mathcal{A}^{z\pm}_{ij\tilde{f}_k} \equiv z^L_{i\tilde{f}_k} z^{L*}_{j\tilde{f}_k} \pm z^R_{i\tilde{f}_k} z^{R*}_{j\tilde{f}_k}, \tag{2.7a}$$
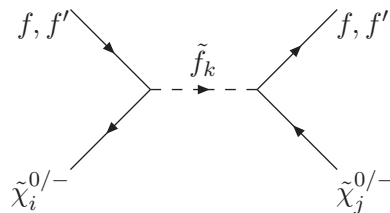
Figure 3. Illustration of the coupling combinations $\mathcal{A}_{ij\tilde{f}_k}^{z\pm}$, $\mathcal{B}_{ij\tilde{f}_k}^{z\pm}$, $z \in \{n,c\}$, arising from sfermion exchange between two neutralino/chargino vertices.

$$\mathcal{B}_{ij\tilde{f}_k}^{z\,\pm} \equiv z_{i\tilde{f}_k}^L\, z_{j\tilde{f}_k}^{R\,*} \pm z_{i\tilde{f}_k}^R\, z_{j\tilde{f}_k}^{L\,*}, \tag{2.7b}$$

with $z \in \{c,n\}$.

The $\mathcal{A}$ combinations correspond to "no chirality flip", and the $\mathcal{B}$ combinations correspond to "one chirality flip". The $\mathcal{B}$ combinations are therefore always proportional to the Yukawa coupling and mass of the fermion involved in the vertex. The left- and right-handed couplings can be equivalently expressed in terms of scalar and pseudoscalar coefficients as $z^L P_L + z^R P_R = z^S - z^P \gamma_5$. This leads to an alternative expression for the $\mathcal{A}$s and $\mathcal{B}$s,

$$\mathcal{A}_{ij\tilde{f}_k}^{z+} = 2z_{i\tilde{f}_k}^S\, z_{j\tilde{f}_k}^{S*} + 2z_{i\tilde{f}_k}^P\, z_{j\tilde{f}_k}^{P*}, \tag{2.8a}$$

$$\mathcal{A}_{ij\tilde{f}_k}^{z-} = 2z_{i\tilde{f}_k}^S\, z_{j\tilde{f}_k}^{P*} + 2z_{i\tilde{f}_k}^P\, z_{j\tilde{f}_k}^{S*}, \tag{2.8b}$$

$$\mathcal{B}_{ij\tilde{f}_k}^{z+} = 2z_{i\tilde{f}_k}^S\, z_{j\tilde{f}_k}^{S*} - 2z_{i\tilde{f}_k}^P\, z_{j\tilde{f}_k}^{P*}, \tag{2.8c}$$

$$\mathcal{B}_{ij\tilde{f}_k}^{z-} = 2z_{i\tilde{f}_k}^P\, z_{j\tilde{f}_k}^{S*} - 2z_{i\tilde{f}_k}^S\, z_{j\tilde{f}_k}^{P*}, \tag{2.8d}$$

which shows the correspondence of $\mathcal{A}^{z+}$ and $\mathcal{B}^{z+}$ to "even numbers of γ_5" on the one hand and $\mathcal{A}^{z-}$ and $\mathcal{B}^{z-}$ to "odd numbers of γ_5" on the other hand. For exchanged indices these coupling combinations satisfy the relations

$$\mathcal{A}_{ij\tilde{f}_k}^{z\,\pm} = + \left(\mathcal{A}_{ji\tilde{f}_k}^{z\,\pm}\right)^*, \tag{2.9a}$$

$$\mathcal{B}_{ij\tilde{f}_k}^{z\,\pm} = \pm \left(\mathcal{B}_{ji\tilde{f}_k}^{z\,\pm}\right)^*. \tag{2.9b}$$

2.2 One-loop results up to $\mathcal{O}(\epsilon)$

In the following we state the SUSY one-loop results up to first order in the dimensional regularization parameter $\epsilon = (4-D)/2$. For reference, the results are expressed in terms of the coupling combinations introduced above. The SUSY one-loop contributions are given by the Feynman diagrams of figure 4. For later purposes, also slightly generalized diagrams are introduced in figure 5, where different neutralino/chargino indices are assigned to the vertices and propagators. It will turn out to be useful to define the following quantities, corresponding to these generalized diagrams:

$$a_\mu^{(\text{n-gen})}\left(\mathcal{A}_{ji\tilde{\mu}_m}^{n\pm}, \mathcal{B}_{ji\tilde{\mu}_m}^{n\pm}, k\right) \equiv \frac{-1}{16\pi^2} \frac{m_\mu^2}{m_{\tilde{\mu}_m}^2} \left\{ \frac{1}{12} \mathcal{A}_{ji\tilde{\mu}_m}^{n\pm} \mathcal{F}_1^N(x_k) + \frac{m_{\tilde{\chi}_i^0}}{6m_\mu} \mathcal{B}_{ji\tilde{\mu}_m}^{n\pm} \mathcal{F}_2^N(x_k) \right\}, \tag{2.10a}$$
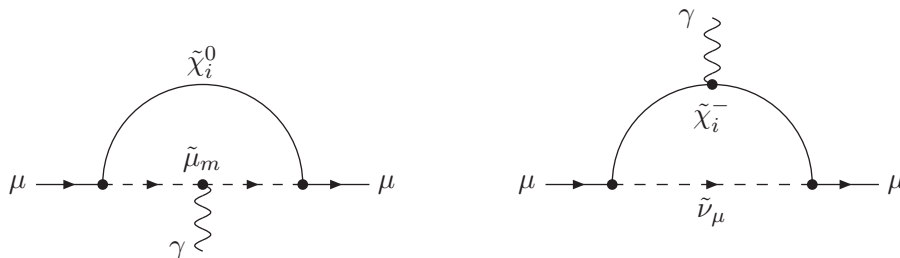
Figure 4. SUSY one-loop diagrams with neutralino-smuon and chargino-sneutrino exchange.
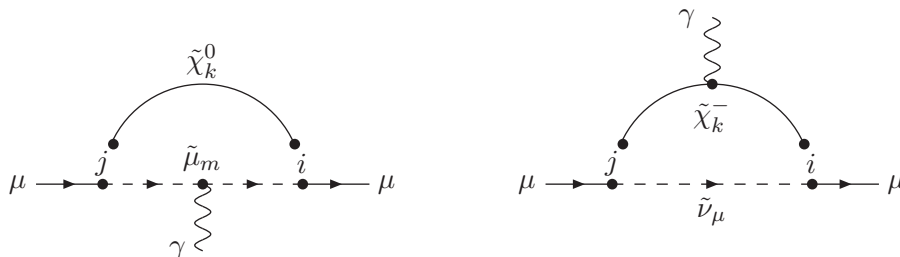

Figure 5. Generalized diagrams, corresponding to eqs. (2.10a), (2.10b). At each vertex different chargino/neutralino indices are applied. These generalized expressions are useful building blocks for expressing one-loop and one-loop counterterm results.

$$a_\mu^{(\text{c-gen})}\Big(\mathcal{A}_{ji\tilde{\nu}_\mu}^{c\pm}, \mathcal{B}_{ji\tilde{\nu}_\mu}^{c\pm}, k\Big) \equiv \frac{1}{16\pi^2}\frac{m_\mu^2}{m_{\tilde{\nu}_\mu}^2}\left\{\frac{1}{12}\mathcal{A}_{ji\tilde{\nu}_\mu}^{c\pm}\mathcal{F}_1^C(x_k) + \frac{m_{\tilde{\chi}_i^-}}{3m_\mu}\mathcal{B}_{ji\tilde{\nu}_\mu}^{c\pm}\mathcal{F}_2^C(x_k)\right\}. \quad (2.10b)$$

The dimensionless mass ratios are defined as $x_k = m_{\tilde{\chi}_k^0}^2/m_{\tilde{\mu}_m}^2$ and $x_k = m_{\tilde{\chi}_k^-}^2/m_{\tilde{\nu}_\mu}^2$ for neutralinos and charginos, respectively. The ϵ-dependent loop functions $\mathcal{F}_{1,2}^{N,C}(x)$ have been given in ref. [51] and are listed for reference in appendix A.

The known SUSY one-loop results for neutralino-smuon and chargino-sneutrino loops can then be expressed in terms of these generic results as

$$a_\mu^{1\text{L}\,\tilde{\chi}^0} = \sum_{i,m} a_\mu^{(\text{n-gen})}\Big(\mathcal{A}_{ii\tilde{\mu}_m}^{n+}, \mathcal{B}_{ii\tilde{\mu}_m}^{n+}, i\Big), \quad (2.11a)$$

$$a_\mu^{1\text{L}\,\tilde{\chi}^\pm} = \sum_{i} a_\mu^{(\text{c-gen})}\Big(\mathcal{A}_{ii\tilde{\nu}_\mu}^{c+}, \mathcal{B}_{ii\tilde{\nu}_\mu}^{c+}, i\Big), \quad (2.11b)$$

respectively. The total SUSY one-loop contribution is $a_\mu^{1\text{L}\,\text{SUSY}} = a_\mu^{1\text{L}\,\tilde{\chi}^0} + a_\mu^{1\text{L}\,\tilde{\chi}^\pm}$.

It shall be stressed that these one-loop contributions involve only the "plus"-coupling combinations $\mathcal{A}^{z+}$, $\mathcal{B}^{z+}$ and only diagonal indices $ii\tilde{\mu}_m$, $ii\tilde{\nu}_\mu$. This will change later in the case of the considered counterterm and two-loop diagrams.

3 Renormalization and counterterms

In this and the subsequent section detailed results of the calculation of the fermion/sfermion-loop contributions to a_μ are presented. This section is devoted to renormalization and the counterterm contributions. The fermion/sfermion-loop contributions
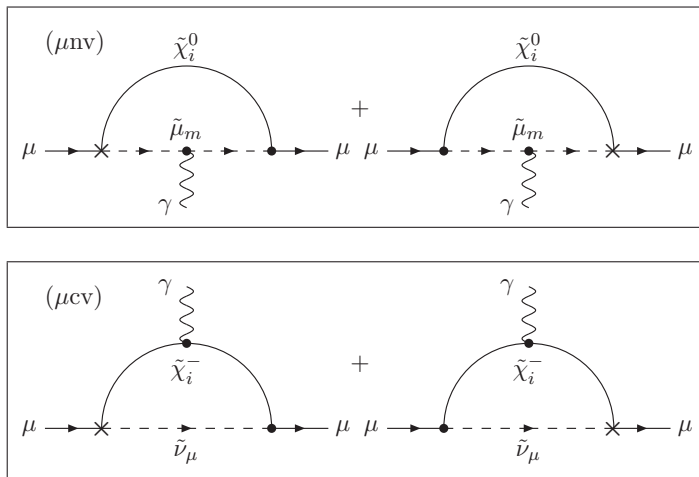
– 8 –

Figure 6. The two classes of counterterm diagrams with counterterm insertions at the external muon vertices. To these counterterm diagrams no corresponding two-loop diagrams exist. The crosses denote counterterm insertions.

$a_\mu^{2\mathrm{L},f\tilde{f}}$ are defined as all two-loop diagrams, where a mixed fermion/sfermion loop is inserted into a SUSY one-loop correction to a_μ, see figure 1, and all SUSY one-loop counterterm diagrams with counterterm insertions from diagrams with only fermions and/or sfermions in the loop.[2] Like pure fermion-loop contributions in the SM, this class of contributions is gauge independent and finite by itself.

The one-loop corrections to a_μ are UV finite. However, divergences arise in the calculation of the two-loop corrections, shown in section 4. Therefore, counterterms have to be introduced, together with appropriate renormalization constants. The counterterm diagrams can be classified according to their topologies into six classes:

- muon vertex counterterm diagrams with insertions of renormalization constants in the vertex with the incoming/outgoing muon of the one-loop neutralino or chargino diagrams, see figure 6(μnv, μcv). There are no corresponding two-loop diagrams with fermion/sfermion loops, hence these counterterm diagrams are finite.

- neutralino counterterm diagrams with insertions of renormalization constants into a neutralino-neutralino-photon vertex or the neutralino self-energy, see figure 7(nv,ns).

- chargino counterterm diagrams with insertions of renormalization constants into the vertex with the external photon or the chargino self-energy, see figure 7(cv,cs).

All renormalization constants have to be computed from one-loop diagrams involving only fermions and/or sfermions in the loop.

---

[2]Diagrams where a pure sfermion loop is attached to a smuon or sneutrino propagator, and the associated counterterm diagrams are excluded. These diagrams arise from sfermion four-point interactions and effectively induce a shift in one of the smuon masses; they are separately gauge independent and finite, straightforward to compute and lead to numerically smaller results. They will be reported on elsewhere.
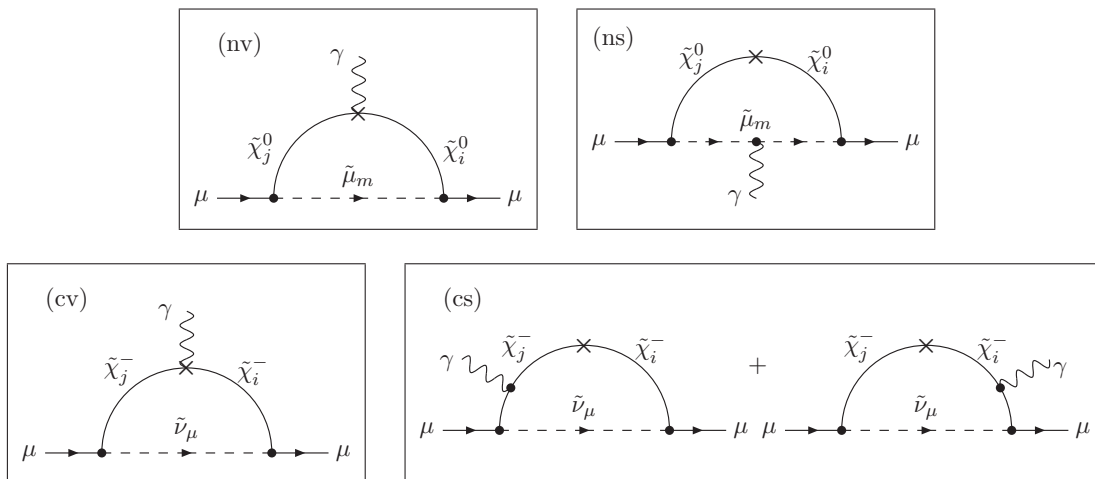
Figure 7. The four classes of counterterm diagrams for which corresponding non-vanishing two-loop diagrams exist. In the (cs) case the sum of the two contributing diagrams is considered. The crosses denote counterterm insertions.

3.1 Definition of α

The anomalous magnetic moment of the muon is proportional to the fine-structure constant α at the one-loop level. For the considered class of two-loop corrections it is necessary to calculate the renormalization of α from the photon vacuum polarization with sfermion and fermion loops, including light quark loops. Since the masses of the light quarks are not known exactly and large QCD corrections arise, a perturbative evaluation of these light quark loops is problematic. The definition of α in the Thomson limit, $\alpha(0)$, would lead to a large intrinsic uncertainty. To avoid this issue we choose the parametrization of the electric charge in terms of $\alpha(M_Z)$, defined by[3]

$$\alpha(M_Z) = \frac{\alpha(0)}{1 - \Delta\alpha(M_Z)}. \tag{3.1}$$

The finite shift $\Delta\alpha(M_Z)$ is defined as the on-shell renormalized photon vacuum polarization from SM leptons and quarks. The light quark contribution can be obtained from experimental data via the optical theorem and dispersion relations. We use the recent determination by ref. [4]:

$$\begin{aligned}
\Delta\alpha &= \Delta\alpha_{\text{leptonic}} + \Delta\alpha_{\text{hadronic}} + \Delta\alpha_{\text{top}} \\
&= 0.031498 + (0.027626 \pm 0.000138) - (0.0000728 \pm 0.0000014).
\end{aligned} \tag{3.2}$$

The choice of $\alpha(M_Z)$ for the parametrization of the one-loop result leads to the following renormalization constant for the electric charge:

$$\frac{\delta e}{e} = \delta Z_e = -\frac{1}{2}\left(\delta Z_{AA} - \frac{s_W}{c_W}\delta Z_{ZA}\right) \tag{3.3}$$

---

[3]This definition of α may not be confused with the $\overline{\text{DR}}$ or $\overline{\text{MS}}$ definition of a running $\alpha(\mu)$.

with the photon-photon and photon-Z field renormalizations, defined in terms of the transverse self-energies Σ_{AA}, Σ_{ZA},

$$\delta Z_{AA} = -\Re\mathfrak{e}\left[\frac{\Sigma_{AA}^{\text{fermions}}(M_Z^2)}{M_Z^2}\right] - \Re\mathfrak{e}\left[\partial_{p^2}\Sigma_{AA}^{\text{others}}(p^2)\right]_{p^2=0}, \tag{3.4a}$$

$$\delta Z_{ZA} = -\Re\mathfrak{e}\left[\frac{2\Sigma_{ZA}(0)}{M_Z^2}\right]. \tag{3.4b}$$

The mixing self-energy $\Sigma_{ZA}(0)$ has only contributions from the non-abelian structure of the theory; it is zero for the considered class of Feynman diagrams. $\Sigma_{AA}^{\text{fermions}}(M_Z)$ refers to all contributions to the photon self-energy with internal SM leptons and quarks, evaluated at the scale M_Z, while $\Sigma_{AA}^{\text{others}}$ denotes all other particle insertions, in our case sfermions.

It should be noted that other schemes, such as replacing $\alpha(0)$ by the muon decay constant G_F, avoid the large QCD uncertainties as well. In ref. [25], table 2, we have shown that the alternative choice of using G_F instead of $\alpha(M_Z)$ for the SUSY one-loop contributions would lead to significantly larger two-loop corrections. Hence we prefer the $\alpha(M_Z)$ parametrization. A full MSSM calculation of a_μ also involves the electroweak SM contributions to a_μ. These are usually parametrized in terms of G_F, whereby the renormalization scheme for the SM [16, 17] and SUSY [19, 48] loop corrections to these SM one-loop diagrams is defined accordingly. It is fully consistent to parametrize the electroweak SM one-loop contributions with G_F and the SUSY one-loop contributions with $\alpha(M_Z)$ at the same time, and we assess this parametrization as optimal for a full MSSM calculation.

3.2 Renormalization constants and scheme

The necessary renormalization constants correspond to the renormalization of the physical parameters appearing at the one-loop level,

$$\delta e,\ \delta M_Z^2,\ \delta M_W^2,\ \delta t_\beta,\ \delta M_1,\ \delta M_2,\ \delta\mu, \tag{3.5}$$

and to the field renormalization of the photon, photon–Z mixing, charginos $\tilde{\chi}_i^-$ and neutralinos $\tilde{\chi}_i^0$ (the latter two field renormalization constants cancel in the sum of all counterterm diagrams),

$$\delta Z_{AA},\ \delta Z_{ZA},\ \delta Z_{\tilde{\chi}^-,ij}^{L/R},\ \delta Z_{\tilde{\chi}^0,ij}^{L/R}. \tag{3.6}$$

As stated above, the renormalization constants have to be computed from one-loop diagrams involving only fermions and/or sfermions in the loop. For this reason, further renormalization constants not listed above, such as smuon mass or muon field renormalization constants vanish.

Charge and photon field renormalization have been defined above. The renormalization scheme defining the remaining renormalization constants is similar to the scheme of refs. [63–68]. It implements an on-shell renormalization of the MSSM [69] as far as possible. The creation and selection of the Feynman diagrams is done with FeynArts [70], using a preliminary model file of ref. [66]. The calculation of the renormalization constants is

done with FormCalc [71]. The gauge-boson masses and s_W are renormalized on-shell by requiring

$$\delta M_Z^2 = \Re \left[\Sigma_{ZZ}(M_Z^2) \right], \tag{3.7}$$

$$\delta M_W^2 = \Re \left[\Sigma_{WW}(M_W^2) \right], \tag{3.8}$$

$$\delta s_W = \frac{c_W^2}{2 s_W} \left(\frac{\delta M_Z^2}{M_Z^2} - \frac{\delta M_W^2}{M_W^2} \right) \tag{3.9}$$

in terms of the transverse self-energies Σ_{ZZ} and Σ_{WW}. The renormalization constant δs_W contains the leading contributions to the quantity $\Delta\rho$ from SM fermion loops and the leading MSSM corrections to $\Delta\rho$ from sfermion loops. This and the discussion of the previous subsection show that the fermion/sfermion-loop corrections to a_μ are sensitive to the two universal quantities $\Delta\alpha(M_Z)$ and $\Delta\rho$.

For the parameter t_β the $\overline{\text{DR}}$ scheme is chosen which has emerged as the best scheme in ref. [72]; for alternative process-dependent schemes see ref. [73]. It can be written in the form given in ref. [74], using self-energies of the physical Higgs bosons h^0, H^0, evaluated at zero Higgs mixing angle $\alpha = 0$:

$$\delta t_\beta = \frac{t_\beta}{2} \left(- \Re \left[\partial_{p^2} \Sigma_{H^0 H^0}(p^2) \right]_{\text{div.}} + \Re \left[\partial_{p^2} \Sigma_{h^0 h^0}(p^2) \right]_{\text{div.}} \right) \Big|_{\alpha=0}. \tag{3.10}$$

Counterterms for $\cos\beta \equiv c_\beta$ and $\sin\beta \equiv s_\beta$ can be derived from that. The reason why δt_β can be reduced to Higgs boson field renormalization at the one-loop level has been clarified recently in refs. [75, 76].

Next, the one-loop masses of the charginos and neutralinos have to be defined. We choose the renormalization of the chargino/neutralino sector as detailed in refs. [63, 64, 77, 78]. The lightest neutralino and both charginos are defined on-shell, which fixes the definitions of $\delta M_1, \delta M_2$ and $\delta\mu$ in the following way (other schemes can be found in ref. [79, 80]):

$$
\begin{aligned}
\delta M_1 = & (N_{11}^*)^{-2} \\
& \times \Bigg\{ \Re \left[\Sigma_{\text{S},11}^{\tilde{\chi}^0,\text{L}}(m_{\tilde{\chi}_1^0}^2) \right] + m_{\tilde{\chi}_1^0} \Re \left[\Sigma_{\text{V},11}^{\tilde{\chi}^0,\text{L}}(m_{\tilde{\chi}_1^0}^2) \right] - (N_{12}^*)^2 \, \delta M_2 + 2 N_{13}^* N_{14}^* \delta\mu \\
& - 2 N_{11}^* \left[N_{13}^* \left(\delta(M_Z c_W c_\beta) - \delta(M_Z s_W c_\beta) \right) \right. \\
& \qquad\qquad \left. - N_{14}^* \left(\delta(M_Z c_W s_\beta) - \delta(M_Z s_W s_\beta) \right) \right] \Bigg\},
\end{aligned}
\tag{3.11}
$$

$$
\begin{aligned}
\delta M_2 = & \frac{1}{2} \left(U_{11}^* U_{22}^* V_{11}^* V_{22}^* - U_{12}^* U_{21}^* V_{12}^* V_{21}^* \right)^{-1} \\
& \times \Bigg\{ U_{22}^* V_{22}^* \left(m_{\tilde{\chi}_1^-} \Re \left[\Sigma_{\text{V},11}^{\tilde{\chi}^-,\text{L}}(m_{\tilde{\chi}_1^-}^2) + \Sigma_{\text{V},11}^{\tilde{\chi}^-,\text{R}}(m_{\tilde{\chi}_1^-}^2) \right] + 2 \Re \left[\Sigma_{\text{S},11}^{\tilde{\chi}^-,\text{L}}(m_{\tilde{\chi}_1^-}^2) \right] \right) \\
& - U_{12}^* V_{12}^* \left(m_{\tilde{\chi}_2^-} \Re \left[\Sigma_{\text{V},22}^{\tilde{\chi}^-,\text{L}}(m_{\tilde{\chi}_2^-}^2) + \Sigma_{\text{V},22}^{\tilde{\chi}^-,\text{R}}(m_{\tilde{\chi}_2^-}^2) \right] + 2 \Re \left[\Sigma_{\text{S},22}^{\tilde{\chi}^-,\text{L}}(m_{\tilde{\chi}_2^-}^2) \right] \right) \\
& - 2 \left(U_{11}^* U_{22}^* - U_{12}^* U_{21}^* \right) V_{12}^* V_{22}^* \delta\left(\sqrt{2} M_W s_\beta \right) \\
& - 2 \left(V_{11}^* V_{22}^* - V_{12}^* V_{21}^* \right) U_{12}^* U_{22}^* \delta\left(\sqrt{2} M_W c_\beta \right) \Bigg\},
\end{aligned}
\tag{3.12}
$$

$$\delta\mu = \frac{1}{2}\left(U_{11}^* U_{22}^* V_{11}^* V_{22}^* - U_{12}^* U_{21}^* V_{12}^* V_{21}^*\right)^{-1}$$

$$\times \left\{ U_{11}^* V_{11}^* \left(m_{\tilde{\chi}_2^-}\,\Re\mathfrak{e}\left[\Sigma_{\mathrm{V},22}^{\tilde{\chi}^-,\mathrm{L}}(m_{\tilde{\chi}_2^-}^2) + \Sigma_{\mathrm{V},22}^{\tilde{\chi}^-,\mathrm{R}}(m_{\tilde{\chi}_2^-}^2)\right] + 2\,\Re\mathfrak{e}\left[\Sigma_{\mathrm{S},22}^{\tilde{\chi}^-,\mathrm{L}}(m_{\tilde{\chi}_2^-}^2)\right]\right) \right.$$

$$- U_{21}^* V_{21}^* \left(m_{\tilde{\chi}_1^-}\,\Re\mathfrak{e}\left[\Sigma_{\mathrm{V},11}^{\tilde{\chi}^-,\mathrm{L}}(m_{\tilde{\chi}_1^-}^2) + \Sigma_{\mathrm{V},11}^{\tilde{\chi}^-,\mathrm{R}}(m_{\tilde{\chi}_1^-}^2)\right] + 2\,\Re\mathfrak{e}\left[\Sigma_{\mathrm{S},11}^{\tilde{\chi}^-,\mathrm{L}}(m_{\tilde{\chi}_1^-}^2)\right]\right) \quad (3.13)$$

$$- 2\left(U_{11}^* U_{22}^* - U_{12}^* U_{21}^*\right) V_{11}^* V_{21}^* \delta\left(\sqrt{2}M_W c_\beta\right)$$

$$\left. - 2\left(V_{11}^* V_{22}^* - V_{12}^* V_{21}^*\right) U_{11}^* U_{21}^* \delta\left(\sqrt{2}M_W s_\beta\right)\right\}.$$

Here the chiral and covariant decomposition of the fermionic self-energies,

$$\Sigma_{ij}^{\tilde{\chi}}(p^2) = \not{p}\left(P_{\mathrm{L}}\Sigma_{\mathrm{V},ij}^{\tilde{\chi},\mathrm{L}}(p^2) + P_{\mathrm{R}}\Sigma_{\mathrm{V},ij}^{\tilde{\chi},\mathrm{R}}(p^2)\right) + \left(P_{\mathrm{L}}\Sigma_{\mathrm{S},ij}^{\tilde{\chi},\mathrm{L}}(p^2) + P_{\mathrm{R}}\Sigma_{\mathrm{S},ij}^{\tilde{\chi},\mathrm{R}}(p^2)\right), \qquad (3.14)$$

has been used. Knowing these quantities, the renormalization constants for all chargino and neutralino masses $\delta m_{\tilde{\chi}_{ij}^-}$ and $\delta m_{\tilde{\chi}_{ij}^0}$ can be derived by applying the usual renormalization procedure for the tree-level mass matrices $\mathcal{X}$ and $\mathcal{Y}$

$$U^* \mathcal{X} V^\dagger = \mathrm{diag}\left(m_{\tilde{\chi}_1^-}, m_{\tilde{\chi}_2^-}\right), \qquad\qquad \left[U^* \delta\mathcal{X} V^\dagger\right]_{ij} = \delta m_{\tilde{\chi}_{ij}^-}, \qquad (3.15\mathrm{a})$$

$$N^* \mathcal{Y} N^\dagger = \mathrm{diag}\left(m_{\tilde{\chi}_1^0}, m_{\tilde{\chi}_2^0}, m_{\tilde{\chi}_3^0}, m_{\tilde{\chi}_4^0}\right), \qquad \left[N^* \delta\mathcal{Y} N^\dagger\right]_{ij} = \delta m_{\tilde{\chi}_{ij}^0}, \qquad (3.15\mathrm{b})$$

with

$$\mathcal{X} = \begin{pmatrix} M_2 & \sqrt{2}M_W s_\beta \\ \sqrt{2}M_W c_\beta & \mu \end{pmatrix}, \quad \mathcal{Y} = \begin{pmatrix} M_1 & 0 & -M_Z s_W c_\beta & M_Z s_W s_\beta \\ 0 & M_2 & M_Z c_W c_\beta & -M_Z c_W s_\beta \\ -M_Z s_W c_\beta & M_Z c_W c_\beta & 0 & -\mu \\ M_Z s_W s_\beta & -M_Z c_W s_\beta & -\mu & 0 \end{pmatrix},$$

$$(3.16)$$

and the matrices U, V and N of the tree-level Singular Value Decomposition and Takagi factorization, respectively.

It should be pointed out that this renormalization scheme is not a good choice for all parameter scenarios. It leads to artificially large corrections if the lightest neutralino is not bino-like which has been discussed in refs. [79, 80] before; it also introduces an artificial singularity for $M_2 = \mu$, because of the explicitly appearing combination of mixing-matrix elements in the denominators of δM_2 and $\delta\mu$; a solution by using a different renormalization scheme would be provided in ref. [79], however in our numerical examples the exact equality $M_2 = \mu$ does not appear.

Finally, the chargino and neutralino fields are renormalized according to the $\overline{\mathrm{DR}}$ definitions

$$\delta Z_{\tilde{\chi}^{0/-},ii}^{\mathrm{L/R}} = -\Re\mathfrak{e}\left[\Sigma_{\mathrm{V},ii}^{\tilde{\chi}^{0/-},\mathrm{L/R}}(m_{\tilde{\chi}_i^{0/-}})\right]_{\mathrm{div.}} \qquad (3.17\mathrm{a})$$

$$\delta Z_{\tilde{\chi}^{0/-},ij}^{\mathrm{L/R}} = \frac{2}{m_{\tilde{\chi}_i^{0/-}}^2 - m_{\tilde{\chi}_j^{0/-}}^2}$$

$$\times \left\{ m_{\tilde{\chi}_j^{0/-}} \left(m_{\tilde{\chi}_j^{0/-}} \, \mathfrak{Re} \left[\Sigma_{\mathrm{V},ij}^{\tilde{\chi}^{0/-},\mathrm{L/R}} (m_{\tilde{\chi}_j^{0/-}}) \right] + m_{\tilde{\chi}_i^{0/-}} \, \mathfrak{Re} \left[\Sigma_{\mathrm{V},ij}^{\tilde{\chi}^{0/-},\mathrm{R/L}} (m_{\tilde{\chi}_j^{0/-}}) \right] \right) \right.$$

$$+ m_{\tilde{\chi}_i^{0/-}} \, \mathfrak{Re} \left[\Sigma_{\mathrm{S},ij}^{\tilde{\chi}^{0/-},\mathrm{L/R}} (m_{\tilde{\chi}_j^{0/-}}) \right] + m_{\tilde{\chi}_j^{0/-}} \, \mathfrak{Re} \left[\Sigma_{\mathrm{S},ij}^{\tilde{\chi}^{0/-},\mathrm{R/L}} (m_{\tilde{\chi}_j^{0/-}}) \right]$$

$$\left. - m_{\tilde{\chi}_i^{0/-}} \delta m_{\tilde{\chi}_{ji}^{0/-}}^{\mathrm{L/R}} - m_{\tilde{\chi}_j^{0/-}} \left(\delta m_{\tilde{\chi}_{ij}^{0/-}}^{\mathrm{L/R}} \right)^* \right\}_{\mathrm{div.}},$$

(3.17b)

with

$$\delta m_{\tilde{\chi}_{ij}^-}^{\mathrm{L}} = \delta m_{\tilde{\chi}_{ij}^-}, \qquad \delta m_{\tilde{\chi}_{ij}^-}^{\mathrm{R}} = \delta m_{\tilde{\chi}_{ji}^-}^*, \qquad \delta m_{\tilde{\chi}_{ij}^0}^{\mathrm{L}} = \delta m_{\tilde{\chi}_{ji}^0}. \qquad (3.17c)$$

The $\overline{\mathrm{DR}}$ definition of $\delta Z_{\tilde{\chi}^-,ij}^{\mathrm{L/R}}$ and $\delta Z_{\tilde{\chi}^0,ij}^{\mathrm{L}}$ leads to results which are numerically more stable than a corresponding on-shell definition. In any case, the field renormalization constants of charginos and neutralinos cancel in the sum of all diagrams, but their inclusion renders the self-energy and vertex diagrams individually finite.

3.3 Counterterms

Now, the explicit results for the six classes of counterterm diagrams are given in terms of the renormalization contants defined above. We use the compact notation for the coupling combinations $\mathcal{A}$ and $\mathcal{B}$ and the abbreviations $a_\mu^{(\text{n-gen})}(\mathcal{A}, \mathcal{B}, k)$ and $a_\mu^{(\text{c-gen})}(\mathcal{A}, \mathcal{B}, k)$ for generalized one-loop results, introduced in sections 2.1 and 2.2. The automated calculation and implementation of the counterterm diagrams has been done using FeynArts [70], OneCalc (part of the TuCalc package) [81] and the a_μ-specific routines developed for [19, 48].

The contribution to a_μ from the finite muon-vertex counterterm diagrams for neutralinos and charginos, see figure 6(μnv,μcv), can be expressed in terms of the abbreviations (2.10a) and (2.10b)

$$a_{\mu\,i\tilde{\mu}_m}^{(\mu\text{nv-ct})} = a_\mu^{(\text{n-gen})} \Bigg(\delta \mathcal{A}_{ii\tilde{\mu}_m}^{n+} + 2 \, \mathfrak{Re} \sum_{k=1}^4 \left[v_{ik}^n \mathcal{A}_{ki\tilde{\mu}_m}^{n+} + a_{ik}^n \mathcal{A}_{ki\tilde{\mu}_m}^{n-} \right],$$

$$\delta \mathcal{B}_{ii\tilde{\mu}_m}^{n+} + 2 \, \mathfrak{Re} \sum_{k=1}^4 \left[v_{ik}^n \mathcal{B}_{ki\tilde{\mu}_m}^{n+} + a_{ik}^n \mathcal{B}_{ki\tilde{\mu}_m}^{n-} \right], i \Bigg), \qquad (3.18a)$$

$$a_{\mu\,i}^{(\mu\text{cv-ct})} = a_\mu^{(\text{c-gen})} \Bigg(\delta \mathcal{A}_{ii\tilde{\nu}_\mu}^{c+} + 2 \, \mathfrak{Re} \sum_{j=1}^2 \left[v_{ij}^c \mathcal{A}_{ji\tilde{\nu}_\mu}^{c+} + a_{ij}^c \mathcal{A}_{ji\tilde{\nu}_\mu}^{c-} \right],$$

$$\delta \mathcal{B}_{ii\tilde{\nu}_\mu}^{c+} + 2 \, \mathfrak{Re} \sum_{j=1}^2 \left[v_{ij}^c \mathcal{B}_{ji\tilde{\nu}_\mu}^{c+} + a_{ij}^c \mathcal{B}_{ji\tilde{\nu}_\mu}^{c-} \right], i \Bigg) \qquad (3.18b)$$

with

$$\delta\mathcal{A}^{z+}_{ij\tilde{f}} = \left(z^L_{i\tilde{f}}\delta z^{L*}_{j\tilde{f}} + z^{L*}_{j\tilde{f}}\delta z^L_{i\tilde{f}}\right) + \left(z^R_{i\tilde{f}}\delta z^{R*}_{j\tilde{f}} + z^{R*}_{j\tilde{f}}\delta z^R_{i\tilde{f}}\right), \tag{3.19a}$$

$$\delta\mathcal{A}^{z-}_{ij\tilde{f}} = \left(z^L_{i\tilde{f}}\delta z^{L*}_{j\tilde{f}} + z^{L*}_{j\tilde{f}}\delta z^L_{i\tilde{f}}\right) - \left(z^R_{i\tilde{f}}\delta z^{R*}_{j\tilde{f}} + z^{R*}_{j\tilde{f}}\delta z^R_{i\tilde{f}}\right), \tag{3.19b}$$

$$\delta\mathcal{B}^{z+}_{ij\tilde{f}} = \left(z^L_{i\tilde{f}}\delta z^{R*}_{j\tilde{f}} + z^{L*}_{j\tilde{f}}\delta z^R_{i\tilde{f}}\right) + \left(z^R_{i\tilde{f}}\delta z^{L*}_{j\tilde{f}} + z^{R*}_{j\tilde{f}}\delta z^L_{i\tilde{f}}\right), \tag{3.19c}$$

$$\delta\mathcal{B}^{z-}_{ij\tilde{f}} = \left(z^L_{i\tilde{f}}\delta z^{R*}_{j\tilde{f}} + z^{L*}_{j\tilde{f}}\delta z^R_{i\tilde{f}}\right) - \left(z^R_{i\tilde{f}}\delta z^{L*}_{j\tilde{f}} + z^{R*}_{j\tilde{f}}\delta z^L_{i\tilde{f}}\right), \tag{3.19d}$$

$$v^n_{ij} = \frac{1}{4}\left(\delta Z^L_{\tilde{\chi}^0,ji} + \delta Z^{L*}_{\tilde{\chi}^0,ji}\right), \tag{3.19e}$$

$$a^n_{ij} = \frac{1}{4}\left(\delta Z^L_{\tilde{\chi}^0,ji} - \delta Z^{L*}_{\tilde{\chi}^0,ji}\right), \tag{3.19f}$$

$$v^c_{ij} = \frac{1}{4}\left(\delta Z^{R*}_{\tilde{\chi}^-,ji} + \delta Z^{L*}_{\tilde{\chi}^-,ji}\right), \tag{3.19g}$$

$$a^c_{ij} = \frac{1}{4}\left(\delta Z^{R*}_{\tilde{\chi}^-,ji} - \delta Z^{L*}_{\tilde{\chi}^-,ji}\right), \tag{3.19h}$$

for $z \in \{c,n\}$ and $\tilde{f} \in \{\tilde{\nu}_\mu, \tilde{\mu}_m\}$, and

$$\delta c^L_{i\tilde{\nu}_\mu} = -\delta g_2 V^*_{i1}, \tag{3.20a}$$

$$\delta c^R_{i\tilde{\nu}_\mu} = \delta y_\mu U_{i2}, \tag{3.20b}$$

$$\delta n^L_{i\tilde{\mu}_m} = \frac{1}{\sqrt{2}}\left(\delta g_1 N^*_{i1} + \delta g_2 N^*_{i2}\right)U^{\tilde{\mu}}_{m1} - \delta y_\mu N^*_{i3}U^{\tilde{\mu}}_{m2}, \tag{3.20c}$$

$$\delta n^R_{i\tilde{\mu}_m} = -\sqrt{2}\delta g_1 N_{i1}U^{\tilde{\mu}}_{m2} - \delta y_\mu N_{i3}U^{\tilde{\mu}}_{m1}, \tag{3.20d}$$

$$\delta y_\mu = \frac{m_\mu g_2}{\sqrt{2}M_W c_\beta}\left(\frac{\delta m_\mu}{m_\mu} + \frac{\delta g_2}{g_2} - \frac{\delta M_W}{M_W} - \frac{\delta c_\beta}{c_\beta}\right), \tag{3.20e}$$

$$\delta g_1 = \frac{e}{c_W}\left(\delta Z_e - \frac{\delta c_W}{c_W}\right), \tag{3.20f}$$

$$\delta g_2 = \frac{e}{s_W}\left(\delta Z_e - \frac{\delta s_W}{s_W}\right), \tag{3.20g}$$

$$\delta c_W = -\frac{s_W}{c_W}\delta s_W. \tag{3.20h}$$

The quantities $\delta\mathcal{A}^{z\pm}$ and $\delta\mathcal{B}^{z\pm}$ correspond to the renormalization of the coupling combinations and contain the entire effect of the parameter renormalization constants. As stressed in the beginning, these counterterm diagrams are finite by themselves, since there are no corresponding two-loop diagrams (as long as field renormalization is included).

Next, the four counterterm classes of figure 7 are considered, starting with the neutralino vertex and neutralino self-energy counterterm diagrams. In each case, only the result for off-diagonal neutralino/chargino indices ij is given; the result for $j = i$ can be obtained by a limiting procedure. The neutralino vertex counterterm diagram of figure 7(nv) is zero,

$$a^{(\text{nv-ct})}_{\mu\,ij\tilde{\mu}_m} = 0. \tag{3.21}$$

In general it would be proportional to δZ_{ZA} which, however, vanishes for the considered class of fermion/sfermion-loop diagrams.

The neutralino self-energy counterterm diagram of figure 7(ns) can be expressed easily with the help of eq. (2.10a):

$$
\begin{aligned}
a_{\mu\,ij\tilde{\mu}_m}^{(\text{ns-ct})} =& \frac{v}{m_{\tilde{\chi}_i^0} - m_{\tilde{\chi}_j^0}} \left[m_{\tilde{\chi}_j^0} a_\mu^{(\text{n-gen})}\Big(\mathcal{A}_{ji\tilde{\mu}_m}^{n+}, \mathcal{B}_{ji\tilde{\mu}_m}^{n+}, j\Big) - m_{\tilde{\chi}_i^0} a_\mu^{(\text{n-gen})}\Big(\mathcal{A}_{ji\tilde{\mu}_m}^{n+}, \mathcal{B}_{ji\tilde{\mu}_m}^{n+}, i\Big) \right] \\
&+ \frac{a}{m_{\tilde{\chi}_i^0} + m_{\tilde{\chi}_j^0}} \left[m_{\tilde{\chi}_j^0} a_\mu^{(\text{n-gen})}\Big(\mathcal{A}_{ji\tilde{\mu}_m}^{n-}, -\mathcal{B}_{ji\tilde{\mu}_m}^{n-}, j\Big) + m_{\tilde{\chi}_i^0} a_\mu^{(\text{n-gen})}\Big(\mathcal{A}_{ji\tilde{\mu}_m}^{n-}, \mathcal{B}_{ji\tilde{\mu}_m}^{n-}, i\Big) \right] \\
&+ \frac{s}{m_{\tilde{\chi}_i^0} - m_{\tilde{\chi}_j^0}} \left[a_\mu^{(\text{n-gen})}\Big(\mathcal{A}_{ji\tilde{\mu}_m}^{n+}, \mathcal{B}_{ji\tilde{\mu}_m}^{n+}, j\Big) - a_\mu^{(\text{n-gen})}\Big(\mathcal{A}_{ji\tilde{\mu}_m}^{n+}, \mathcal{B}_{ji\tilde{\mu}_m}^{n+}, i\Big) \right] \\
&+ \frac{p}{m_{\tilde{\chi}_i^0} + m_{\tilde{\chi}_j^0}} \left[a_\mu^{(\text{n-gen})}\Big(\mathcal{A}_{ji\tilde{\mu}_m}^{n-}, \mathcal{B}_{ji\tilde{\mu}_m}^{n-}, i\Big) - a_\mu^{(\text{n-gen})}\Big(\mathcal{A}_{ji\tilde{\mu}_m}^{n-}, -\mathcal{B}_{ji\tilde{\mu}_m}^{n-}, j\Big) \right].
\end{aligned}
\tag{3.22}
$$

Here the constants v, a, s, p correspond to a generic counterterm Feynman rule given by $i\ell(v - a\gamma_5) + i(s - p\gamma_5)$; they have to be replaced by the following renormalization constants:

$$
v = \frac{1}{4}\left(\delta Z_{\tilde{\chi}^0,ij}^L + \delta Z_{\tilde{\chi}^0,ji}^{L*} + \delta Z_{\tilde{\chi}^0,ji}^L + \delta Z_{\tilde{\chi}^0,ij}^{L*} \right),
\tag{3.23a}
$$

$$
a = \frac{1}{4}\left(\delta Z_{\tilde{\chi}^0,ij}^L + \delta Z_{\tilde{\chi}^0,ji}^{L*} - \delta Z_{\tilde{\chi}^0,ji}^L - \delta Z_{\tilde{\chi}^0,ij}^{L*} \right),
\tag{3.23b}
$$

$$
\begin{aligned}
s =& -\frac{1}{4}m_{\tilde{\chi}_i^0}\left(\delta Z_{\tilde{\chi}^0,ij}^{L*} + \delta Z_{\tilde{\chi}^0,ij}^L \right) - \frac{1}{4}m_{\tilde{\chi}_j^0}\left(\delta Z_{\tilde{\chi}^0,ji}^{L*} + \delta Z_{\tilde{\chi}^0,ji}^L \right) \\
& -\frac{1}{2}\left(\delta m_{\tilde{\chi}^0,ji}^* + \delta m_{\tilde{\chi}^0,ij} \right),
\end{aligned}
\tag{3.23c}
$$

$$
\begin{aligned}
p =& -\frac{1}{4}m_{\tilde{\chi}_i^0}\left(\delta Z_{\tilde{\chi}^0,ij}^{L*} - \delta Z_{\tilde{\chi}^0,ij}^L \right) - \frac{1}{4}m_{\tilde{\chi}_j^0}\left(\delta Z_{\tilde{\chi}^0,ji}^{L*} - \delta Z_{\tilde{\chi}^0,ji}^L \right) \\
& -\frac{1}{2}\left(\delta m_{\tilde{\chi}^0,ji}^* - \delta m_{\tilde{\chi}^0,ij} \right).
\end{aligned}
\tag{3.23d}
$$

Several differences between the counterterm result (3.22) and the standard one-loop result (2.11a) are noteworthy. Off-diagonal couplings with indices $ji\tilde{\mu}_m$ and the "minus"-coupling combinations $\mathcal{A}^-$ and $\mathcal{B}^-$ appear. Characteristically, only the a- and p-terms involve the "minus"-coupling combinations. These terms also involve denominators with sums of the neutralino masses instead of their differences. Note also that the $\mathcal{B}^-$s in some terms appear with negative prefactor. Importantly, thanks to partial fractioning, the counterterm results can be expressed in terms of the generalized one-loop result of eq. (2.10a) and therefore of the standard one-loop functions which depend only on a single mass ratio.

The chargino vertex counterterm diagram, i.e. the diagram with counterterm insertion at the photon-chargino-chargino vertex, has a slightly more complicated structure. The chargino vertex counterterm diagram of figure 7(cv) with the generic counterterm Feynman

rule $\gamma^\mu(v - a\gamma_5)$ leads to the expression

$$a_{\mu\,ij}^{(\text{cv-ct})} = \frac{1}{16\pi^2} \frac{m_\mu^2}{m_{\tilde{\nu}_\mu}^2} \left\{ \frac{1}{12} \left(v\mathcal{A}_{ji\tilde{\nu}_\mu}^{c+} - a\mathcal{A}_{ji\tilde{\nu}_\mu}^{c-} \right) \mathcal{F}_1^C(x_j, x_i) \right.$$
$$+ v\frac{\mathcal{B}_{ji\tilde{\nu}_\mu}^{c+}}{6m_\mu} \left[(m_{\tilde{\chi}_j^-} + m_{\tilde{\chi}_i^-})\mathcal{F}_2^C(x_j, x_i) + 6(m_{\tilde{\chi}_j^-} - m_{\tilde{\chi}_i^-})\mathcal{F}_3^C(x_j, x_i) \right]$$
$$\left. + a\frac{\mathcal{B}_{ji\tilde{\nu}_\mu}^{c-}}{6m_\mu} \left[(m_{\tilde{\chi}_j^-} - m_{\tilde{\chi}_i^-})\mathcal{F}_2^C(x_j, x_i) + 6(m_{\tilde{\chi}_j^-} + m_{\tilde{\chi}_i^-})\mathcal{F}_3^C(x_j, x_i) \right] \right\}. \tag{3.24}$$

It cannot be written in terms of the generalized one-loop result. Instead, and as an additional complication, eq. (3.24) contains new loop functions depending on two mass ratios, given in the appendix. Consistency with the standard one-loop result is reflected in the relations

$$\mathcal{F}_{1,2}^C(x_i, x_i) = \mathcal{F}_{1,2}^C(x_i), \qquad \mathcal{F}_3^C(x_i, x_i) = 0. \tag{3.25}$$

The generic constants v and a have to be replaced by

$$v = \frac{1}{4} \left(\delta Z_{\tilde{\chi}^-,ji}^{R*} + \delta Z_{\tilde{\chi}^-,ji}^{L*} + \delta Z_{\tilde{\chi}^-,ij}^{R} + \delta Z_{\tilde{\chi}^-,ij}^{L} \right), \tag{3.26a}$$

$$a = \frac{1}{4} \left(\delta Z_{\tilde{\chi}^-,ji}^{R*} - \delta Z_{\tilde{\chi}^-,ji}^{L*} + \delta Z_{\tilde{\chi}^-,ij}^{R} - \delta Z_{\tilde{\chi}^-,ij}^{L} \right). \tag{3.26b}$$

Finally, the chargino self-energy counterterm contribution is obtained by summing up the two chargino self-energy counterterm diagrams of figure 7(cs). The result combines all complications of the previous terms and reads

$$a_{\mu\,ij}^{(\text{cs-ct})} = \frac{v}{m_{\tilde{\chi}_i^-} - m_{\tilde{\chi}_j^-}} \left[m_{\tilde{\chi}_j^-} a_\mu^{(\text{c-gen})}\left(\mathcal{A}_{ji\tilde{\nu}_\mu}^{c+}, \mathcal{B}_{ji\tilde{\nu}_\mu}^{c+}, j \right) - m_{\tilde{\chi}_i^-} a_\mu^{(\text{c-gen})}\left(\mathcal{A}_{ji\tilde{\nu}_\mu}^{c+}, \mathcal{B}_{ji\tilde{\nu}_\mu}^{c+}, i \right) \right]$$

$$+ \frac{a}{m_{\tilde{\chi}_i^-} + m_{\tilde{\chi}_j^-}} \left[m_{\tilde{\chi}_j^-} a_\mu^{(\text{c-gen})}\left(\mathcal{A}_{ji\tilde{\nu}_\mu}^{c-}, -\mathcal{B}_{ji\tilde{\nu}_\mu}^{c-}, j \right) + m_{\tilde{\chi}_i^-} a_\mu^{(\text{c-gen})}\left(\mathcal{A}_{ji\tilde{\nu}_\mu}^{c-}, \mathcal{B}_{ji\tilde{\nu}_\mu}^{c-}, i \right) \right]$$

$$+ \frac{s}{m_{\tilde{\chi}_i^-} - m_{\tilde{\chi}_j^-}} \left[a_\mu^{(\text{c-gen})}\left(\mathcal{A}_{ji\tilde{\nu}_\mu}^{c+}, \mathcal{B}_{ji\tilde{\nu}_\mu}^{c+}, j \right) - a_\mu^{(\text{c-gen})}\left(\mathcal{A}_{ji\tilde{\nu}_\mu}^{c+}, \mathcal{B}_{ji\tilde{\nu}_\mu}^{c+}, i \right) \right]$$

$$+ \frac{p}{m_{\tilde{\chi}_i^-} + m_{\tilde{\chi}_j^-}} \left[a_\mu^{(\text{c-gen})}\left(\mathcal{A}_{ji\tilde{\nu}_\mu}^{c-}, \mathcal{B}_{ji\tilde{\nu}_\mu}^{c-}, i \right) - a_\mu^{(\text{c-gen})}\left(\mathcal{A}_{ji\tilde{\nu}_\mu}^{c-}, -\mathcal{B}_{ji\tilde{\nu}_\mu}^{c-}, j \right) \right]$$

$$- \frac{1}{16\pi^2} \frac{m_\mu^2}{m_{\tilde{\nu}_\mu}^2} \left\{ \frac{1}{12} \left(v\mathcal{A}_{ji\tilde{\nu}_\mu}^{c+} - a\mathcal{A}_{ji\tilde{\nu}_\mu}^{c-} \right) \mathcal{F}_1^C(x_j, x_i) \right.$$

$$+ v\frac{\mathcal{B}_{ji\tilde{\nu}_\mu}^{c+}}{6m_\mu} \left[(m_{\tilde{\chi}_j^-} + m_{\tilde{\chi}_i^-})\mathcal{F}_2^C(x_j, x_i) + 6(m_{\tilde{\chi}_j^-} - m_{\tilde{\chi}_i^-})\mathcal{F}_3^C(x_j, x_i) \right]$$

$$\left. + a\frac{\mathcal{B}_{ji\tilde{\nu}_\mu}^{c-}}{6m_\mu} \left[(m_{\tilde{\chi}_j^-} - m_{\tilde{\chi}_i^-})\mathcal{F}_2^C(x_j, x_i) + 6(m_{\tilde{\chi}_j^-} + m_{\tilde{\chi}_i^-})\mathcal{F}_3^C(x_j, x_i) \right] \right\}. \tag{3.27}$$
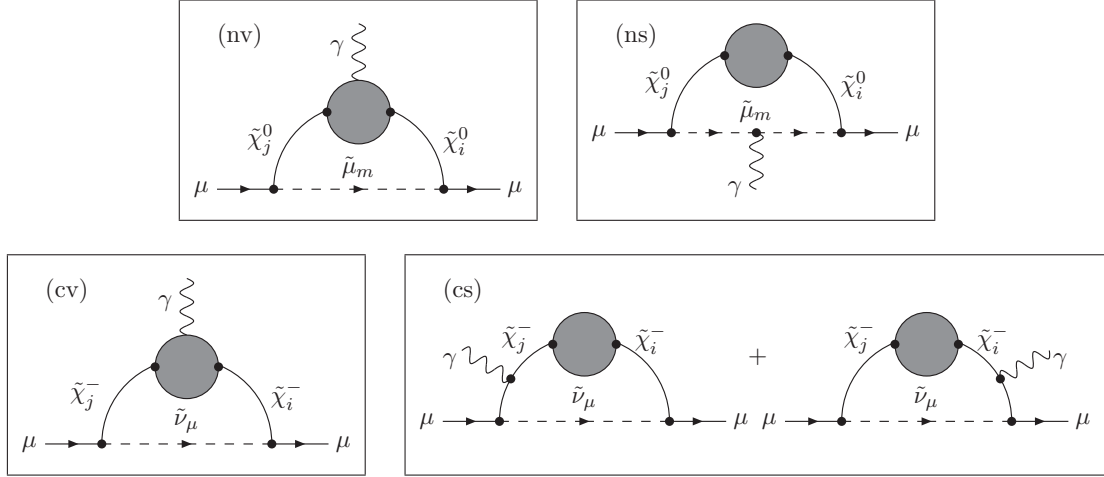
Figure 8. The four classes of two-loop diagrams with fermion/sfermion loop insertions into the neutralino vertex (nv), neutralino self-energy (ns), chargino vertex (cv), and chargino self-energy (cs). In the (cs) case always the sum of the two contributing diagrams is considered. The dark circles denote fermion/sfermion-loop insertions.

The generic constants v, a, s, p have to be replaced by

$$v = \frac{1}{4}\left(\delta Z^{L*}_{\tilde{\chi}^-,ji} + \delta Z^{R*}_{\tilde{\chi}^-,ji} + \delta Z^{L}_{\tilde{\chi}^-,ij} + \delta Z^{R}_{\tilde{\chi}^-,ij}\right), \tag{3.28a}$$

$$a = \frac{1}{4}\left(\delta Z^{L*}_{\tilde{\chi}^-,ji} - \delta Z^{R*}_{\tilde{\chi}^-,ji} + \delta Z^{L}_{\tilde{\chi}^-,ij} - \delta Z^{R}_{\tilde{\chi}^-,ij}\right), \tag{3.28b}$$

$$s = -\frac{1}{4}m_{\tilde{\chi}^-_i}\left(\delta Z^{L}_{\tilde{\chi}^-,ij} + \delta Z^{R}_{\tilde{\chi}^-,ij}\right) - \frac{1}{4}m_{\tilde{\chi}^-_j}\left(\delta Z^{L*}_{\tilde{\chi}^-,ji} + \delta Z^{R*}_{\tilde{\chi}^0,ji}\right)$$
$$\qquad -\frac{1}{2}\left(\delta m_{\tilde{\chi}^-,ji} + \delta m^*_{\tilde{\chi}^-,ij}\right), \tag{3.28c}$$

$$p = -\frac{1}{4}m_{\tilde{\chi}^-_i}\left(\delta Z^{L}_{\tilde{\chi}^-,ij} - \delta Z^{R}_{\tilde{\chi}^-,ij}\right) - \frac{1}{4}m_{\tilde{\chi}^-_j}\left(\delta Z^{R*}_{\tilde{\chi}^-,ji} - \delta Z^{L*}_{\tilde{\chi}^-,ji}\right)$$
$$\qquad -\frac{1}{2}\left(\delta m_{\tilde{\chi}^-,ji} - \delta m^*_{\tilde{\chi}^-,ij}\right). \tag{3.28d}$$

We highlight several characteristic properties which are shared by the more complicated two-loop contributions discussed below: off-diagonal coupling combinations with indices ji and the "minus"-coupling combinations $\mathcal{A}^-$ and $\mathcal{B}^-$ appear. Some parts of the counterterm results can be reduced by partial fractioning to loop functions that appear already in the standard one-loop results, some parts involve more complicated loop functions that depend on two mass ratios. Results at $\mathcal{O}(\epsilon^0)$ for generic diagrams similar to these counterterm diagrams have already been computed in ref. [82].

4 Two-loop contributions

The two-loop diagrams with a closed fermion/sfermion loop can be classified according to their topologies, as shown in figure 8, where the fermion/sfermion loops are denoted by dark circles. There are four classes:

- neutralino diagrams with an inner fermion/sfermion loop generating either an effective three-point neutralino-neutralino-photon vertex (nv), or a neutralino self-energy (ns). The inner loops are shown in more detail in figures 9 and 10.

- chargino diagrams with an inner fermion/sfermion loop generating either an effective three-point chargino-chargino-photon vertex (cv), or a chargino self-energy (cs). The inner loops are shown in more detail in figures 11 and 12.

There are no fermion/sfermion-loop corrections to the external vertices involving the muons, which is the reason why the counterterm diagrams in figure 6(μnv, μcv) are finite.

The computation of the diagrams has been carried out in two different ways. The first way uses the procedure described in refs. [19, 48] and is based on standard techniques for evaluating two-loop integrals, reduction to master integrals, large mass expansion and automated analytical simplification.

The second computation is completely different and uses the technique of Barr-Zee diagrams [58]. In the simplest Barr-Zee diagrams a closed loop generates an effective γ–γ-Higgs vertex. The computational strategy is to first compute the inner one-loop diagram alone using a Feynman parametrization, simplify it, and then insert it into the second loop diagram. By performing the second loop integration one obtains an integral representation of the full two-loop diagram. This Barr-Zee technique has been employed to compute several classes of contributions to electric [58, 83, 84] and magnetic dipole moments [49, 50, 85, 86]. In the latter references either fermion or sfermion loops generate a γ-vector-Higgs interaction. The diagrams considered in this paper can be regarded as supersymmetric counterparts to this, since the fermion/sfermion loops of figures 9 and 11 effectively generate γ-gaugino-higgsino interactions.

Compared to the previous applications of the method used by Barr and Zee the diagrams considered here are more complicated for three reasons:

- There is one more heavy mass scale in the diagram. As a consequence the two-loop results depend on four dimensionless mass ratios instead of three.

- The QED Ward identity constrains the results for the inner loops. As a consequence the inner loops in the references quoted above can be simplified to expressions which depend only on a single covariant and a single scalar function. However, in our case the Ward identity allows four such covariants already in the simplest case.

- The inner loops can be ultraviolet divergent. Apart from the requirement of renormalization this implies that the outer loop has to be computed to higher orders in the dimensional regularization parameter $\epsilon = (4 - D)/2$.

In the following the calculation and the results of the four classes of figure 8 are described in detail. The results are expressed in terms of generic neutralino and chargino couplings, defined in section 2.1. All results will be given only for $i \neq j$; for the case $i = j$ a limit can be performed.

In the neutralino cases we will close with some remarks on the structure of the results, similar to the remarks at the end of section 3. We will be briefer in the chargino cases, where the structure of the results is similar.

4.1 Notations for the neutralino results

We first introduce abbreviations which help us to write the neutralino two-loop results in a compact way.

The Feynman parametrization of the inner loops leads to a denominator of the form $w(1-w)\,\ell^2 - (1-w)\,m_f^2 - w\,m_{\tilde{f}}^2$, which depends on the Feynman parameter w. This defines a propagator denominator

$$\mathcal{D}_{f\tilde{f}_k}(\ell) \equiv \ell^2 - m_{f\tilde{f}_k}^2(w) \tag{4.1}$$

with momentum ℓ and an effective mass

$$m_{f\tilde{f}_k}^2(w) \equiv \frac{m_f^2}{w} + \frac{m_{\tilde{f}_k}^2}{1-w}. \tag{4.2}$$

The quantities m_f and $m_{\tilde{f}}$ denote fermion and sfermion masses, respectively. Due to partial integration also the derivative of the denominator appears, so it is convenient to introduce the abbreviation

$$g_w(\ell^2, m_f^2, m_{\tilde{f}_k}^2) \equiv \frac{(1-2w)\,\ell^2 + m_f^2 - m_{\tilde{f}_k}^2}{1-w}, \tag{4.3}$$

which is related to this derivative. In the case of neutralinos the results depend on the electric charge Q_f of the inner fermion, which equals $+\frac{2}{3}, -\frac{1}{3}, -1$ for up-type quarks, down-type quarks and charged leptons, respectively. The color factor N_C is 1 for leptons and 3 for quarks. The results further depend on the dimensionless mass ratios defined as

$$N_i \equiv \frac{m_i^2}{m_{\tilde{\mu}_m}^2}, \quad N_j \equiv \frac{m_j^2}{m_{\tilde{\mu}_m}^2}, \quad N_f \equiv \frac{m_f^2}{m_{\tilde{\mu}_m}^2}, \quad N_{\tilde{f}_k} \equiv \frac{m_{\tilde{f}_k}^2}{m_{\tilde{\mu}_m}^2}, \quad N_{f\tilde{f}_k} \equiv \frac{m_{f\tilde{f}_k}^2(w)}{m_{\tilde{\mu}_m}^2}, \tag{4.4}$$

where the neutralino masses are defined as $m_{i,j} \equiv m_{\tilde{\chi}_{i,j}^0}$ and $m_{\tilde{\mu}_m}$ is the smuon mass. It is also useful to introduce the following abbreviations for logarithms

$$l_z \equiv \log N_z, \quad L(m^2) \equiv \log \frac{m^2}{\mu_{\text{DRED}}^2}. \tag{4.5}$$

Here μ_{DRED} is the scale of dimensional regularization/dimensional reduction (there is no difference between the two schemes for the considered class of contributions). This scale does not drop out of the final, renormalized two-loop result because of the $\overline{\text{DR}}$ renormalization of $\tan\beta$.
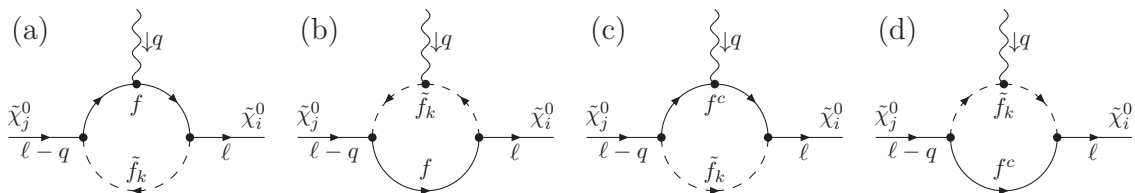
Figure 9. Feynman diagrams contributing to the neutralino vertex insertion. The sum of these diagrams is denoted as $i\Gamma^{0\mu}_{ij\tilde{f}_k}(\ell)$. The momenta flow in the directions indicated by the arrows.

4.2 Neutralino vertex contributions

The neutralino vertex diagrams, shown in figure 8(nv), constitute the only ultraviolet finite class of two-loop diagrams containing a closed fermion/sfermion loop. They show the closest similarity to the Barr-Zee type diagrams calculated in refs. [49, 50, 85, 86]. For each fermion/sfermion pair, there are four different inner loop diagrams, shown in figure 9, which generate an effective $\tilde{\chi}^0\tilde{\chi}^0\gamma$ interaction. This three-point function is calculated to first order in the photon momentum q. The use of Feynman parameter representation then yields the form of a Feynman propagator with an effective mass defined in eq. (4.2) and simplifies the subsequent calculation.

For a generic fermion/sfermion pair $(f, \tilde{f}_k)$, the sum of the four inner loop diagrams of figure 9 results in

$$
\Gamma^{0\mu}_{ij\tilde{f}_k}(\ell) = \frac{eQ_f}{16\pi^2} \int_0^1 \frac{\mathrm{d}w}{2} \left[\left(\overline{\mathcal{A}}^{n+}_{ij\tilde{f}_k} - \overline{\mathcal{A}}^{n-}_{ij\tilde{f}_k}\gamma^5 \right) \frac{\ell\!\!\!/ q\!\!\!/ \gamma^\mu - \ell\!\!\!/ q^\mu + q\!\!\!/\ell^\mu - (\ell\cdot q)\gamma^\mu}{\mathcal{D}_{f\tilde{f}_k}(\ell)} \right.
$$
$$
\left. + \left(\overline{\mathcal{B}}^{n+}_{ij\tilde{f}_k} - \overline{\mathcal{B}}^{n-}_{ij\tilde{f}_k}\gamma^5 \right) \frac{m_f}{w} \frac{q\!\!\!/\gamma^\mu - q^\mu}{\mathcal{D}_{f\tilde{f}_k}(\ell)} \right]. \tag{4.6}
$$

The appearing coupling combinations correspond to the imaginary and real parts of the coupling constants involved:

$$
\overline{\mathcal{A}}^{n\pm}_{ij\tilde{f}_k} \equiv \mathcal{A}^{n\pm}_{ij\tilde{f}_k} \mp \mathcal{A}^{n\pm*}_{ij\tilde{f}_k}, \tag{4.7a}
$$
$$
\overline{\mathcal{B}}^{n\pm}_{ij\tilde{f}_k} \equiv \mathcal{B}^{n\pm}_{ij\tilde{f}_k} \mp \mathcal{B}^{n\pm*}_{ij\tilde{f}_k}. \tag{4.7b}
$$

The result of eq. (4.6) can be divided into four parts according to these four different coupling combinations.

Apparently, the QED Ward identity $q_\mu\Gamma^{0\mu}_{ij\tilde{f}_k}(\ell) = 0$ is manifestly valid for each of the four parts separately. In line with the interpretation from section 2.1, the chirality-conserving $\mathcal{A}$ combinations appear in terms with odd powers of γ-matrices; the chirality-flipping $\mathcal{B}$ combinations in the ones with even powers. Further, the "plus"-combinations appear without γ_5; the "minus"-combinations with γ_5.

Inserting eq. (4.6) into the outer loop, performing the loop integration and extracting a_μ yields

$$
a^{(\mathrm{nv})}_{\mu\,ijm\tilde{f}_k} = \int_0^1 \mathrm{d}w \Bigg[\mathcal{A}^{n+}_{ji\tilde{\mu}_m} \left(\overline{\mathcal{A}}^{n+}_{ij\tilde{f}_k} \mathcal{T}^{nv+}_{AA} + \overline{\mathcal{B}}^{n+}_{ij\tilde{f}_k} \mathcal{T}^{nv+}_{AB} \right) + \mathcal{B}^{n+}_{ji\tilde{\mu}_m} \left(\overline{\mathcal{A}}^{n+}_{ij\tilde{f}_k} \mathcal{T}^{nv+}_{BA} + \overline{\mathcal{B}}^{n+}_{ij\tilde{f}_k} \mathcal{T}^{nv+}_{BB} \right)
$$
$$
+ \mathcal{A}^{n-}_{ji\tilde{\mu}_m} \left(\overline{\mathcal{A}}^{n-}_{ij\tilde{f}_k} \mathcal{T}^{nv-}_{AA} + \overline{\mathcal{B}}^{n-}_{ij\tilde{f}_k} \mathcal{T}^{nv-}_{AB} \right) + \mathcal{B}^{n-}_{ji\tilde{\mu}_m} \left(\overline{\mathcal{A}}^{n-}_{ij\tilde{f}_k} \mathcal{T}^{nv-}_{BA} + \overline{\mathcal{B}}^{n-}_{ij\tilde{f}_k} \mathcal{T}^{nv-}_{BB} \right) \Bigg].
$$
(4.8)

The loop functions $\mathcal{T}$ are either symmetric or antisymmetric in i, j and read

$$
\mathcal{T}^{nv\pm}_{AA} = \left(\frac{1}{16\pi^2} \right)^2 \frac{N_C Q_f}{4} \frac{m_\mu^2}{m_{\tilde{\mu}_m}^2} \frac{m_i}{m_i \mp m_j}
$$
$$
\times \left[\frac{1 - N_{f\tilde{f}_k} + l_{f\tilde{f}_k} N_{f\tilde{f}_k}^2}{(1 - N_{f\tilde{f}_k})^2 (N_{f\tilde{f}_k} - N_i)} - \frac{1 - N_i + l_i N_i^2}{(1 - N_i)^2 (N_{f\tilde{f}_k} - N_i)} \right] + (i \leftrightarrow j),
$$
(4.9a)

$$
\mathcal{T}^{nv\pm}_{AB} = \left(\frac{1}{16\pi^2} \right)^2 \frac{N_C Q_f}{4w} \frac{m_\mu^2 m_f}{m_{\tilde{\mu}_m}^2} \frac{1}{\pm m_i - m_j}
$$
$$
\times \left[\frac{1 - N_{f\tilde{f}_k} + l_{f\tilde{f}_k} N_{f\tilde{f}_k}^2}{(1 - N_{f\tilde{f}_k})^2 (N_{f\tilde{f}_k} - N_i)} - \frac{1 - N_i + l_i N_i^2}{(1 - N_i)^2 (N_{f\tilde{f}_k} - N_i)} \right] \pm (i \leftrightarrow j),
$$
(4.9b)

$$
\mathcal{T}^{nv\pm}_{BA} = \left(\frac{1}{16\pi^2} \right)^2 \frac{N_C Q_f}{4} m_\mu \frac{1}{m_i \mp m_j}
$$
$$
\times \left[-\frac{l_{f\tilde{f}_k} N_{f\tilde{f}_k}^2}{(1 - N_{f\tilde{f}_k})(N_{f\tilde{f}_k} - N_i)} + \frac{l_i N_i^2}{(1 - N_i)(N_{f\tilde{f}_k} - N_i)} \right] \pm (i \leftrightarrow j),
$$
(4.9c)

$$
\mathcal{T}^{nv\pm}_{BB} = \left(\frac{1}{16\pi^2} \right)^2 \frac{N_C Q_f}{2w} \frac{m_\mu m_f}{m_{\tilde{\mu}_m}^2} \frac{m_i m_j}{m_i^2 - m_j^2}
$$
$$
\times \left[-\frac{l_{f\tilde{f}_k} N_{f\tilde{f}_k}}{(1 - N_{f\tilde{f}_k})(N_{f\tilde{f}_k} - N_i)} + \frac{l_i N_i}{(1 - N_i)(N_{f\tilde{f}_k} - N_i)} \right] + (i \leftrightarrow j).
$$
(4.9d)

The notation $\pm(i \leftrightarrow j)$ indicates adding or subtracting the preceding expression with i and j exchanged.

We close with some comments on the structure of the results. The $\mathcal{A}^+, \mathcal{B}^+$-terms and the $\mathcal{A}^-, \mathcal{B}^-$-terms in the inner loop generate the vector and axial vector parts of the $\tilde{\chi}^0 \tilde{\chi}^0 \gamma$ interaction and further terms without/with γ_5, respectively. They combine with the coupling combinations of the outer loop similarly to v and a in eq. (3.24), such that only "++" and "−−" coupling combinations exist in eq. (4.8). The index structure of the outer loop, $ji\tilde{\mu}_m$, matches the index structure $ij\tilde{f}_k$ of the inner loop.

An important property of the $\mathcal{B}$-terms of the inner loop is that they are all proportional to the inner fermion mass m_f. This factor is needed in the inner loop because of the chirality-flipping nature of the $\mathcal{B}$ coupling combinations. As a result, the $\mathcal{B}$-terms of the inner loop can be sizeable only for third-generation insertions. In contrast, the $\mathcal{B}$-terms
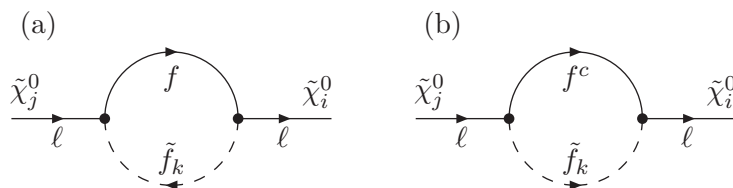
Figure 10. Feynman diagrams contributing to the neutralino self-energy insertion $i\Sigma^0_{ij\tilde{f}_k}(\ell)$.

of the outer loop are always important; as already at one-loop, they are $\tan\beta$-enhanced compared to the $\mathcal{A}$-terms of the outer loop.

The loop functions appearing in the two-loop results of eqs. (4.9) depend on three mass ratios, $N_i, N_j, N_{f\tilde{f}_k}$. The neutralino vertex contributions are particularly simple in this respect, since the masses m_f and $m_{\tilde{f}_k}$ of the inner loop do not appear individually but only in the combination $N_{f\tilde{f}_k}$.

4.3 Neutralino self-energy contributions

The next diagram class in our consideration is the one corresponding to figure 8(ns), where the inner loop generates a neutralino self-energy. For each fermion/sfermion pair, the corresponding one-loop insertions are given by the two Feynman diagrams shown in figure 10. The sum of these diagrams yields the effective self-energy insertion $i\Sigma^0_{ij\tilde{f}_k}(\ell)$, given by

$$
\Sigma^0_{ij\tilde{f}_k}(\ell) = \frac{1}{16\pi^2} \int_0^1 \frac{\mathrm{d}w}{2} \left[\left(\widetilde{\mathcal{A}}^{n+}_{ij\tilde{f}_k} - \widetilde{\mathcal{A}}^{n-}_{ij\tilde{f}_k} \gamma^5 \right) w\ell \left(\frac{1}{\epsilon} - L(m^2_{\tilde{f}_k}) + \frac{g_w(\ell^2, m^2_f, m^2_{\tilde{f}_k})/2}{\mathcal{D}_{f\tilde{f}_k}(\ell)} \right) \right.
$$
$$
\left. + \left(\widetilde{\mathcal{B}}^{n+}_{ij\tilde{f}_k} - \widetilde{\mathcal{B}}^{n-}_{ij\tilde{f}_k} \gamma^5 \right) m_f \left(\frac{1}{\epsilon} - L(m^2_{\tilde{f}_k}) + \frac{g_w(\ell^2, m^2_f, m^2_{\tilde{f}_k})}{\mathcal{D}_{f\tilde{f}_k}(\ell)} \right) \right].
\tag{4.10}
$$

Compared to the neutralino vertex contributions in eqs. (4.7), the coupling combinations appear with opposite signs:

$$
\widetilde{\mathcal{A}}^{n\pm}_{ij\tilde{f}_k} \equiv \mathcal{A}^{n\pm}_{ij\tilde{f}_k} \pm \mathcal{A}^{n\pm*}_{ij\tilde{f}_k},
\tag{4.11a}
$$
$$
\widetilde{\mathcal{B}}^{n\pm}_{ij\tilde{f}_k} \equiv \mathcal{B}^{n\pm}_{ij\tilde{f}_k} \pm \mathcal{B}^{n\pm*}_{ij\tilde{f}_k}.
\tag{4.11b}
$$

Similar to the previous case, the chirality-conserving $\mathcal{A}$-combinations appear in the terms with odd powers of γ-matrices, the chirality-flipping $\mathcal{B}$-couplings in those without γ-matrix. Also the "plus"("minus")-combinations appear without(with) γ_5.

Inserting eq. (4.10) into the two-loop diagrams of figure 8(ns) and performing the loop integration yields a rather compact expression for a_μ. The divergent part can be trivially

read off from combining eqs. (3.22) and (4.10). The finite part is given by:

$$
a_{\mu\,ijm\tilde{f}_k}^{(\mathrm{ns})} = \int_0^1 \mathrm{d}w \Bigg[\mathcal{A}_{ji\tilde{\mu}_m}^{n+} \left(\widetilde{\mathcal{A}}_{ij\tilde{f}_k}^{n+} \mathcal{T}_{AA}^{ns+} + \widetilde{\mathcal{B}}_{ij\tilde{f}_k}^{n+} \mathcal{T}_{AB}^{ns+} \right) + \mathcal{B}_{ji\tilde{\mu}_m}^{n+} \left(\widetilde{\mathcal{A}}_{ij\tilde{f}_k}^{n+} \mathcal{T}_{BA}^{ns+} + \widetilde{\mathcal{B}}_{ij\tilde{f}_k}^{n+} \mathcal{T}_{BB}^{ns+} \right)
$$
$$
+ \mathcal{A}_{ji\tilde{\mu}_m}^{n-} \left(\widetilde{\mathcal{A}}_{ij\tilde{f}_k}^{n-} \mathcal{T}_{AA}^{ns-} + \widetilde{\mathcal{B}}_{ij\tilde{f}_k}^{n-} \mathcal{T}_{AB}^{ns-} \right) + \mathcal{B}_{ji\tilde{\mu}_m}^{n-} \left(\widetilde{\mathcal{A}}_{ij\tilde{f}_k}^{n-} \mathcal{T}_{BA}^{ns-} + \widetilde{\mathcal{B}}_{ij\tilde{f}_k}^{n-} \mathcal{T}_{BB}^{ns-} \right) \Bigg].
$$
(4.12)

Each of the loop functions $\mathcal{T}_{XY}^{ns\pm}$ can be expressed in terms of two simpler functions $\mathcal{T}_{XY}^{ns1}$ and $\mathcal{T}_{XY}^{ns2}$, such that the dependence on $N_{f\tilde{f}_k}$ and N_i/N_j is essentially separated:

$$
\mathcal{T}_{AA}^{ns\pm} = \left(\frac{1}{16\pi^2} \right)^2 N_C \frac{m_\mu^2}{m_{\tilde{\mu}_m}^2} \frac{m_i}{m_i \mp m_j} \left[\mathcal{T}_{AA}^{ns1} + \mathcal{T}_{AA}^{ns2} \right] + (i \leftrightarrow j),
\tag{4.13a}
$$

$$
\mathcal{T}_{AB}^{ns\pm} = \left(\frac{1}{16\pi^2} \right)^2 N_C \frac{m_\mu^2 m_{f'}}{m_{\tilde{\mu}_m}^2} \frac{1}{\pm m_i - m_j} \left[\mathcal{T}_{AB}^{ns1} + \mathcal{T}_{AB}^{ns2} \right] \pm (i \leftrightarrow j),
\tag{4.13b}
$$

$$
\mathcal{T}_{BA}^{ns\pm} = \left(\frac{1}{16\pi^2} \right)^2 N_C m_\mu \frac{1}{m_i \mp m_j} \left[\mathcal{T}_{BA}^{ns1} + \mathcal{T}_{BA}^{ns2} \right] \pm (i \leftrightarrow j),
\tag{4.13c}
$$

$$
\mathcal{T}_{BB}^{ns\pm} = \left(\frac{1}{16\pi^2} \right)^2 N_C \frac{m_\mu m_{f'}}{m_{\tilde{\mu}_m}^2} \frac{m_i}{\pm m_i - m_j} \left[\mathcal{T}_{BB}^{ns1} + \mathcal{T}_{BB}^{ns2} \right] + (i \leftrightarrow j),
\tag{4.13d}
$$

with

$$
\mathcal{T}_{AA}^{ns1} = w \, \frac{g_w(N_{f\tilde{f}_k}, N_f, N_{\tilde{f}_k})}{N_{f\tilde{f}_k} - N_i} \frac{F_1^N(N_{f\tilde{f}_k})}{48},
\tag{4.14a}
$$

$$
\mathcal{T}_{AA}^{ns2} = \Bigg(-4L(m_{\tilde{\mu}_m}^2) - l_i - 2l_{\tilde{f}_k}
$$
$$
- \frac{1}{6N_i^2} + \frac{1}{N_i} + \frac{5}{2} + \frac{N_i}{3} - 2w \frac{g_w(N_i, N_f, N_{\tilde{f}_k})}{N_{f\tilde{f}_k} - N_i} \Bigg) \frac{F_1^N(N_i)}{96} + \frac{1 - 8N_i - 4N_i^2}{288 N_i^2},
\tag{4.14b}
$$

$$
\mathcal{T}_{AB}^{ns1} = \frac{g_w(N_{f\tilde{f}_k}, N_f, N_{\tilde{f}_k})}{N_{f\tilde{f}_k} - N_i} \frac{F_1^N(N_{f\tilde{f}_k})}{24},
\tag{4.14c}
$$

$$
\mathcal{T}_{AB}^{ns2} = \Bigg(-4L(m_{\tilde{\mu}_m}^2) - l_i - 2l_{\tilde{f}_k}
$$
$$
- \frac{1}{6N_i^2} + \frac{1}{N_i} + \frac{5}{2} + \frac{N_i}{3} - 2 \frac{g_w(N_i, N_f, N_{\tilde{f}_k})}{N_{f\tilde{f}_k} - N_i} \Bigg) \frac{F_1^N(N_i)}{48} + \frac{1 - 8N_i}{144 N_i^2},
\tag{4.14d}
$$

$$
\mathcal{T}_{BA}^{ns1} = w \, \frac{g_w(N_{f\tilde{f}_k}, N_f, N_{\tilde{f}_k})}{N_{f\tilde{f}_k} - N_i} \frac{N_{f\tilde{f}_k} F_2^N(N_{f\tilde{f}_k}) - 3}{24},
\tag{4.14e}
$$

$$
\mathcal{T}_{BA}^{ns2} = \Bigg(-4L(m_{\tilde{\mu}_m}^2) - l_i - 2l_{\tilde{f}_k}
$$
$$
- \frac{1}{2N_i^2} + \frac{2}{N_i} + \frac{1}{2} + N_i - 2w \frac{g_w(N_i, N_f, N_{\tilde{f}_k})}{N_{f\tilde{f}_k} - N_i} \Bigg) \frac{N_i F_2^N(N_i) - 3}{48} - \frac{3 - 15N_i}{96 N_i^2},
\tag{4.14f}
$$

$$\mathcal{T}_{BB}^{ns1} = \frac{g_w(N_{f\tilde{f}_k}, N_f, N_{\tilde{f}_k})}{N_{f\tilde{f}_k} - N_i} \frac{F_2^N(N_{f\tilde{f}_k})}{12}, \tag{4.14g}$$

$$\mathcal{T}_{BB}^{ns2} = \left(-4L(m_{\tilde{\mu}_m}^2) - l_i - 2l_{\tilde{f}_k} \right.$$
$$\left. + \frac{1}{2N_i^2} + 2 + \frac{N_i}{2} - 2\frac{g_w(N_i, N_f, N_{\tilde{f}_k})}{N_{f\tilde{f}_k} - N_i} \right) \frac{F_2^N(N_i)}{24} - \frac{1 + N_i}{16N_i}, \tag{4.14h}$$

The comments at the end of section 4.2 apply here as well. However, the loop functions are now more complicated. The masses m_f and $m_{\tilde{f}_k}$ appear not only via the combination $N_{f\tilde{f}_k}$ but also explicitly via N_f and $N_{\tilde{f}_k}$. Their dependence is localized to the abbreviation g_w, which already appears in the inner loop, i.e. the self energy eq. (4.10). In spite of this complication, the loop functions in eq. (4.13) could be partially expressed in terms of the one-loop functions $F_{1,2}^N$. This is similar to the corresponding counterterm diagram in figure 7(ns), eq. (3.22).

4.4 Notations for the chargino results

We now turn to the chargino results. Since the chargino is negatively charged, the inner loop contains the fermion f', which is the U(2) doublet partner of the fermion f. In analogy to the neutralino case we introduce an effective mass

$$m_{f'\tilde{f}_k}^2(w) \equiv \frac{m_{f'}^2}{w} + \frac{m_{\tilde{f}_k}^2}{1-w}, \tag{4.15}$$

and its corresponding propagator denominator

$$\mathcal{D}_{f'\tilde{f}_k}(\ell) \equiv \ell^2 - m_{f'\tilde{f}_k}^2(w). \tag{4.16}$$

As mentioned in section 2.1, the chargino interactions in the Lagrangian (2.1) can be rewritten using flipping rules for the anti-up-type fermions. Recalling the $(f', \tilde{f})$ combinations in eq. (2.4) we apply $Q_{u^c} = -\frac{2}{3}$ for anti-up-type quarks, $Q_d = -\frac{1}{3}$ for down-type quarks, and $Q_l = -1$ for leptons. In this way, the relation for charge conservation $Q_{f'} - Q_{\tilde{f}_k} = Q_{\tilde{\chi}^-} = -1$ is always valid. The chargino results further depend on the color factor N_C of the inner fermion, the chargino masses $m_{i,j} \equiv m_{\tilde{\chi}_{i,j}^-}$ and the dimensionless mass ratios

$$C_i \equiv \frac{m_i^2}{m_{\tilde{\nu}_\mu}^2}, \quad C_j \equiv \frac{m_j^2}{m_{\tilde{\nu}_\mu}^2}, \quad C_{f'} \equiv \frac{m_{f'}^2}{m_{\tilde{\nu}_\mu}^2}, \quad C_{\tilde{f}_k} \equiv \frac{m_{\tilde{f}_k}^2}{m_{\tilde{\nu}_\mu}^2}, \quad C_{f'\tilde{f}_k} \equiv \frac{m_{f'\tilde{f}_k}^2(w)}{m_{\tilde{\nu}_\mu}^2}. \tag{4.17}$$

The logarithms defined in eq. (4.5) are modified to

$$l_z \equiv \log C_z, \quad L(m^2) \equiv \log \frac{m^2}{\mu_{\text{DRED}}^2} \tag{4.18}$$
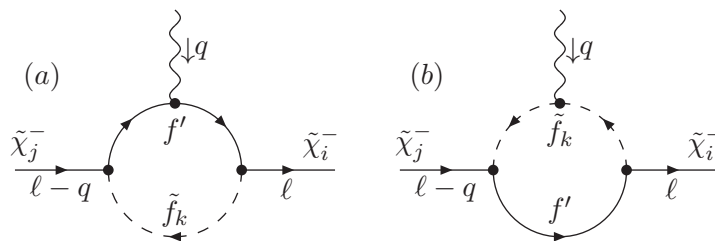
for the chargino case.

Figure 11. Feynman diagrams for the chargino vertex insertion $i\Gamma^{-\,\mu}_{ij\tilde{f}_k}(\ell)$. The possible insertions are given in eq. (2.4) and involve only negative fermions and positive sfermions.

4.5 Chargino vertex contributions

The chargino vertex contributions are shown in figure 8(cv). The corresponding one-loop insertions are shown in figure 11 and can be written as:

$$
\Gamma^{-\,\mu}_{ij\tilde{f}_k}(\ell) = \frac{eQ_{f'}}{16\pi^2}\int_0^1 \frac{\mathrm{d}w}{2}\left\{ \left(\mathcal{A}^{c+}_{ij\tilde{f}_k} - \mathcal{A}^{c-}_{ij\tilde{f}_k}\gamma_5\right)\frac{\slashed{\ell}\slashed{q}\gamma^\mu - \slashed{\ell}q^\mu + \slashed{q}\ell^\mu - (\ell\cdot q)\gamma^\mu}{\mathcal{D}_{f'\tilde{f}_k}(\ell)} \right.
$$
$$
\left. + \left(\mathcal{B}^{c+}_{ij\tilde{f}_k} - \mathcal{B}^{c-}_{ij\tilde{f}_k}\gamma_5\right)\frac{m_{f'}}{w}\frac{\slashed{q}\gamma^\mu - q^\mu}{\mathcal{D}_{f'\tilde{f}_k}(\ell)} \right\}
$$
$$
-\frac{eQ_{\tilde{\chi}^-}}{16\pi^2}\int_0^1 \frac{\mathrm{d}w}{2}\left\{ \left(\mathcal{A}^{c+}_{ij\tilde{f}_k} - \mathcal{A}^{c-}_{ij\tilde{f}_k}\gamma_5\right)w\right.
$$
$$
\times\left[\left(\frac{1}{\epsilon} - L(m^2_{\tilde{f}_k})\right)\gamma^\mu - 2\frac{(\ell\cdot q)\,\slashed{\ell}\,\ell^\mu}{\mathcal{D}^2_{f'\tilde{f}_k}(\ell)} \right.
$$
$$
\left. + \frac{\slashed{q}\ell^\mu + \slashed{\ell}q^\mu + (\ell\cdot q)\gamma^\mu - 2\,\slashed{\ell}\,\ell^\mu + g_w(\ell^2,m^2_{f'},m^2_{\tilde{f}_k})\gamma^\mu/2}{\mathcal{D}_{f'\tilde{f}_k}(\ell)} \right]
$$
$$
\left. + \left(\mathcal{B}^{c+}_{ij\tilde{f}_k} - \mathcal{B}^{c-}_{ij\tilde{f}_k}\gamma_5\right)m_{f'}\left[-2\frac{(\ell\cdot q)\ell^\mu}{\mathcal{D}^2_{f'\tilde{f}_k}(\ell)} + \frac{q^\mu - 2\ell^\mu}{\mathcal{D}_{f'\tilde{f}_k}(\ell)} \right] \right\}.
$$
(4.19)

The part proportional to the inner fermion charge $Q_{f'}$ can be written in exactly the same way as the neutralino vertex corrections. The remaining terms proportional to $Q_{\tilde{\chi}^-}$ have no neutralino counterpart. They are divergent and have a far more involved structure.

Inserting eq. (4.19) into the outer loop and integrating over the loop momentum yields for the finite part

$$
a^{(cv)}_{\mu\,ij\tilde{f}_k} = \int_0^1 \mathrm{d}w\left[\mathcal{A}^{c+}_{ji\tilde{\nu}_\mu}\left(\mathcal{A}^{c+}_{ij\tilde{f}_k}\mathcal{T}^{cv+}_{AA} + \mathcal{B}^{c+}_{ij\tilde{f}_k}\mathcal{T}^{cv+}_{AB}\right) + \mathcal{B}^{c+}_{ji\tilde{\nu}_\mu}\left(\mathcal{A}^{c+}_{ij\tilde{f}_k}\mathcal{T}^{cv+}_{BA} + \mathcal{B}^{c+}_{ij\tilde{f}_k}\mathcal{T}^{cv+}_{BB}\right) \right.
$$
$$
\left. + \mathcal{A}^{c-}_{ji\tilde{\nu}_\mu}\left(\mathcal{A}^{c-}_{ij\tilde{f}_k}\mathcal{T}^{cv-}_{AA} + \mathcal{B}^{c-}_{ij\tilde{f}_k}\mathcal{T}^{cv-}_{AB}\right) + \mathcal{B}^{c-}_{ji\tilde{\nu}_\mu}\left(\mathcal{A}^{c-}_{ij\tilde{f}_k}\mathcal{T}^{cv-}_{BA} + \mathcal{B}^{c-}_{ij\tilde{f}_k}\mathcal{T}^{cv-}_{BB}\right) \right].
$$
(4.20)

Now the loop functions have a significantly more involved structure. On the one hand this is due to the additional terms in the inner loop, and on the other hand it is caused by the

outer loop, for which the counterterm result of eq. (3.24) already provides an illustration. For the loop functions we find the following expressions

$$
\mathcal{T}_{AA}^{cv\pm} = \left(\frac{1}{16\pi^2}\right)^2 N_C \frac{m_\mu^2}{m_{\tilde\nu_\mu}^2}\left[\frac{1}{C_i - C_j}\left(\frac{\mathcal{T}_{AA}^{cv1a}(C_{f'\tilde f_k}) - \mathcal{T}_{AA}^{cv1a}(C_i)}{C_{f'\tilde f_k} - C_i} + \mathcal{T}_{AA}^{cv2}(C_i)\right)\right.
$$
$$
\left.\pm \frac{m_i m_j}{m_i^2 - m_j^2}\frac{\mathcal{T}_{AA}^{cv1b}(C_{f'\tilde f_k}) - \mathcal{T}_{AA}^{cv1b}(C_i)}{C_{f'\tilde f_k} - C_i}\right] + (i \leftrightarrow j), \tag{4.21a}
$$

$$
\mathcal{T}_{AB}^{cv\pm} = \left(\frac{1}{16\pi^2}\right)^2 N_C \frac{m_\mu^2 m_{f'}}{m_{\tilde\nu_\mu}^2}\frac{1}{\pm m_i - m_j}\frac{1}{w}\left[\frac{\mathcal{T}_{AB}^{cv1}(C_{f'\tilde f_k}) - \mathcal{T}_{AB}^{cv1}(C_i)}{C_{f'\tilde f_k} - C_i}\right] \pm (i \leftrightarrow j), \tag{4.21b}
$$

$$
\mathcal{T}_{BA}^{cv\pm} = \left(\frac{1}{16\pi^2}\right)^2 N_C m_\mu\left[\frac{1}{m_i \mp m_j}\left(\frac{\mathcal{T}_{BA}^{cv1a}(C_{f'\tilde f_k}) - \mathcal{T}_{BA}^{cv1a}(C_i)}{C_{f'\tilde f_k} - C_i} + \mathcal{T}_{BA}^{cv2a}\right)\right.
$$
$$
\left.+ \frac{1}{m_i \pm m_j}\left(\frac{\mathcal{T}_{BA}^{cv1b}}{C_{f'\tilde f_k} - C_i} + \mathcal{T}_{BA}^{cv2b}\right)\right] \pm (i \leftrightarrow j), \tag{4.21c}
$$

$$
\mathcal{T}_{BB}^{cv\pm} = \left(\frac{1}{16\pi^2}\right)^2 N_C \frac{m_\mu m_{f'}}{m_{\tilde\nu_\mu}^2}\left[\frac{\pm 1}{C_i - C_j}\frac{\mathcal{T}_{BB}^{cv1}(C_{f'\tilde f_k}) - \mathcal{T}_{BB}^{cv1}(C_i)}{C_{f'\tilde f_k} - C_i}\right.
$$
$$
\left.+ \frac{m_i m_j}{m_i^2 - m_j^2}\frac{\mathcal{T}_{BB}^{cv1b}(C_{f'\tilde f_k}) - \mathcal{T}_{BB}^{cv1b}(C_i)}{C_{f'\tilde f_k} - C_i}\right] + (i \leftrightarrow j), \tag{4.21d}
$$

with

$$
\mathcal{T}_{AA}^{cv1a}(C_x) = \frac{Q_{f'}}{4}\frac{C_x(1 - C_x + l_x C_x^2)}{(1 - C_x)^2} + \frac{w}{4}\frac{1 - C_x + l_x C_x^3}{(1 - C_x)^2} + \frac{w}{24(1 - w)}\frac{1}{(1 - C_x)^3}
$$
$$
\times\left[2 - 6C_x + 4C_x^2 - 3l_x C_x^3 + l_x C_x^4 + (C_{f'} - C_{\tilde f_k})C_x(2 - 2C_x + 3l_x C_x - l_x C_x^2)\right], \tag{4.22a}
$$

$$
\mathcal{T}_{AA}^{cv1b}(C_x) = \frac{Q_{f'}}{4}\frac{1 - C_x + l_x C_x^2}{(1 - C_x)^2} + \frac{w}{12}\frac{3 - 8C_x + 5C_x^2 - 2l_x C_x^3}{(1 - C_x)^3}, \tag{4.22b}
$$

$$
\mathcal{T}_{AA}^{cv2}(C_x) = \left[-12L(m_{\tilde\nu_\mu}^2) - 6l_{\tilde f_k} - 3l_x + 5 - \frac{6}{C_x}\right]\frac{C_x\left(2 - 2C_x + 3l_x C_x - l_x C_x^2\right)}{144\left(1 - C_x\right)^3}
$$
$$
+ \frac{1 + 2l_x C_x - C_x^2}{12\left(1 - C_x\right)^3}, \tag{4.22c}
$$

$$
\mathcal{T}_{AB}^{cv1}(C_x) = \mathcal{T}_{AA}^{cv1b}(C_x), \tag{4.22d}
$$

$$
\mathcal{T}_{BA}^{cv1a}(C_x) = -\frac{Q_{f'}}{4}\frac{l_x C_x^2}{1 - C_x} + \frac{w}{8}\left[\frac{2}{1 - C_x} + \frac{l_x C_x^2(1 + C_x)}{(1 - C_x)^2}\right]
$$
$$
- \frac{1}{16}w\, g_w(C_{f'\tilde f_k}, C_{f'}, C_{\tilde f_k})\left[\frac{1}{1 - C_x} + \frac{l_x C_x(2 - C_x)}{(1 - C_x)^2}\right], \tag{4.22e}
$$

$$
\mathcal{T}_{BA}^{cv1b} = \frac{1}{16}w\, g_w(C_{f'\tilde f_k}, C_{f'}, C_{\tilde f_k})\left[\frac{l_i C_i(C_i^2 - 2C_j + C_i C_j)}{(C_i - C_j)(1 - C_i)^2} + \frac{C_i}{1 - C_i} + \right.
$$
$$
\left.+ \frac{l_{f'\tilde f_k}C_{f'\tilde f_k}^2}{1 - C_{f'\tilde f_k}}\left(\frac{2}{C_i - C_j} - \frac{1}{C_{f'\tilde f_k} - C_i}\right)\right] - \frac{w}{8}\frac{l_i C_i^2}{1 - C_i}, \tag{4.22f}
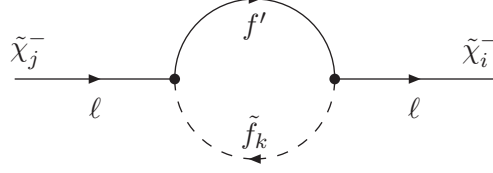$$

Figure 12. Feynman diagram for the chargino self-energy insertion $i\Sigma^-_{ij\tilde{f}_k}(\ell)$.

$$\mathcal{T}^{cv2a}_{BA} = \frac{C_i\left(-3 + 3C_i - 4l_i + l_iC_i + 2l_i^2 - l_i^2C_i\right)}{32\left(1 - C_i\right)^2}$$
$$+ \frac{1}{16}\left[2L(m^2_{\tilde{\nu}_\mu}) + l_{\tilde{f}_k} - w\frac{1 - 2w}{1 - w}\right] \times \left[\frac{l_i\left(2 - C_i\right)C_i}{\left(1 - C_i\right)^2} + \frac{C_i}{1 - C_i}\right], \tag{4.22g}$$

$$\mathcal{T}^{cv2b}_{BA} = \mathcal{T}^{cv2a}_{BA} + \frac{\left(3l_i - l_i^2\right)C_i^2}{16\left(1 - C_i\right)\left(C_i - C_j\right)}$$
$$- \frac{1}{8}\left[2L(m^2_{\tilde{\nu}_\mu}) + l_{\tilde{f}_k} - w\frac{1 - 2w}{1 - w}\right] \times \left[\frac{l_iC_i^2}{\left(1 - C_i\right)\left(C_i - C_j\right)}\right], \tag{4.22h}$$

$$\mathcal{T}^{cv1}_{BB}(C_x) = \frac{1 - C_x + l_xC_x^2}{4\left(1 - C_x\right)^2}, \tag{4.22i}$$

$$\mathcal{T}^{cv1b}_{BB}(C_x) = -\frac{Q_{f'}}{2w}\frac{l_xC_x}{1 - C_x} + \frac{1 - C_x + l_xC_x^2}{4\left(1 - C_x\right)^2} \tag{4.22j}$$

In some of these functions an explicit argument C_x is specified, which is specialized in eqs. (4.21) to $C_x \in \{C_i, C_j, C_{f'\tilde{f}_k}\}$.

4.6 Chargino self-energy contributions

The last class of diagrams is the one corresponding to figure 8(cs), where the fermion/sfermion loop generates a chargino self-energy. Figure 12 shows the chargino self-energy one-loop diagram. The result has the same structure as the corresponding neutralino self-energy result, see eq. (4.10),

$$\Sigma^-_{ij\tilde{f}_k}(\ell) = \frac{1}{16\pi^2}\int_0^1 \frac{dw}{2}\left[\left(\mathcal{A}^{c+}_{ij\tilde{f}_k} - \mathcal{A}^{c-}_{ij\tilde{f}_k}\gamma^5\right)w\ell\left(\frac{1}{\epsilon} - L(m^2_{\tilde{f}_k}) + \frac{g_w(\ell^2, m^2_{f'}, m^2_{\tilde{f}_k})/2}{\mathcal{D}_{f'\tilde{f}_k}(\ell)}\right)\right.$$
$$+ \left.\left(\mathcal{B}^{c+}_{ij\tilde{f}_k} - \mathcal{B}^{c-}_{ij\tilde{f}_k}\gamma^5\right)m_f\left(\frac{1}{\epsilon} - L(m^2_{\tilde{f}_k}) + \frac{g_w(\ell^2, m^2_{f'}, m^2_{\tilde{f}_k})}{\mathcal{D}_{f'\tilde{f}_k}(\ell)}\right)\right]. \tag{4.23}$$

This self-energy vertex can be inserted in the outer loop in two different ways, as shown in figure 8(cs). Inserting the self-energy result into the two-loop diagrams, the following contribution to a_μ is obtained:

$$a^{(cs)}_{\mu\, ij\tilde{f}_k} = \int_0^1 dw\Big[\mathcal{A}^{c+}_{ji\tilde{\nu}_\mu}\left(\mathcal{A}^{c+}_{ij\tilde{f}_k}\mathcal{T}^{cs+}_{AA} + \mathcal{B}^{c+}_{ij\tilde{f}_k}\mathcal{T}^{cs+}_{AB}\right) + \mathcal{B}^{c+}_{ji\tilde{\nu}_\mu}\left(\mathcal{A}^{c+}_{ij\tilde{f}_k}\mathcal{T}^{cs+}_{BA} + \mathcal{B}^{c+}_{ij\tilde{f}_k}\mathcal{T}^{cs+}_{BB}\right)$$
$$+ \mathcal{A}^{c-}_{ji\tilde{\nu}_\mu}\left(\mathcal{A}^{c-}_{ij\tilde{f}_k}\mathcal{T}^{cs-}_{AA} + \mathcal{B}^{c-}_{ij\tilde{f}_k}\mathcal{T}^{cs-}_{AB}\right) + \mathcal{B}^{c-}_{ji\tilde{\nu}_\mu}\left(\mathcal{A}^{c-}_{ij\tilde{f}_k}\mathcal{T}^{cs-}_{BA} + \mathcal{B}^{c-}_{ij\tilde{f}_k}\mathcal{T}^{cs-}_{BB}\right)\Big]. \tag{4.24}$$

As is clear from the corresponding one-loop counterterm diagrams of figure 7(cs), eq. (3.27), the chargino self-energy corrections lead to the most complicated two-loop expressions. It would result in very long formulas for the loop functions $\mathcal{T}_{XY}^{cs\pm}$ to express the $\mathcal{O}(\epsilon^0)$-result like in the previous cases. Hence we employ the ϵ-dependent one-loop functions defined with two variables $\mathcal{F}_{1,2,3}^C(C_j, C_i)$. The $\mathcal{O}(\epsilon^0)$-part can then be obtained by evaluating the following expressions explicitly.

Furthermore, the particular structure of the one-loop self-energy result is used. All terms have the form of a counterterm insertion, possibly multiplied with an additional propagator and w-dependent rational functions, which can be split off:

$$\mathcal{T}_{XA}^{cs\pm} = \left(\frac{1}{16\pi^2}\right)^2 \left[\left(\frac{1}{\epsilon} - L(m_{\tilde{\nu}_\mu}^2) - l_{\tilde{f}_k} - \frac{2w-1}{2(1-w)}\right)\mathcal{T}_{XA}^{cs1\pm} + \frac{g_w(C_{f'\tilde{f}_k}, C_{f'}, C_{\tilde{f}_k})}{2}\mathcal{T}_{XA}^{cs2\pm}\right]w, \tag{4.25a}$$

$$\mathcal{T}_{XB}^{cs\pm} = \left(\frac{1}{16\pi^2}\right)^2 \left[\left(\frac{1}{\epsilon} - L(m_{\tilde{\nu}_\mu}^2) - l_{\tilde{f}_k} - \frac{2w-1}{1-w}\right)\mathcal{T}_{XB}^{cs1\pm} + g_w(C_{f'\tilde{f}_k}, C_{f'}, C_{\tilde{f}_k})\mathcal{T}_{XB}^{cs2\pm}\right], \tag{4.25b}$$

where $X \in \{A, B\}$. The individual results for the coefficients of the w-dependent functions are

$$\mathcal{T}_{AA}^{cs1\pm} = -\frac{N_C}{24}\frac{m_\mu^2}{m_{\tilde{\nu}_\mu}^2}\frac{m_i}{m_i \mp m_j}\left[\mathcal{F}_1^C(C_i) + \mathcal{F}_1^C(C_j, C_i)\right] + (i \leftrightarrow j), \tag{4.26a}$$

$$\mathcal{T}_{AA}^{cs2\pm} = \frac{N_C}{24}\frac{m_\mu^2}{m_{\tilde{\nu}_\mu}^2}\frac{m_i}{m_i \mp m_j}\frac{1}{C_{f'\tilde{f}_k} - C_i} \tag{4.26b}$$
$$\times \left[\mathcal{F}_1^C(C_i) - \mathcal{F}_1^C(C_{f'\tilde{f}_k}, C_i) - \mathcal{F}_1^C(C_j, C_{f'\tilde{f}_k}) + \mathcal{F}_1^C(C_j, C_i)\right] + (i \leftrightarrow j),$$

$$\mathcal{T}_{AB}^{cs1\pm} = -\frac{N_C}{24}\frac{m_\mu^2}{m_{\tilde{\nu}_\mu}^2}m_{f'}\frac{1}{\pm m_i - m_j}\mathcal{F}_1^C(C_i) \pm (i \leftrightarrow j), \tag{4.26c}$$

$$\mathcal{T}_{AB}^{cs2\pm} = \frac{N_C}{24}\frac{m_\mu^2}{m_{\tilde{\nu}_\mu}^2}m_{f'}\frac{1}{\pm m_i - m_j}\frac{1}{C_{f'\tilde{f}_k} - C_i} \tag{4.26d}$$
$$\times \left[\mathcal{F}_1^C(C_i) - \mathcal{F}_1^C(C_{f'\tilde{f}_k}, C_i) - \mathcal{F}_1^C(C_j, C_{f'\tilde{f}_k}) + \mathcal{F}_1^C(C_j, C_i)\right] \pm (i \leftrightarrow j),$$

$$\mathcal{T}_{BA}^{cs1\pm} = -\frac{N_C}{12}\frac{m_\mu}{m_{\tilde{\nu}_\mu}^2}\frac{m_i}{m_i \mp m_j}$$
$$\times \left[2m_i\mathcal{F}_2^C(C_i) + (m_i \pm m_j)\mathcal{F}_2^C(C_j, C_i) - 6(m_i \mp m_j)\mathcal{F}_3^C(C_j, C_i)\right] \pm (i \leftrightarrow j), \tag{4.26e}$$

$$\mathcal{T}_{BA}^{cs2\pm} = -\frac{N_C}{12}\frac{m_\mu}{m_{\tilde{\nu}_\mu}^2}\frac{m_i}{m_i \mp m_j}\frac{1}{C_{f'\tilde{f}_k} - C_i}$$
$$\times \left[2m_i\left(-\mathcal{F}_2^C(C_i) + \mathcal{F}_2^C(C_{f'\tilde{f}_k}, C_i)\right) + (m_i \pm m_j)\left(\mathcal{F}_2^C(C_j, C_{f'\tilde{f}_k}) - \mathcal{F}_2^C(C_j, C_i)\right)\right.$$
$$\left. + 6(m_i \mp m_j)\left(\mathcal{F}_3^C(C_j, C_i) - \mathcal{F}_3^C(C_j, C_{f'\tilde{f}_k})\right)\right] + (i \leftrightarrow j), \tag{4.26f}$$

$$\mathcal{T}_{BB}^{cs1\pm} = -\frac{N_C}{6} \frac{m_\mu m_{f'}}{m_{\tilde{\nu}_\mu}^2} \frac{m_i}{\pm m_i - m_j} \mathcal{F}_2^{\mathrm{C}}(C_i) + (i \leftrightarrow j), \tag{4.26g}$$

$$\mathcal{T}_{BB}^{cs2\pm} = -\frac{N_C}{12} \frac{m_\mu m_{f'}}{m_{\tilde{\nu}_\mu}^2} \frac{1}{\pm m_i - m_j} \frac{1}{C_{f'\tilde{f}_k} - C_i}$$
$$\times \Big[2m_i \Big(-\mathcal{F}_2^{\mathrm{C}}(C_i) + \mathcal{F}_2^{\mathrm{C}}(C_{f'\tilde{f}_k}, C_i) \Big) + (m_i \pm m_j) \Big(\mathcal{F}_2^{\mathrm{C}}(C_j, C_{f'\tilde{f}_k}) - \mathcal{F}_2^{\mathrm{C}}(C_j, C_i) \Big)$$
$$+ 6(m_i \mp m_j) \Big(\mathcal{F}_3^{\mathrm{C}}(C_j, C_i) - \mathcal{F}_3^{\mathrm{C}}(C_j, C_{f'\tilde{f}_k}) \Big) \Big] + (i \leftrightarrow j).$$

5 Overview of input parameters and benchmark scenarios

In the remaining three sections the phenomenological behaviour of the results is discussed. The present section gives an overview of the input parameters and useful benchmark parameter scenarios; then a compact approximation is provided, and finally the parameter dependence of the fermion/sfermion-loop contributions to a_μ is analyzed in detail.

The fermion/sfermion-loop contributions to a_μ depend on the following fifteen parameters.

- One-loop parameters:

$$\mu, M_1, M_2, M_E, M_L, \tan\beta. \tag{5.1}$$

Of course, all parameters of the one-loop SUSY contributions appear again.

- Two-loop sfermion-mass parameters appearing in the inner loop:

$$M_U, M_D, M_Q, M_{U3}, M_{D3}, M_{Q3}, M_{E3}, M_{L3}. \tag{5.2}$$

The additional sensitivity on these sfermion masses of all generations is one of the most important properties of the fermion/sfermion-loop contributions. For simplicity, the sfermion-mass parameters of the first two generations are set equal; hence the first-generation slepton masses do not appear as free parameters here.

- Stop A-parameter:

$$A_t. \tag{5.3}$$

All other A-parameters appear only multiplied with small fermion masses and are neglected.

In our analysis all parameters are considered to be real quantities, and generation mixing is neglected. SM input parameters are defined as in ref. [87]:

$$M_W = (80.385 \pm 0.015)\,\mathrm{GeV}, \qquad m_t = (173.5 \pm 0.6 \pm 0.8)\,\mathrm{GeV},$$
$$M_Z = (91.1876 \pm 0.0021)\,\mathrm{GeV}, \quad m_\mu = (105.6583715 \pm 0.0000035)\,\mathrm{MeV}. \tag{5.4}$$

Since we define $\tan\beta$ in the $\overline{\mathrm{DR}}$ renormalization scheme, the final result also depends on the scale μ_{DRED}, which we always set to the SPS1a value $\mu_{\mathrm{DRED}} = 454.7\,\mathrm{GeV}$ [88].

	BM1	BM2	BM3	BM4
μ[GeV]	350	1300	4000	-160
$\tan\beta$	40	40	40	50
M_1[GeV]	150	150	150	140
M_2[GeV]	300	300	300	2000
M_E[GeV]	400	400	400	200
M_L[GeV]	400	400	400	2000
$a_\mu^{\mathrm{1L\,SUSY}}[10^{-10}]$	44.02	26.95	46.78	15.98

Table 1. Definition of the benchmark points; see also ref. [25]. In BM1, all one-loop masses are similar; in BM2, the μ-parameter is increased by a factor 4. In BM3, the μ-parameter is very large and the bino-exchange contribution dominates. In BM4, the contribution from the right-handed smuon dominates.

In the following numerical discussions, the benchmark points for the one-loop parameters, introduced in ref. [25] and defined in table 1, are used repeatedly. They characterize qualitatively different regions of the one-loop parameter space, where the one-loop result is dominated by different mass-insertion diagrams (see refs. [27, 45, 47]).

- BM1: all one-loop masses are similar; the one-loop contribution to a_μ is dominated by the chargino mass-insertion diagram $a_\mu^{1L}(\tilde{W}-\tilde{H}, \tilde{\nu}_\mu)$ with wino-Higgsino exchange.

- BM2: the μ-parameter is increased by a factor ~ 4. The one-loop chargino contribution $a_\mu^{1L}(\tilde{W}-\tilde{H}, \tilde{\nu}_\mu)$ and the bino-exchange contribution $a_\mu^{1L}(\tilde{B}, \tilde{\mu}_L-\tilde{\mu}_R)$ are similar. The well-known benchmark point SPS1a [88] has a similar characteristic.

- BM3: the μ-parameter is very large. All one-loop contributions involving higgsinos are suppressed, and the bino-exchange contribution $a_\mu^{1L}(\tilde{B}, \tilde{\mu}_L-\tilde{\mu}_R)$ dominates. Parameter scenarios with this characteristic have been studied extensively also in refs. [30, 38] recently.

- BM4: the parameters are chosen such that the right-handed smuon contribution $a_\mu^{1L}(\tilde{B}-\tilde{H}, \tilde{\mu}_R)$ dominates: M_2 and M_L are heavy, and the other three one-loop mass parameters are light. The μ-parameter is negative to allow for a positive contribution to a_μ. Parameter scenarios with this characteristic have been studied recently also in ref. [89].

6 Leading logarithmic approximation

As a first step of the numerical discussion, a very compact approximate formula is provided. It can be easily implemented, and it captures many features of the qualitative and quantitative behaviour of the exact result. The approximation is based on the leading logarithms of the result.

As discussed in ref. [25], the fermion/sfermion-loop contributions are logarithmically enhanced if the sfermions in the inner loop become heavy. This non-decoupling behaviour can be understood in an effective field theory. If heavy sfermions are integrated out, the effective field theory is not supersymmetric anymore, and gaugino and higgsino couplings can differ from the corresponding gauge and Yukawa couplings.

Based on this idea, we start from the one-loop result, approximated by mass-insertion diagrams, see refs. [27, 45, 47].[4] In the form given in ref. [47] the approximation reads

$$a_\mu^{\text{1L SUSY,M.I.}} = a_\mu^{\text{1L}}(\tilde{W}\text{--}\tilde{H}, \tilde{\nu}_\mu) + a_\mu^{\text{1L}}(\tilde{W}\text{--}\tilde{H}, \tilde{\mu}_L) + a_\mu^{\text{1L}}(\tilde{B}\text{--}\tilde{H}, \tilde{\mu}_L)$$
$$+ a_\mu^{\text{1L}}(\tilde{B}\text{--}\tilde{H}, \tilde{\mu}_R) + a_\mu^{\text{1L}}(\tilde{B}, \tilde{\mu}_L\text{--}\tilde{\mu}_R), \tag{6.1}$$

with

$$a_\mu^{\text{1L}}(\tilde{W}\text{--}\tilde{H}, \tilde{\nu}_\mu) = \frac{g_2^2}{8\pi^2} \frac{m_\mu^2 M_2}{m_{\tilde{\nu}_\mu}^4} \mu \tan\beta \, F_a\left(\frac{M_2^2}{m_{\tilde{\nu}_\mu}^2}, \frac{\mu^2}{m_{\tilde{\nu}_\mu}^2}\right), \tag{6.2a}$$

$$a_\mu^{\text{1L}}(\tilde{W}\text{--}\tilde{H}, \tilde{\mu}_L) = -\frac{g_2^2}{16\pi^2} \frac{m_\mu^2 M_2}{M_{L2}^4} \mu \tan\beta \, F_b\left(\frac{M_2^2}{M_{L2}^2}, \frac{\mu^2}{M_{L2}^2}\right), \tag{6.2b}$$

$$a_\mu^{\text{1L}}(\tilde{B}\text{--}\tilde{H}, \tilde{\mu}_L) = \frac{g_1^2}{16\pi^2} \frac{m_\mu^2 M_1}{M_{L2}^4} \mu \tan\beta \, F_b\left(\frac{M_1^2}{M_{L2}^2}, \frac{\mu^2}{M_{L2}^2}\right), \tag{6.2c}$$

$$a_\mu^{\text{1L}}(\tilde{B}\text{--}\tilde{H}, \tilde{\mu}_R) = -\frac{g_1^2}{8\pi^2} \frac{m_\mu^2 M_1}{M_{E2}^4} \mu \tan\beta \, F_b\left(\frac{M_1^2}{M_{E2}^2}, \frac{\mu^2}{M_{E2}^2}\right), \tag{6.2d}$$

$$a_\mu^{\text{1L}}(\tilde{B}, \tilde{\mu}_L\text{--}\tilde{\mu}_R) = \frac{g_1^2}{8\pi^2} \frac{m_\mu^2}{M_1^3} \mu \tan\beta \, F_b\left(\frac{M_{L2}^2}{M_1^2}, \frac{M_{E2}^2}{M_1^2}\right). \tag{6.2e}$$

The loop functions appearing here are defined as

$$F_a(x, y) = -\frac{G_3(x) - G_3(y)}{x - y}, \tag{6.3a}$$

$$F_b(x, y) = -\frac{G_4(x) - G_4(y)}{x - y}, \tag{6.3b}$$

with

$$G_3(x) = \frac{1}{2(x-1)^3}\Big[(x-1)(x-3) + 2\log x\Big], \tag{6.4a}$$

$$G_4(x) = \frac{1}{2(x-1)^3}\Big[(x-1)(x+1) - 2x\log x\Big]. \tag{6.4b}$$

---

[4]Note that we only use $a_\mu^{\text{1L SUSY,M.I.}}$ and the definitions of eq. (6.2) as building blocks in an approximation of the two-loop results. They should not be used in a precision evaluation of the SUSY one-loop contributions, since the error can be significant.

In terms of these expressions, the leading logarithmic approximation of the fermion/sfermion two-loop contributions, $a_\mu^{2\mathrm{L},f\tilde{f}\,\mathrm{LL}}$, is given by

$$
\begin{aligned}
a_\mu^{2\mathrm{L},f\tilde{f}\,\mathrm{LL}} = {}& a_\mu^{1\mathrm{L}}(\tilde{W}\text{–}\tilde{H}, \tilde{\nu}_\mu)\left(\Delta_{g_2} + \Delta_{\tilde{H}} + \Delta_{\tilde{W}\tilde{H}} + \Delta_{t_\beta} + 0.015\right), \\
& + a_\mu^{1\mathrm{L}}(\tilde{W}\text{–}\tilde{H}, \tilde{\mu}_L)\left(\Delta_{g_2} + \Delta_{\tilde{H}} + \Delta_{\tilde{W}\tilde{H}} + \Delta_{t_\beta} + 0.015\right), \\
& + a_\mu^{1\mathrm{L}}(\tilde{B}\text{–}\tilde{H}, \tilde{\mu}_L)\left(\Delta_{g_1} + \Delta_{\tilde{H}} + \Delta_{\tilde{B}\tilde{H}} + \Delta_{t_\beta} + 0.015\right), \qquad (6.5) \\
& + a_\mu^{1\mathrm{L}}(\tilde{B}\text{–}\tilde{H}, \tilde{\mu}_R)\left(\Delta_{g_1} + \Delta_{\tilde{H}} + \Delta_{\tilde{B}\tilde{H}} + \Delta_{t_\beta} + 0.04\right), \\
& + a_\mu^{1\mathrm{L}}(\tilde{B}, \tilde{\mu}_L\text{–}\tilde{\mu}_R)\left(\Delta_{g_1} + \Delta_{t_\beta} + 0.03\right).
\end{aligned}
$$

The shifts Δ_{g_1}, Δ_{g_2}, $\Delta_{\tilde{H}}$, $\Delta_{\tilde{B}\tilde{H}}$, $\Delta_{\tilde{W}\tilde{H}}$ and Δ_{t_β} are defined as follows:

$$
\begin{aligned}
\Delta_{g_1} = {}& \frac{g_1^2}{16\pi^2}\frac{4}{3}\bigg(\frac{8}{3}\log\frac{M_U}{m_{\mathrm{SUSY}}} + \frac{4}{3}\log\frac{M_{U3}}{m_{\mathrm{SUSY}}} + \frac{2}{3}\log\frac{M_D}{m_{\mathrm{SUSY}}} + \frac{1}{3}\log\frac{M_{D3}}{m_{\mathrm{SUSY}}} \\
& \qquad + \frac{1}{3}\log\frac{M_Q}{m_{\mathrm{SUSY}}} + \frac{1}{6}\log\frac{M_{Q3}}{m_{\mathrm{SUSY}}} + \log\frac{M_{E3}}{m_{\mathrm{SUSY}}} + \frac{1}{2}\log\frac{M_{L3}}{m_{\mathrm{SUSY}}}\bigg), \qquad (6.6\text{a})
\end{aligned}
$$

$$
\Delta_{g_2} = \frac{g_2^2}{16\pi^2}\frac{4}{3}\left(3\log\frac{M_Q}{m_{\mathrm{SUSY}}} + \frac{3}{2}\log\frac{M_{Q3}}{m_{\mathrm{SUSY}}} + \frac{1}{2}\log\frac{M_{L3}}{m_{\mathrm{SUSY}}}\right), \qquad (6.6\text{b})
$$

$$
\begin{aligned}
\Delta_{\tilde{H}} = {}& \frac{1}{16\pi^2}\frac{1}{2}\bigg(3y_t^2\log\frac{M_{U3}}{m_{\mathrm{SUSY}}} + 3y_b^2\log\frac{M_{D3}}{m_{\mathrm{SUSY}}} + 3(y_t^2+y_b^2)\log\frac{M_{Q3}}{m_{\mathrm{SUSY}}} \\
& \qquad + y_\tau^2\log\frac{M_{E3}}{m_{\mathrm{SUSY}}} + y_\tau^2\log\frac{M_{L3}}{m_{\mathrm{SUSY}}}\bigg), \qquad (6.6\text{c})
\end{aligned}
$$

$$
\Delta_{\tilde{B}\tilde{H}} = \frac{1}{16\pi^2}y_t^2\left(2\log\frac{M_{Q3}}{m_{\mathrm{SUSY}}} - 8\log\frac{M_{U3}}{m_{\mathrm{SUSY}}}\right), \qquad (6.6\text{d})
$$

$$
\Delta_{\tilde{W}\tilde{H}} = \frac{1}{16\pi^2}y_t^2\left(-6\log\frac{M_{Q3}}{m_{\mathrm{SUSY}}}\right), \qquad (6.6\text{e})
$$

$$
\Delta_{t_\beta} = \frac{1}{16\pi^2}(3y_b^2 - 3y_t^2 + y_\tau^2)\log\frac{\mu_{\mathrm{DRED}}}{m_{\mathrm{SUSY}}}, \qquad (6.6\text{f})
$$

where $m_{\mathrm{SUSY}} = \min(|\mu|, |M_1|, |M_2|, M_{L2}, M_{E2})$. The gauge and Yukawa coupling constants in the coefficients are given in eq. (2.6).

Here, Δ_{g_1} and Δ_{g_2} are effective shifts to the gaugino couplings of the bino and wino, respectively. The logarithms of the inner sfermion masses appear weighted with the respective squared gauge couplings. $\Delta_{\tilde{H}}$ corresponds to the higgsino self energies and contains logarithms multiplied with squared Yukawa couplings. Here, the 1st and 2nd generation Yukawa couplings are neglected. $\Delta_{\tilde{B}\tilde{H}}$ and $\Delta_{\tilde{W}\tilde{H}}$ correspond to effective $\tilde{B}$–$\tilde{H}$ and $\tilde{W}$–$\tilde{H}$ transitions generated by fermion/sfermion loops. Δ_{t_β} arises from $\overline{\mathrm{DR}}$ renormalization of $\tan\beta$ and contains μ_{DRED}. The non-logarithmic numerical constants appearing in eq. (6.5) approximate the typical magnitude of the additional non-logarithmic contributions. They have been obtained by fitting eq. (6.5) to the exact result for the data points shown in figure 13.

We briefly summarize the terms which are neglected by this approximation and state criteria when the approximation is expected to fail.

	BM1	BM2	BM3	BM4
$a_\mu^{\mathrm{1L\,SUSY}}[10^{-10}]$	44.02	26.95	46.78	15.98
$a_\mu^{\mathrm{1L\,SUSY,M.I.}}[10^{-10}]$	44.69	27.25	47.41	17.59
$r = a_\mu^{2\mathrm{L},f\tilde{f}}/a_\mu^{\mathrm{1L\,SUSY}}$	0.041	0.045	0.047	0.049
$r_{\mathrm{LL}} = a_\mu^{2\mathrm{L},f\tilde{f}\,\mathrm{LL}}/a_\mu^{\mathrm{1L\,SUSY}}$	0.040	0.043	0.047	0.053

Table 2. Comparison of exact results and corresponding approximation formulas. The first and the third line are taken from ref. [25].
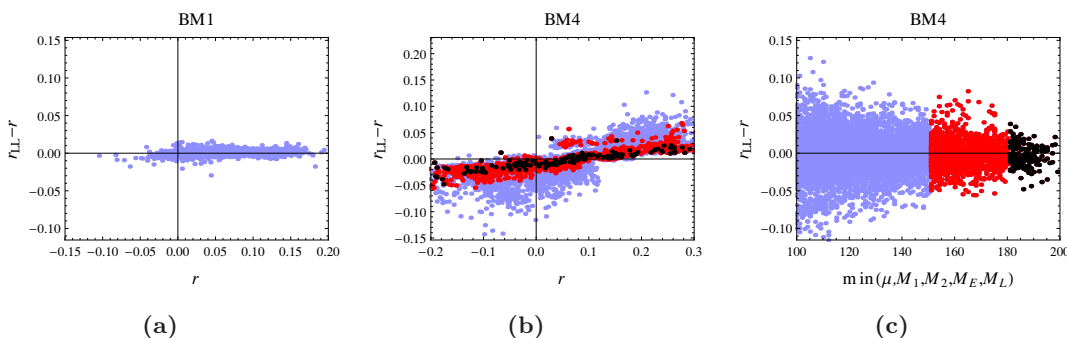
Figure 13. The exact result for $r \equiv a_\mu^{2\mathrm{L},f\tilde{f}}/a_\mu^{\mathrm{1L\,SUSY}}$ compared with the approximation expressed as $r_{\mathrm{LL}} \equiv a_\mu^{2\mathrm{L},f\tilde{f}\,\mathrm{LL}}/a_\mu^{\mathrm{1L\,SUSY}}$. The mass parameters are chosen randomly around the benchmark points BM1 and BM4, with the ranges given in table 3. The first and second figure show $r_{\mathrm{LL}} - r$ as a function of r, the third figure shows $r_{\mathrm{LL}} - r$ as a function of the minimum SUSY mass $\min(|\mu|, |M_1|, |M_2|, M_E, M_L)$. The light blue points correspond to the same data points as the ones used for figure 5 of ref. [25], the red (black) points to a minimum SUSY mass bigger than 150 (180) GeV.

- Already the one-loop approximation in eqs. (6.2) neglects terms with a relative suppression of the orders $\mathcal{O}(1/\tan\beta)$ and $\mathcal{O}(M_Z^2/M_{\mathrm{SUSY}}^2)$, where M_{SUSY} denotes the relevant SUSY masses appearing at the one-loop level. Hence, the two-loop approximation becomes invalid if $\tan\beta$ or M_{SUSY} become too small.

- The dependence on the inner sfermion masses beyond leading logarithms, in particular the behaviour for small inner sfermion masses and large mixing, is neglected. Furthermore, the dependence on all one-loop parameters μ, M_1, M_2, M_L, M_E and $\tan\beta$ (beyond the one-loop dependence) is neglected and replaced by the numerical constants in eq. (6.5).

We have verified that the approximation is in good agreement with the results for the benchmark points BM1...BM4 from ref. [25].[5] Table 2 shows a comparison of the results

---

[5]Some of the benchmark points involve equal mass parameters, $M_E = M_L$, $M_2 = M_L$. A direct evaluation of the approximation formulas for these benchmark points would suffer from the artificial singularities of the loop functions $F_a(x,y)$ and $F_b(x,y)$ for $x = y$. These are avoided in the numerical evaluation of the approximations in table 2 by shifting the mass parameters of the benchmark points in a numerically

	BM1	BM4
μ[GeV]	$[100, 200]$	$[-200, -100]$
$\tan \beta$	40	50
M_1[GeV]	$[100, 200]$	$[100, 200]$
M_2[GeV]	$[200, 400]$	$[1000, 3000]$
M_E[GeV]	$[200, 500]$	$[100, 300]$
M_L[GeV]	$[200, 500]$	$[1000, 3000]$

Table 3. Scan intervals for the least restrictive light blue parameter regions of figure 13.

from ref. [25] (repeated in the first and third line) with the corresponding one-loop and leading log approximations (second and fourth line). Also, all entries of table 3 of ref. [25] are reproduced well, except for the coefficient of $\log(M_{U3})$ in the case of BM4. The reason is that BM4 has very small SUSY masses, so it is outside the region of approximation validity. Figure 13 quantifies how well the approximation works. It compares the approximate results with the exact ones, normalized to the one-loop result, for a random set of parameters. The same data set as for figure 5 of ref. [25] has been used, see table 3 for the one-loop masses; the other eight sfermion-mass parameters appearing in the inner loop are varied in the range $[10^3, 10^6]$ GeV.

The scatter plot around BM1, figure 13(a), shows an almost perfect agreement between approximate and exact results. For almost all data points, the difference is at most 1% of the one-loop result. Hence, the approximation represents a significant improvement compared to the fit formula given in ref. [25] with fixed coefficients of the logarithms.

For the scatter plot around BM4, figure 13(b), the improvement compared to the fit formula of ref. [25] is only marginal. This is due to the smallness of the SUSY masses in these data points. The blue/red/black points in figure 13(b) are the points for which the minimum SUSY mass is $\geq 100/150/180$GeV, respectively. Figure 13(c) shows the same data points as a function of the minimum SUSY mass. The figures confirm that the approximation quickly improves as the ratio M_{SUSY}/M_Z increases.

7   Numerical analysis

In this section the parameter dependence of the fermion/sfermion-loop contributions to a_μ is analyzed in detail. To begin with, we recall that the fifteen relevant parameters can be devided into one-loop parameters, two-loop sfermion-mass parameters for the inner loops, and the stop A-parameter, see section 5:

$$\mu, M_1, M_2, M_E, M_L, \tan \beta,$$
$$M_U, M_D, M_Q, M_{U3}, M_{D3}, M_{Q3}, M_{E3}, M_{L3},$$
$$A_t.$$

---

insignificant way, but such that all mass parameters are different. Note that this problem is not present in the exact result.

As stated above, the additional sensitivity on the sfermion masses of all generations is a distinctive feature of the fermion/sfermion-loop contributions.

The dependence on all parameters is studied systematically, starting with the region of large two-loop sfermion masses, where the leading logarithmic approximation of section 6 is valid. Then, the focus is set on smaller inner sfermion masses and the influence of stop mixing.

We also briefly recall the benchmark points for the one-loop parameters, introduced in ref. [25] and in section 5, table 1. They characterize qualitatively different regions of the one-loop parameter space, in particular, BM1 is a point where all one-loop masses are similar. BM3 is a point where the bino-exchange contribution strongly dominates, and BM4 is a point where the right-handed smuon contribution dominates.

7.1 Parameter region of the leading logarithmic approximation

The leading logarithmic behaviour has been studied extensively in ref. [25], and it can be well understood from the approximation $a_\mu^{2\mathrm{L}, f\tilde{f}\,\mathrm{LL}}$ in section 6. The approximation is expected to be valid if the hierarchy (2-loop sfermion masses) $\gg$ (1-loop masses) $\gg M_Z$ holds. In practice it is already good for one-loop masses above around $200\,\mathrm{GeV}$ and two-loop masses around $1\,\mathrm{TeV}$, as shown in figure 13.

The largest two-loop contributions can arise from the correction factors $\Delta_{\tilde{W}\tilde{H}}$ and $\Delta_{\tilde{B}\tilde{H}}$, which contain the logarithms of M_{U3} and M_{Q3} multiplied with the top-Yukawa coupling and large prefactors. These large logarithms are effective if the one-loop contribution is dominated by $a_\mu^{1\mathrm{L}}(\tilde{W}-\tilde{H}, \tilde{\nu}_\mu)$ or $a_\mu^{1\mathrm{L}}(\tilde{B}-\tilde{H}, \tilde{\mu}_R)$, as in BM1 or BM4. In these cases, the logarithms can drive the two-loop corrections up to 15% (30%) of the one-loop contributions for two-loop masses in the $20\,\mathrm{TeV}$ ($1000\,\mathrm{TeV}$) range.

On the other hand, in the case that $a_\mu^{1\mathrm{L}}(\tilde{B}, \tilde{\mu}_L-\tilde{\mu}_R)$ dominates at the one-loop level, as in BM3, the two-loop corrections are smaller since the leading logarithms are suppressed by the small gauge coupling g_1^2. In this case, the two-loop corrections remain below 10% of the one-loop contributions for two-loop masses up to $1000\,\mathrm{TeV}$. The parameter region where $a_\mu^{1\mathrm{L}}(\tilde{B}, \tilde{\mu}_L-\tilde{\mu}_R)$ dominates has also been investigated in ref. [38]. There, analytical results have been given for the leading logarithm if not only sfermion masses but also the wino and higgsino masses M_2 and μ are set to a common, very large scale.

7.2 Decomposition of contributions

To deepen the understanding of the fermion/sfermion-loop corrections, we now show how the full result is decomposed into the individual two-loop and counterterm contributions. The parameters are still chosen such that the leading logarithmic approximation $a_\mu^{2\mathrm{L}, f\tilde{f}\,\mathrm{LL}}$ in section 6 is valid. Figure 14 shows two such parameter scenarios, considered already in ref. [25]. In both panels, the upper half shows the full result for the fermion/sfermion-loop corrections, and the lower half shows the following individual contributions:

- $BA(\tilde{\chi}^\pm), BA(\tilde{\chi}^0)$: all genuine chargino/neutralino two-loop contributions with coupling combination $\mathcal{BA}$, as given in section 4. These contributions are $\tan\beta$-enhanced
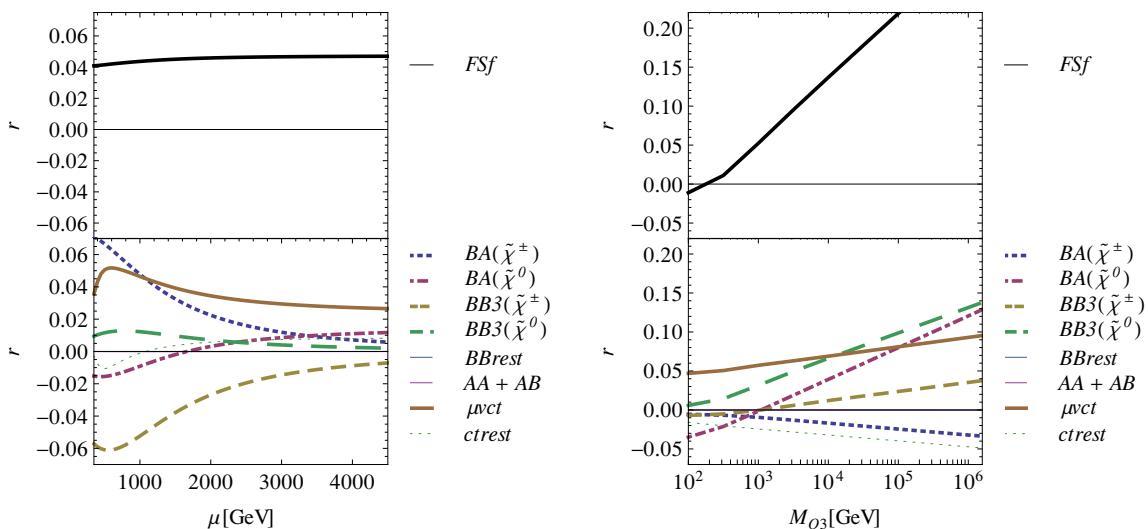
Figure 14. Full result $r \equiv a_\mu^{2\text{L}, f\tilde{f}} / a_\mu^{1\text{L SUSY}}$ and individual contributions as defined in section 7.2, for two different scenarios. Left: one-loop parameters as in BM1, BM2, BM3 except that μ is varied, and $M_{U,D,Q,U3,D3,Q3} = 7$ TeV, $M_{E3,L3} = 3$ TeV. Right: one-loop parameters as in BM4, two-loop parameters as before, except that $M_{U3} = 1$ TeV and M_{Q3} is varied.

due to the couplings $\mathcal{B}$ of the outer loop. They do not involve an explicit factor of the inner fermion mass.

- $BB3(\tilde{\chi}^\pm), BB3(\tilde{\chi}^0)$: all genuine chargino/neutralino two-loop contributions with couplings $\mathcal{BB}$, but only from third generation fermion/sfermion pairs. These are $\tan\beta$-enhanced and proportional to the mass of the inner fermion, due to the coupling combination $\mathcal{B}$ of the inner loop.

- $BBrest$: all remaining contributions of the type $\mathcal{BB}$. These contributions are suppressed by a factor of the first or second generation fermion from the inner loop.

- $AA + AB$: all genuine two-loop contributions involving the coupling combinations $\mathcal{AA}$ or $\mathcal{AB}$. These are not $\tan\beta$-enhanced and expected to be small.

- μvct: all counterterm contributions from the external muon vertex, i.e. of the classes (μnv) and (μcv). These counterterms are individually finite, contain $\Delta\rho$, and are the only contributions which involve pure fermion and pure sfermion loops.

- $ctrest$: all remaining counterterm contributions.

The parameters of figure 14 are chosen as follows: in the left panel, the one-loop parameters are set as in BM1, BM2, BM3 except that μ is varied. The sfermion masses are set to $M_{U,D,Q,U3,D3,Q3} = 7$ TeV and $M_{E3,L3} = 3$ TeV (see table 2 of ref. [25]). In the right panel, the one-loop parameters are set as in BM4, the two-loop parameters as before, except that $M_{U3} = 1$ TeV and M_{Q3} is varied (see figure 6 of ref. [25]).

The full result in the left panel is always around 4%, in agreement with the result of ref. [25], and this result is well described by the leading logarithmic approximation of
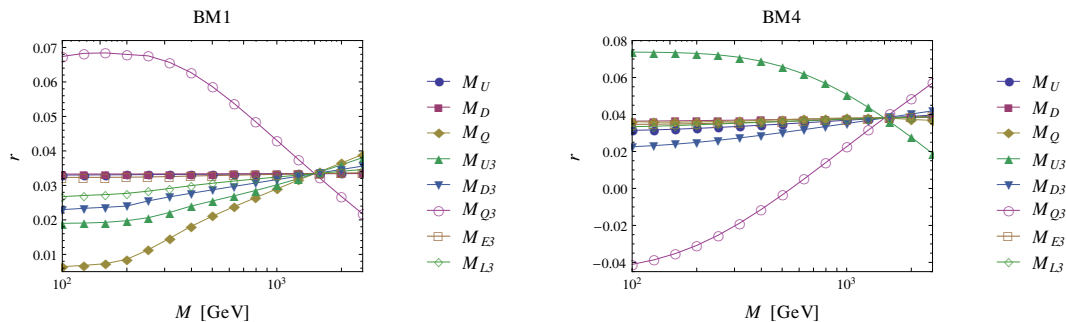
Figure 15. Relative correction $r \equiv a_\mu^{2\mathrm{L}, f\tilde{f}}/a_\mu^{1\mathrm{L}\,\mathrm{SUSY}}$ from fermion/sfermion loops for the benchmark points BM1 and BM4 as a function of each sfermion mass parameter. One sfermion mass is varied at a time; the remaining sfermion masses are set to $1.5\,\mathrm{TeV}$, and $A_t = 0$.

section 6. Among the contributions listed above, only BA, $BB3$, and the counterterms are sizeable. This is expected, as discussed above. For small values of μ, many individual contributions are large and there are strong cancellations. For larger μ, in the BM2 and BM3 region, the $a_\mu^{1\mathrm{L}}(\tilde{B}, \tilde{\mu}_L - \tilde{\mu}_R)$ one-loop contribution becomes dominant. All two-loop corrections are therefore governed by the small gauge coupling g_1^2, and the individual two-loop contributions become smaller. For all μ, the muon-vertex counterterms μvct almost account for the full result.

In the right figure the muon-vertex counterterms do not dominate the full result. Since in the scenario of BM4 the bino-higgsino exchange is most important, the neutralino contributions of the type $BA(\tilde{\chi}^0)$ and $BB3(\tilde{\chi}^0)$ are most important. They rise logarithmically, while the chargino contributions are much smaller and cancel each other to a large extent.

7.3 Behaviour for small inner sfermion masses

Figure 15 shows the general behaviour of $a_\mu^{2\mathrm{L}, f\tilde{f}}$ if one of the inner sfermion masses is varied at a time in the range $100 \ldots 2500\,\mathrm{GeV}$ and can be viewed as an extension of figure 4 of ref. [25] to smaller sfermion masses. Since the approximation of section 6 cannot be expected to be valid over the whole mass range, figure 15 quantifies when and to what extent the exact dependence on the inner sfermion masses differs from a purely logarithmic one. In the left (right) panel of figure 15 the one-loop parameters are set to the values of benchmark point BM1 (BM4). The inner sfermion masses are set to $1.5\,\mathrm{TeV}$ as a standard value and all A-parameters are set to zero.

Both plots show the familiar logarithmic dependence on the inner sfermion masses, as long as the masses remain sufficiently large. For inner sfermion masses below $500\,\mathrm{GeV}$ the contributions saturate, and the difference between the leading logarithmic approximation and the exact result can be quite sizeable.

The mass scale of $500\,\mathrm{GeV}$ can be compared with the typical mass scale of the one-loop parameters in BM1 and BM4, which is $300\,\mathrm{GeV}$ and $200\,\mathrm{GeV}$, respectively. Generally, therefore, the leading logarithmic approximation can be expected to work well only as long as the inner sfermion masses are at least twice as large as the one-loop masses in the outer
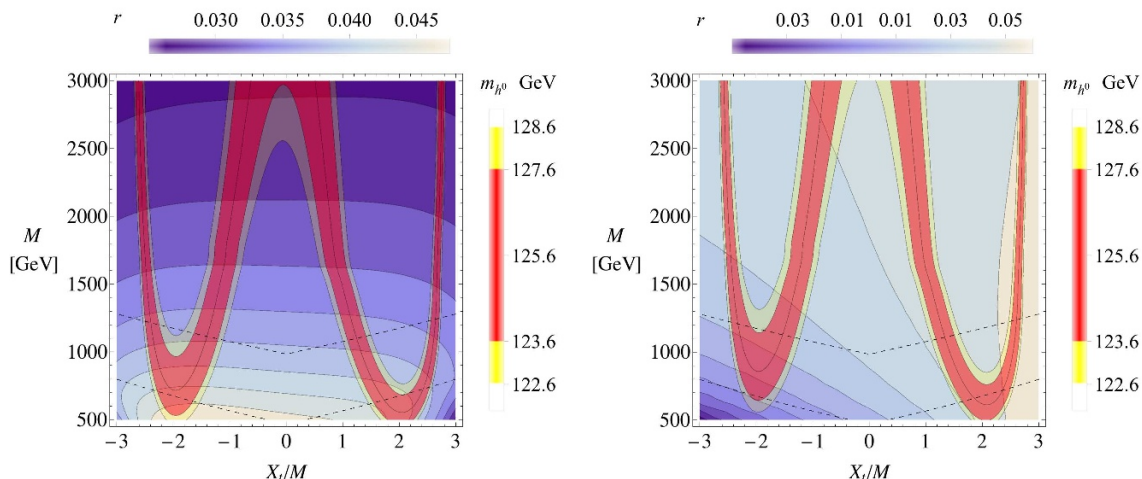
Figure 16. The dependence of $r \equiv a_\mu^{2\text{L},f\tilde{f}}/a_\mu^{1\text{L SUSY}}$ on $M \equiv M_{Q3} = M_{U3} = M_{D3}$ and the ratio X_t/M. All other squark and the third generation slepton masses are set to 1.5 TeV. The one-loop parameters are set to the values of BM1 in the left and of BM4 in the right panel. The red and yellow bands indicate the mass of the lightest Higgs boson. The dashed lines depict the thresholds for a lighter stop mass of 500 GeV or 1 TeV.

loop. For smaller inner sfermion masses, the exact result can be expected to be smaller than the approximated one.

7.4 Dependence on stop mixing

The discovery of a Higgs-like particle at the LHC constrains the allowed parameter space of the MSSM. If stop mixing is not allowed, i.e. $A_t = 0$, its rather high mass can be accomodated only by very heavy stops with a mass of several TeV. In contrast, a non-zero mixing allows for stop masses below the TeV scale.

So far, all trilinear A-parameters were set to zero in the discussion of $a_\mu^{2\text{L},f\tilde{f}}$. Now, the influence of stop mixing, induced by $A_t \neq 0$, is studied. A_t and the associated stop-mixing parameter $X_t = (A_t - \mu^*/t_\beta)$ enter the calculation of a_μ at the two-loop level through the mixing matrices of the stops in the inner loop.

Figure 16 compares the influence of a normalized X_t on both $a_\mu^{2\text{L},f\tilde{f}}$ and the Higgs-boson mass. It shows contour plots in the plane of the universal SUSY breaking parameter $M \equiv M_{Q3} = M_{U3} = M_{D3}$ and X_t/M. Contours are drawn for both $a_\mu^{2\text{L},f\tilde{f}}/a_\mu^{1\text{L SUSY}}$ and m_{h^0}; the latter is computed using FeynHiggs [74, 90–92]. The dashed lines at the bottom depict the thresholds where the mass of the lighter stop falls below 500 GeV and 1 TeV, respectively. The input parameters besides M and X_t in figure 16 are chosen as $M_Q = M_U = M_D = M_{E3} = M_{L3} = 1.5$ TeV; the one-loop parameters are chosen as in benchmark points BM1 (left) and BM4 (right).

For the Higgs-boson mass we find the well-known dependence on X_t/M as an approximate fourth order polynomial. In particular the dependence is approximately symmetric for $X_t \leftrightarrow -X_t$. For $a_\mu^{2\text{L},f\tilde{f}}$, however, the dependence is approximately linear. In the case of BM4, X_t/M has a pronounced influence. Moving from $X_t/M = -2$ to $X_t/M = +2$
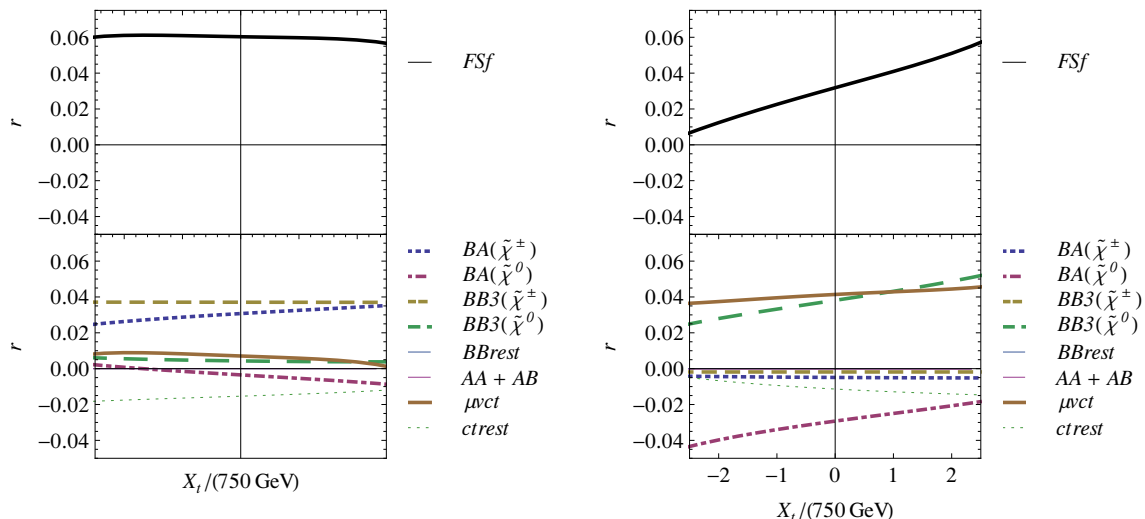
Figure 17. Full result $r \equiv a_\mu^{2\mathrm{L}, f\tilde{f}}/a_\mu^{1\mathrm{L\,SUSY}}$ and individual contributions as defined in section 7.2, for the scenarios of figure 16, but with fixed $M = 750\,\mathrm{GeV}$.

changes the a_μ correction from 1% to 5% at $M = 750$ GeV, and by an even larger amount for smaller M. In the case of BM1, however, the influence of X_t is tiny.

Again, a deeper understanding of this behaviour can be obtained by considering the decomposition of contributions introduced in section 7.2. Figure 17 shows plots corresponding to the parameter choices of figure 16, but at fixed $M = 750$ GeV. The style is as in figure 14. In the left plot, based on BM1, wino-higgsino mass-insertion diagrams dominate. As a result, the BA-contributions of charginos and neutralinos (from stop/bottom and stop/top loops generating a wino-higgsino transition) have the strongest dependence on the mixing parameter. Accidentally these contributions cancel out to a large extent, and the full result is almost insensitive to the choice of X_t. In the right plot, based on BM4 with bino-higgsino dominance, only the BA and $BB3$ contributions of the neutralinos are important. Since they have positive slopes and add up constructively the full result is very sensitive to the mixing parameter.

These considerations also show that the behaviour found for BM1 and BM4 is typical for the behaviour in the larger parameter regions represented by these benchmark points.

7.5 Particular scenarios with extremely small SUSY masses

In the previous sections the behaviour of $a_\mu^{2\mathrm{L}, f\tilde{f}}$ has been studied in a quite generic way. Now, special parameter scenarios are considered in which particular SUSY masses can be very small, without violating experimental bounds. We focus on the following three cases:

- light stop and large stop-mass splitting, in the scenario of ref. [93]: this scenario fixes the stop sector in a particular way, such that the lighter stop mass is as small as the one-loop masses; we study $a_\mu^{2\mathrm{L}, f\tilde{f}}$ for several choices of the one-loop parameters.

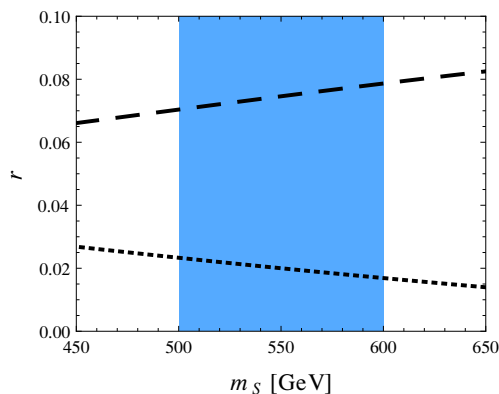- light stau scenario of ref. [94]: this scenario essentially fixes the two-loop parameters

Figure 18. Full result $r \equiv a_\mu^{2\text{L},f\tilde{f}}/a_\mu^{1\text{L SUSY}}$ for the scenario of ref. [93], $M_{U3} = 200\,\text{GeV}$, $A_t^2 = 6M_{U3}M_{Q3}$, as a function of $m_S = (m_{\tilde{t}_1}m_{\tilde{t}_2})^{1/2}$. The one-loop parameters are defined for slightly modified benchmark points BM1 (dotted) and BM4 (dashed), respectively.

for $a_\mu^{2\text{L},f\tilde{f}}$ as well as most one-loop parameters, such that both staus can be lighter than the one-loop masses.

- light smuon, chargino and neutralino masses and extremely small $\tan\beta$, in the scenario of ref. [95]: this scenario fixes all one-loop parameters, such that none of the usual hierarchies ($\tan\beta \gg 1$, $M_{\text{SUSY}} \gg M_Z$) is valid; we study the dependence on the two-loop parameters.

Light stop scenario: In ref. [93], arguments are put forward in favour of a very light right-handed stop with almost degenerate neutralino, together with large A_t and a heavier left-handed stop. This parameter choice is of interest for $a_\mu^{2\text{L},f\tilde{f}}$ since a large left/right stop-mass splitting can lead to particularly large logarithmic corrections. However, the scenario of ref. [93] differs from the scenarios considered so far in the present paper or in ref. [25], because it combines large stop-mass splitting with large stop mixing, and because one stop is so light that the leading logarithmic approximation cannot be expected to be valid.

Figure 18 shows the result for $r \equiv a_\mu^{2\text{L},f\tilde{f}}/a_\mu^{1\text{L SUSY}}$ if the stop and neutralino parameters are chosen according to this scenario. According to ref. [93] the right-handed stop mass M_{U3} is set to $200\,\text{GeV}$, and M_{Q3} is varied such that the quantity $m_S = (m_{\tilde{t}_1}m_{\tilde{t}_2})^{1/2}$ is in the range $500\ldots600\,\text{GeV}$, depicted by the blue shaded area in figure 18. The trilinear mixing parameter is always set to $A_t^2 = 6M_{U3}M_{Q3} \approx 6m_S^2$. All remaining two-loop mass parameters equal $1.5\,\text{TeV}$. The one-loop parameters are not fixed by the scenario of ref. [93], except for the requirement that the lightest neutralino is $30\ldots40\,\text{GeV}$ lighter than the lightest stop. Hence we set the one-loop parameters to the values of either BM1 or BM4, with the modifications $M_1 = 178\,\text{GeV}$ (BM1-like scenario), $M_1 = 190\,\text{GeV}$ and $\mu = -220\,\text{GeV}$ (BM4-like scenario).

The results can be understood by comparing with figure 15, where $A_t = 0$. There, varying down the value of M_{U3} from $1.5\,\text{TeV}$ to $200\,\text{GeV}$ for BM1 leads to a relative
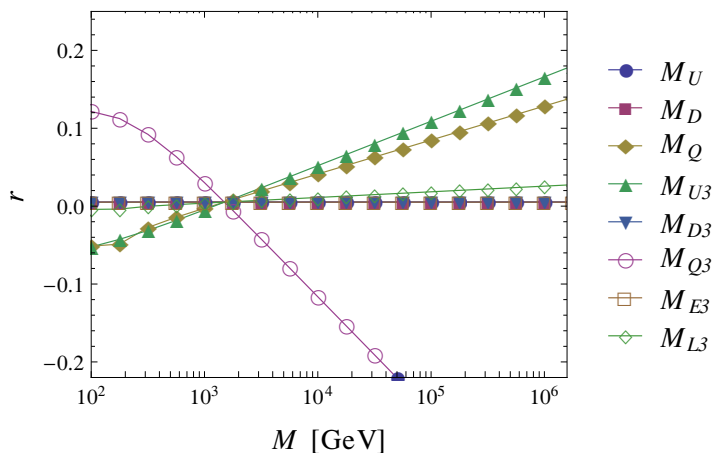
Figure 19. Relative correction $r \equiv a_\mu^{2L, f\tilde{f}}/a_\mu^{1L\,SUSY}$ as in figure 15, except that the one-loop parameters are set to the scenario of ref. [95] with light one-loop masses, see eq. (7.6).

reduction of $r \equiv a_\mu^{2L, f\tilde{f}}/a_\mu^{1L\,SUSY}$ from $\approx 3\%$ to $\approx 2\%$ for BM1. In the BM4-like scenario the reduction of M_{U3} has an even larger impact on the final result and r increases from $\approx 4\%$ up to $\approx 7\%$. The large A_t present in figure 18 and the slightly different one-loop parameters do not significantly modify the result.

Light stau scenario: in ref. [94], benchmark scenarios for the MSSM Higgs sector are proposed which are in agreement with the most recent experimental data. One of them contains a very light stau. This scenario is of interest for the evaluation of $a_\mu^{2L, f\tilde{f}}$ since it constitutes an example where the sfermion mass in the inner loop can be lighter than the one-loop masses in the outer loop, i.e. the opposite of the situation in which the leading logarithmic approximation is valid.

According to ref. [94] we consider the following parameter choice:

$$\tan\beta = 25, \qquad \mu = 500\,\text{GeV}, \qquad M_2 = 200\,\text{GeV}, \qquad M_1 = 95.61\,\text{GeV}, \tag{7.1}$$

$$M_L = M_E = 400\,\text{GeV}, \qquad\qquad M_{L3} = M_{E3} = 245\,\text{GeV}, \tag{7.2}$$

$$M_{Q3} = M_{U3} = M_{D3} = 1\,\text{TeV}, \qquad A_t = A_b = 1620\,\text{GeV}. \tag{7.3}$$

All other sfermion mass parameters are set to 1.5 TeV. This leads to the following results for $a_\mu^{1L\,SUSY}$ and $r \equiv a_\mu^{2L, f\tilde{f}}/a_\mu^{1L\,SUSY}$:

$$a_\mu^{1L\,SUSY} = 26.25 \times 10^{-10}, \tag{7.4}$$

$$r = 0.0289. \tag{7.5}$$

The input parameters are similar to BM1, so the result can be compared to figure 15. In that figure, the BM1 result for r with very small stau masses is slightly below 0.03, like in eq. (7.5).

Light one-loop masses and small tanβ: In ref. [95] a scenario is considered where a chargino, a neutralino, a slepton and a sneutrino are all lighter than the Z boson, and it

is demonstrated that such a scenario cannot be ruled out by current experimental data. In that scenario $\tan\beta$ takes the very small value of $\tan\beta = 1.5$. For a_μ this scenario is interesting since all usual approximations are invalid: $\tan\beta$ is small, and the usually $\tan\beta$-suppressed terms become important; likewise, the approximation (1-loop masses) $\gg M_Z$ fails.

We consider the following parameter choice:

$$\tan\beta = 1.5, \quad \mu = 149\,\text{GeV}, \quad M_2 = 160\,\text{GeV}, \quad M_1 = 1\,\text{TeV},$$
$$M_L = 76\,\text{GeV}, \quad M_E = 1\,\text{TeV}, \tag{7.6}$$

which is similar to the choice made in ref. [95] but avoids the singularity for $\mu = M_2$ in the chargino-mass renormalization constants. This choice fixes all one-loop parameters and thus $a_\mu^{\text{1L SUSY}}$. The small masses, together with the small $\tan\beta$, lead to an interesting value in the ballpark of the deviation (1.1),

$$a_\mu^{\text{1L SUSY}} = 16.29 \times 10^{-10}. \tag{7.7}$$

The two-loop corrections can be large, too, as shown in figure 19. Like figure 15 it shows the two-loop corrections if one of the inner sfermion masses is varied at a time, while all others remain at the standard value of 1.5 TeV. If all inner sfermion masses are 1.5 TeV, the two-loop corrections accidentally cancel. But whenever either M_{Q3}, M_{U3}, or M_Q is varied away from 1.5 TeV, large corrections arise.

The pattern of the individual slopes in figure 19 is similar to the one in figure 15 for BM1, but the slopes are much larger. They cannot be predicted by the approximation of section 6 for the reasons mentioned above. Positive and negative corrections of around 10% are possible if the inner sfermion masses are in the sub-TeV or few-TeV region. For smaller inner sfermion masses, there is a slight saturation effect, but less pronounced compared to figure 15.

Because of the very peculiar nature of the parameter scenario eq. (7.6), it is instructive to consider again the decomposition of the contributions, as in section 7.2. Figure 20 shows two corresponding plots; the left one corresponds to the M_{U3} line, the right one to the M_{Q3} line of figure 19. Several features are noteworthy. First, in contrast to the previous cases, only $BB3(\tilde\chi^-)$, μvct and $ctrest$ are sizeable; all other contributions are very small. This observation is particularly interesting as $\tan\beta$ is very small, and the $\tan\beta$-suppressed $AA + AB$ contributions could have been expected to play a more important role. Furthermore, there is always a strong cancellation between $ctrest$ and the other contributions. In the left plot the M_{U3} dependence is dictated by the muon-vertex counterterms. All other contributions are almost insensitive to M_{U3}. In the right plot the situation is slighly different, and the full M_{Q3} dependence is governed by a combination of the $BB3(\tilde\chi^-)$, μvct and $ctrest$ contributions.

8 Conclusions

The calculation of the fermion/sfermion-loop contributions extends the known results of the MSSM two-loop contributions to a_μ in several important ways.
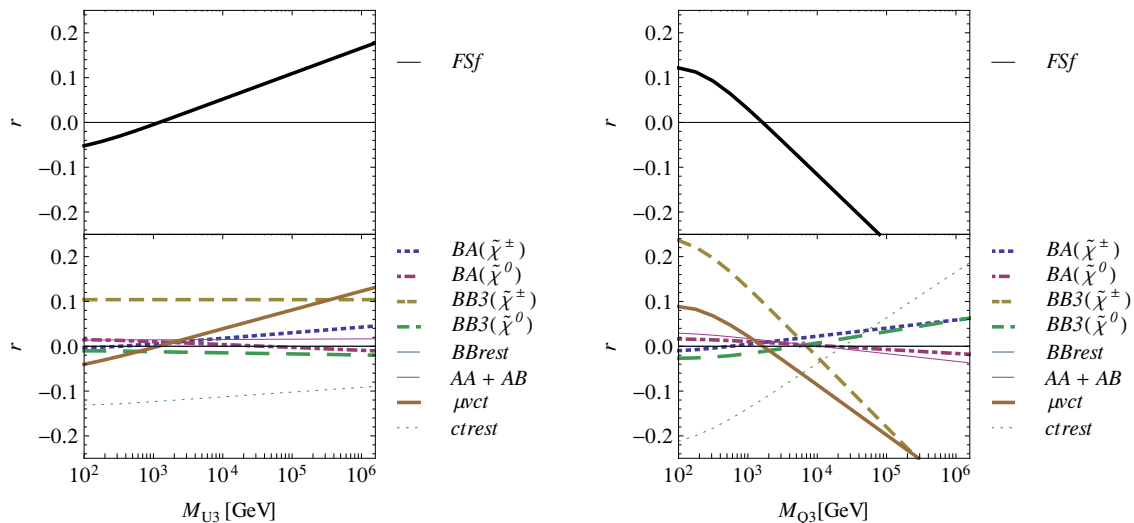
Figure 20. Full result $r \equiv a_\mu^{2\mathrm{L}, f\tilde{f}}/a_\mu^{1\mathrm{L\,SUSY}}$ and individual contributions as defined in section 7.2, for the scenario of ref. [95] and figure 19. The one-loop parameters are chosen as in eq. (7.6). Left: M_{U3} line of figure 19, Right: M_{Q3} line of figure 19,

- It is an exact evaluation of the fermion/sfermion-loop corrections to MSSM one-loop diagrams and all associated counterterm diagrams. The two-loop diagrams contain the maximum number of different mass scales possible in the MSSM.

- It introduces a dependence of a_μ on the squarks and sleptons of all generations. As shown already in ref. [25] this sensitivity is strong: the contributions are logarithmically enhanced by heavy sfermions in the inner loop, and they can be the largest SUSY two-loop contributions.

- It eliminates the ambiguity from parametrizing the one-loop contributions either in terms of α, $\alpha(M_Z)$, or G_F. This is due to the fact that the counterterms contain in particular the leading contributions to the large quantities $\Delta\alpha$ and $\Delta\rho$ from light and heavy SM quarks and leptons.

In the present paper, full details of the calculation and analytical results, as well as a complete survey of the numerical behaviour have been given.

A very compact approximation formula was provided in section 6. It can be easily implemented in any code for numerical evaluation, and it is available as Mathematica code.[6] This compact formula is based on the leading logarithms and numerical constants approximating the non-logarithmic terms. It is a good approximation in large regions of the parameter space, and it also provides qualitative understanding of the parameter dependence of the result.

The largest possible two-loop corrections can be obtained from loops involving stops or sbottoms due to their large Yukawa couplings; these Yukawa-enhanced corrections can

---

[6]The Mathematica implementation of the approximation formula of section 6 can be obtained from http://iktp.tu-dresden.de/?id=theory-software.

be positive or negative, depending on the hierarchy between left- and right-handed stop masses. Large two-loop corrections can also arise from 1st/2nd generation squarks due to their large multiplicity and SU(2) gauge coupling. Generally, for inner sfermion masses in the sub-TeV or few-TeV range, the two-loop corrections can be around 10% of the SUSY one-loop contributions to a_μ.

Even if certain or all relevant SUSY masses become small, such that the leading logarithmic approximation fails, the corrections can be sizeable. We have considered three examples of experimentally allowed scenarios with extremely light stop, light stau, or light slepton and chargino masses. In all cases the total SUSY contribution to a_μ can be in the ballpark of the deviation (1.1), and the two-loop corrections are up to 10%.

The computation of the fermion/sfermion-loop correction represents an important step towards the full two-loop calculation of a_μ in the MSSM. On a technical level, the diagrams involve 2 light and up to 5 different heavy mass scales. This is a higher number than for all previously considered a_μ two-loop corrections, and it is the maximum number possible in the MSSM. The standard two-loop techniques based on integration by parts lead to very cumbersome expressions. Our second, alternative calculation based on an iterated one-loop calculation leads to elegant final analytical results in terms of a one-dimensional Feynman parameter integration.

It is interesting to compare the fermion/sfermion-loop corrections to other SUSY two-loop contributions to the muon magnetic moment. Up to now, two classes of corrections to SUSY one-loop diagrams were known. The first are photonic, or QED corrections [51, 52], which are dominated by QED logarithms and amount to around $(-7 \ldots - 9)\%$ in typical parameter regions. The second is a universal $(\tan\beta)^2$-enhanced correction arising from a shift of the muon Yukawa coupling [53]. In large regions of the MSSM parameter space, particularly for approximately degenerate SUSY masses, the $(\tan\beta)^2$-corrections are positive (for positive $a_\mu^{1L\,SUSY}$) and can partially or fully compensate the photonic corrections for large $\tan\beta$. Further, two-loop corrections to SM one-loop diagrams from SUSY particle loops have been fully evaluated in ref. [19, 48], and they amount to around 2% of $a_\mu^{1L\,SUSY}$ for degenerate masses. However, these corrections decouple for heavy SUSY particles.

Hence, the fermion/sfermion-loop corrections can be as large as any of the previously known corrections. For all these corrections either the exact result or a useful approximation formula can be easily implemented. Numerical comparisons between all these known two-loop results can be found in ref. [25].

The remaining MSSM two-loop corrections to a_μ comprise SUSY one-loop diagrams with a second loop with gauge or Higgs boson or neutralino/chargino exchange. These remaining corrections depend on a subset of parameters of the fermion/sfermion-loop corrections, hence their parameter dependence will be more straightforward. Nevertheless, their evaluation will be important to reduce the theory error of the SUSY prediction of a_μ below the experimental uncertainty of the future a_μ experiments.

Acknowledgments

A Loop functions for one-loop diagrams

The one-loop functions with a single mass ratio read

$$\mathcal{F}_i^C(x) = F_i^C(x)[1 - \epsilon\, L(m_{\tilde{\nu}_\mu}^2)] + \epsilon\, F_{i\epsilon}^C(x), \tag{A.1}$$

$$\mathcal{F}_i^N(x) = F_i^N(x)[1 - \epsilon\, L(m_{\tilde{\mu}}^2)] + \epsilon\, F_{i\epsilon}^N(x), \tag{A.2}$$

where we have used the abbreviation

$$L(m^2) = \log\frac{m^2}{\mu_{\text{DRED}}^2} \tag{A.3}$$

with the dimensional-regularization scale μ_{DRED}, and the well-known functions

$$F_1^C(x) = \frac{2}{(1-x)^4}\Big[2 + 3x - 6x^2 + x^3 + 6x\log x\Big], \tag{A.4}$$

$$F_2^C(x) = \frac{3}{2(1-x)^3}\Big[-3 + 4x - x^2 - 2\log x\Big], \tag{A.5}$$

$$F_1^N(x) = \frac{2}{(1-x)^4}\Big[1 - 6x + 3x^2 + 2x^3 - 6x^2\log x\Big], \tag{A.6}$$

$$F_2^N(x) = \frac{3}{(1-x)^3}\Big[1 - x^2 + 2x\log x\Big], \tag{A.7}$$

normalized such that $F_i^j(1) = 1$. The functions for the ϵ-dependent parts are defined as

$$F_{1\epsilon}^C(x) = F_1^C(x)\left(\frac{-x^3 + 6x^2 + 15x + 2 - 6x\log x}{12x}\right) + \frac{x^2 - 8x - 4}{6x}, \tag{A.8}$$

$$F_{2\epsilon}^C(x) = F_2^C(x)\left(\frac{-2x^2 + 8x + 6 - 4\log x}{8}\right) + \frac{3x - 15}{8}, \tag{A.9}$$

$$F_{1\epsilon}^N(x) = F_1^N(x)\left(\frac{2x^3 + 15x^2 + 6x - 1 - 6x^2\log x}{12x^2}\right) + \frac{1 - 8x - 4x^2}{6x^2}, \tag{A.10}$$

$$F_{2\epsilon}^N(x) = F_2^N(x)\left(\frac{x^2 + 4x + 1 - 2x\log x}{4x}\right) - \frac{3x + 3}{4x}, \tag{A.11}$$

and are normalized to $F_{i\epsilon}^j(1) = 0$.

The one-loop functions with two mass ratios can be related to the loop functions of single mass ratios. For $k = 1, 2$, we have

$$\mathcal{F}_k^C(x_i, x_j) = \frac{\mathcal{G}_k^C(x_i) - \mathcal{G}_k^C(x_j)}{x_i - x_j} \qquad (k = 1, 2), \tag{A.12}$$

where

$$\mathcal{G}_k^C(x) = \int \mathcal{F}_k^C(x) \qquad\qquad (k = 1, 2). \qquad\qquad (A.13)$$

In this way the $\mathcal{G}_{1,2}^C$ are defined up to irrelevant constants. The third chargino one-loop function can be expressed in terms of new one-variable functions as

$$\mathcal{F}_3^C(x_i, x_j) = \frac{\mathcal{G}_{3a}^C(x_i) + \mathcal{G}_{3a}^C(x_j)}{x_i - x_j} + \frac{\mathcal{G}_{3b}^C(x_i) - \mathcal{G}_{3b}^C(x_j)}{(x_i - x_j)^2} \qquad\qquad (A.14)$$

with

$$\mathcal{G}_{3a}^C(x) = -\frac{x[1 - \epsilon\, L(m_{\tilde{\nu}_\mu}^2)]}{8(x-1)^2} \Big[-2(-1 + x + (x-2)\log x) \\ + \epsilon\left(3 - 3x - (x-4)\log x + (x-2)\log^2 x\right) \Big], \qquad\qquad (A.15)$$

$$\mathcal{G}_{3b}^C(x) = \frac{x^2 \log x[1 - \epsilon\, L(m_{\tilde{\nu}_\mu}^2)]}{4(x-1)} \Big[-2 - 3\epsilon + \epsilon \log x \Big]. \qquad\qquad (A.16)$$

Similarly to the case with only one mass ratio, the one-loop functions can be decomposed into terms of $\mathcal{O}(\epsilon^0, \epsilon^1)$, as

$$\mathcal{F}_k^C(x_i, x_j) = F_k^C(x_i, x_j)[1 - \epsilon\, L(m_{\tilde{\nu}_\mu}^2)] + \epsilon\, F_{k\epsilon}^C(x_i, x_j), \qquad\qquad (A.17)$$
$$\mathcal{G}_k^C(x) = G_k^C(x)[1 - \epsilon\, L(m_{\tilde{\nu}_\mu}^2)] + \epsilon\, G_{k\epsilon}^C(x), \qquad\qquad (A.18)$$

with

$$F_k^C(x_i, x_i) = F_k^C(x_i), \qquad F_{k\epsilon}^C(x_i, x_i) = F_{k\epsilon}^C(x_i), \qquad (k \in \{1, 2, 3\}) \qquad (A.19)$$
$$F_3^C(x_i) = 0, \qquad\qquad F_{3\epsilon}^C(x_i) = 0. \qquad\qquad (A.20)$$

For reference we list the explicit expressions for the G_k^C and $G_{k\epsilon}^C$ are as follows:

$$G_1^C(x) = \frac{2x(-2 + (2 - 3\log x)x + x^2 \log x)}{(-1 + x)^3}, \qquad\qquad (A.21)$$

$$G_{1\epsilon}^C(x) = \frac{x(-22 + (22 - 27\log x + 9\log^2 x)x + (5\log x - 3\log^2 x)x^2)}{3(-1 + x)^3}, \qquad (A.22)$$

$$G_2^C(x) = \frac{3(-1 + x - 2x\log x + x^2 \log x)}{2(-1 + x)^2}, \qquad\qquad (A.23)$$

$$G_{2\epsilon}^C(x) = \frac{3(-3 + (3 - 4\log x + 2\log^2 x)x + (\log x - \log^2 x)x^2)}{4(-1 + x)^2}, \qquad (A.24)$$

$$G_{3a}^C(x) = \frac{x(-1 - 2\log x + (1 + \log x)x)}{4(-1 + x)^2}, \qquad\qquad (A.25)$$

$$G_{3a\epsilon}^C(x) = \frac{x(-3 - 4\log x + 2\log^2 x + (3 + \log x - \log^2 x)x)}{8(-1 + x)^2}, \qquad (A.26)$$

$$G_{3b}^C(x) = -\frac{x^2 \log x}{2(-1 + x)}, \qquad\qquad (A.27)$$

$$G_{3b\epsilon}^C(x) = \frac{x^2(-3\log x + \log^2 x)}{4(-1 + x)}. \qquad\qquad (A.28)$$

References

[1] Muon G-2 collaboration, G. Bennett et al., *Final Report of the Muon E821 Anomalous Magnetic Moment Measurement at BNL*, *Phys. Rev.* **D 73** (2006) 072003 [`hep-ex/0602035`] [InSPIRE].

[2] T. Aoyama, M. Hayakawa, T. Kinoshita and M. Nio, *Complete Tenth-Order QED Contribution to the Muon g-2*, *Phys. Rev. Lett.* **109** (2012) 111808 [`arXiv:1205.5370`] [InSPIRE].

[3] M. Davier, A. Hoecker, B. Malaescu and Z. Zhang, *Reevaluation of the Hadronic Contributions to the Muon g-2 and to alpha(MZ)*, *Eur. Phys. J.* **C 71** (2011) 1515 [*Erratum ibid.* **C 72** (2012) 1874] [`arXiv:1010.4180`] [InSPIRE].

[4] K. Hagiwara, R. Liao, A.D. Martin, D. Nomura and T. Teubner, $(g-2)_\mu$ *and* $\alpha(M_Z^2)$ *re-evaluated using new precise data*, *J. Phys.* **G 38** (2011) 085003 [`arXiv:1105.3149`] [InSPIRE].

[5] M. Benayoun, P. David, L. DelBuono and F. Jegerlehner, *An Update of the HLS Estimate of the Muon g-2*, *Eur. Phys. J.* **C 73** (2013) 2453 [`arXiv:1210.7184`] [InSPIRE].

[6] F. Jegerlehner and R. Szafron, $\rho^0 - \gamma$ *mixing in the neutral channel pion form factor* F_π^e *and its role in comparing* e^+e^- *with* τ *spectral functions*, *Eur. Phys. J.* **C 71** (2011) 1632 [`arXiv:1101.2872`] [InSPIRE].

[7] F. Jegerlehner and A. Nyffeler, *The Muon g-2*, *Phys. Rept.* **477** (2009) 1 [`arXiv:0902.3360`] [InSPIRE].

[8] J. Prades, E. de Rafael and A. Vainshtein, *Hadronic Light-by-Light Scattering Contribution to the Muon Anomalous Magnetic Moment*, `arXiv:0901.0306` [InSPIRE].

[9] T. Goecke, C.S. Fischer and R. Williams, *Hadronic light-by-light scattering in the muon g-2: a Dyson-Schwinger equation approach*, *Phys. Rev.* **D 83** (2011) 094006 [*Erratum ibid.* **D 86** (2012) 099901] [`arXiv:1012.3886`] [InSPIRE].

[10] J. Bijnens and M.Z. Abyaneh, *The hadronic light-by-light contribution to the muon anomalous magnetic moment and renormalization group for EFT*, *EPJ Web Conf.* **37** (2012) 01007 [`arXiv:1208.3548`] [InSPIRE].

[11] P. Masjuan and M. Vanderhaeghen, *Ballpark prediction for the hadronic light-by-light contribution to the muon* $(g-2)_\mu$, `arXiv:1212.0357` [InSPIRE].

[12] T. Blum, M. Hayakawa and T. Izubuchi, *Hadronic corrections to the muon anomalous magnetic moment from lattice QCD*, `PoS(Lattice 2012)022` [`arXiv:1301.2607`] [InSPIRE].

[13] ATLAS collaboration, *Combined measurements of the mass and signal strength of the Higgs-like boson with the ATLAS detector using up to 25 fb^{-1} of proton-proton collision data*, [ATLAS-CONF-2013-014](#) (2013).

[14] CMS collaboration, *Combination of standard model Higgs boson searches and measurements of the properties of the new boson with a mass near 125 GeV*, [CMS-PAS-HIG-13-005](#).

[15] C. Gnendiger, D. Stöckinger and H. Stöckinger-Kim, *The electroweak contributions to* $(g-2)_\mu$ *after the Higgs boson mass measurement*, *Phys. Rev.* **D 88** (2013) 053005 [`arXiv:1306.5546`] [ɪɴSPIRE].

[16] A. Czarnecki, B. Krause and W.J. Marciano, *Electroweak Fermion loop contributions to the muon anomalous magnetic moment*, *Phys. Rev.* **D 52** (1995) 2619 [`hep-ph/9506256`] [ɪɴSPIRE].

[17] A. Czarnecki, B. Krause and W.J. Marciano, *Electroweak corrections to the muon anomalous magnetic moment*, *Phys. Rev. Lett.* **76** (1996) 3267 [`hep-ph/9512369`] [ɪɴSPIRE].

[18] A. Czarnecki, W.J. Marciano and A. Vainshtein, *Refinements in electroweak contributions to the muon anomalous magnetic moment*, *Phys. Rev.* **D 67** (2003) 073006 [*Erratum ibid.* **D 73** (2006) 119901] [`hep-ph/0212229`] [ɪɴSPIRE].

[19] S. Heinemeyer, D. Stöckinger and G. Weiglein, *Electroweak and supersymmetric two-loop corrections to* $(g-2)_\mu$, *Nucl. Phys.* **B 699** (2004) 103 [`hep-ph/0405255`] [ɪɴSPIRE].

[20] T. Gribouk and A. Czarnecki, *Electroweak interactions and the muon g-2: Bosonic two-loop effects*, *Phys. Rev.* **D 72** (2005) 053016 [`hep-ph/0509205`] [ɪɴSPIRE].

[21] J.P. Miller, E.d. Rafael, B.L. Roberts and D. Stöckinger, *Muon (g-2): Experiment and Theory*, *Ann. Rev. Nucl. Part. Sci.* **62** (2012) 237 [ɪɴSPIRE].

[22] R.M. Carey et al., *The New (g-2) Experiment: A proposal to measure the muon anomalous magnetic moment to* ± 0.14 *ppm precision*, FERMILAB-PROPOSAL-0989 (2009) [ɪɴSPIRE].

[23] B.L. Roberts, *Status of the Fermilab Muon* $(g-2)$ *Experiment*, *Chin. Phys.* **C 34** (2010) 741 [`arXiv:1001.2898`] [ɪɴSPIRE].

[24] J-PARC NEW G-2/EDM EXPERIMENT collaboration, H. Iinuma, *New approach to the muon g-2 and EDM experiment at J-PARC*, *J. Phys. Conf. Ser.* **295** (2011) 012032 [ɪɴSPIRE].

[25] H. Fargnoli, C. Gnendiger, S. Paßehr, D. Stöckinger and H. Stöckinger-Kim, *Non-decoupling two-loop corrections to* $(g-2)_\mu$ *from fermion/sfermion loops in the MSSM*, *Phys. Lett.* **B 726** (2013) 717 [`arXiv:1309.0980`] [ɪɴSPIRE].

[26] A. Czarnecki and W.J. Marciano, *The Muon anomalous magnetic moment: A Harbinger for 'new physics'*, *Phys. Rev.* **D 64** (2001) 013014 [`hep-ph/0102122`] [ɪɴSPIRE].

[27] D. Stöckinger, *The Muon Magnetic Moment and Supersymmetry*, *J. Phys.* **G 34** (2007) R45 [`hep-ph/0609168`] [ɪɴSPIRE].

[28] R. Benbrik et al., *Confronting the MSSM and the NMSSM with the Discovery of a Signal in the two Photon Channel at the LHC*, *Eur. Phys. J.* **C 72** (2012) 2171 [`arXiv:1207.1096`] [ɪɴSPIRE].

[29] A. Arbey, M. Battaglia, A. Djouadi and F. Mahmoudi, *The Higgs sector of the phenomenological MSSM in the light of the Higgs boson discovery*, *JHEP* **09** (2012) 107 [`arXiv:1207.1348`] [ɪɴSPIRE].

[30] M. Endo, K. Hamaguchi, S. Iwamoto and T. Yoshinaga, *Muon* $g-2$ *vs LHC in Supersymmetric Models*, *JHEP* **01** (2014) 123 [`arXiv:1303.4256`] [ɪɴSPIRE].

[31] M. Ibe, S. Matsumoto, T.T. Yanagida and N. Yokozaki, *Heavy Squarks and Light Sleptons in Gauge Mediation From the viewpoint of 125 GeV Higgs Boson and Muon g-2*, *JHEP* **03** (2013) 078 [`arXiv:1210.3122`] [ɪɴSPIRE].

[32] G. Bhattacharyya, B. Bhattacherjee, T.T. Yanagida and N. Yokozaki, *A natural scenario for heavy colored and light uncolored superpartners*, *Phys. Lett.* **B 725** (2013) 339 [arXiv:1304.2508] [inSPIRE].

[33] T. Cheng and T. Li, *Electroweak Supersymmetry (EWSUSY) in the NMSSM*, *Phys. Rev.* **D 88** (2013) 015031 [arXiv:1305.3214] [inSPIRE].

[34] M. Ibe, T.T. Yanagida and N. Yokozaki, *Muon g-2 and 125 GeV Higgs in Split-Family Supersymmetry*, *JHEP* **08** (2013) 067 [arXiv:1303.6995] [inSPIRE].

[35] S. Mohanty, S. Rao and D. Roy, *Reconciling the muon $g-2$ and dark matter relic density with the LHC results in nonuniversal gaugino mass models*, *JHEP* **09** (2013) 027 [arXiv:1303.5830] [inSPIRE].

[36] S. Akula and P. Nath, *Gluino-driven Radiative Breaking, Higgs Boson Mass, Muon $\mathbf{g-2}$ and the Higgs Diphoton Decay in SUGRA Unification*, *Phys. Rev.* **D 87** (2013) 115022 [arXiv:1304.5526] [inSPIRE].

[37] J.L. Evans, M. Ibe, S. Shirai and T.T. Yanagida, *A 125GeV Higgs Boson and Muon g-2 in More Generic Gauge Mediation*, *Phys. Rev.* **D 85** (2012) 095004 [arXiv:1201.2611] [inSPIRE].

[38] M. Endo, K. Hamaguchi, T. Kitahara and T. Yoshinaga, *Probing Bino contribution to muon $g-2$*, *JHEP* **11** (2013) 013 [arXiv:1309.3065] [inSPIRE].

[39] P. Bechtle et al., *Constrained Supersymmetry after two years of LHC data: a global view with Fittino*, *JHEP* **06** (2012) 098 [arXiv:1204.4199] [inSPIRE].

[40] C. Balázs, A. Buckley, D. Carter, B. Farmer and M. White, *Should we still believe in constrained supersymmetry?*, *Eur. Phys. J.* **C 73** (2013) 2563 [arXiv:1205.1568] [inSPIRE].

[41] O. Buchmueller et al., *The CMSSM and NUHM1 in Light of 7 TeV LHC, B_s to $\mu^+\mu^-$ and XENON100 Data*, *Eur. Phys. J.* **C 72** (2012) 2243 [arXiv:1207.7315] [inSPIRE].

[42] M. Endo, K. Hamaguchi, S. Iwamoto, T. Kitahara and T. Moroi, *Reconstructing Supersymmetric Contribution to Muon Anomalous Magnetic Dipole Moment at ILC*, *Phys. Lett.* **B 728** (2014) 274 [arXiv:1310.4496] [inSPIRE].

[43] D.W. Hertzog, J.P. Miller, E. de Rafael, B. Lee Roberts and D. Stöckinger, *The Physics case for the new muon (g-2) experiment*, arXiv:0705.4617 [inSPIRE].

[44] C. Adam, J.-L. Kneur, R. Lafaye, T. Plehn, M. Rauch and D. Zerwas, *Measuring Unification*, *Eur. Phys. J.* **C 71** (2011) 1520 [arXiv:1007.2190] [inSPIRE].

[45] T. Moroi, *The Muon anomalous magnetic dipole moment in the minimal supersymmetric standard model*, *Phys. Rev.* **D 53** (1996) 6565 [*Erratum ibid.* **D 56** (1997) 4424] [hep-ph/9512396] [inSPIRE].

[46] S.P. Martin and J.D. Wells, *Muon anomalous magnetic dipole moment in supersymmetric theories*, *Phys. Rev.* **D 64** (2001) 035003 [hep-ph/0103067] [inSPIRE].

[47] G.-C. Cho, K. Hagiwara, Y. Matsumoto and D. Nomura, *The MSSM confronts the precision electroweak data and the muon g-2*, *JHEP* **11** (2011) 068 [arXiv:1104.1769] [inSPIRE].

[48] S. Heinemeyer, D. Stöckinger and G. Weiglein, *Two loop SUSY corrections to the anomalous magnetic moment of the muon*, *Nucl. Phys.* **B 690** (2004) 62 [hep-ph/0312264] [inSPIRE].

[49] A. Arhrib and S. Baek, *Two loop Barr-Zee type contributions to $(g-2)_\mu$ in the MSSM*, *Phys. Rev.* **D 65** (2002) 075002 [hep-ph/0104225] [inSPIRE].

[50] C.-H. Chen and C. Geng, *The Muon anomalous magnetic moment from a generic charged Higgs with SUSY*, *Phys. Lett.* **B 511** (2001) 77 [hep-ph/0104151] [INSPIRE].

[51] P. von Weitershausen, M. Schafer, H. Stöckinger-Kim and D. Stöckinger, *Photonic SUSY Two-Loop Corrections to the Muon Magnetic Moment*, *Phys. Rev.* **D 81** (2010) 093004 [arXiv:1003.5820] [INSPIRE].

[52] G. Degrassi and G. Giudice, *QED logarithms in the electroweak corrections to the muon anomalous magnetic moment*, *Phys. Rev.* **D 58** (1998) 053007 [hep-ph/9803384] [INSPIRE].

[53] S. Marchetti, S. Mertens, U. Nierste and D. Stöckinger, tan β-*enhanced supersymmetric corrections to the anomalous magnetic moment of the muon*, *Phys. Rev.* **D 79** (2009) 013010 [arXiv:0808.1530] [INSPIRE].

[54] T.-F. Feng, L. Sun and X.-Y. Yang, *The Two loop supersymmetric corrections to lepton anomalous dipole moments in split supersymmetry scenarios*, *Phys. Rev.* **D 77** (2008) 116008 [arXiv:0805.0653] [INSPIRE].

[55] T.-F. Feng, L. Sun and X.-Y. Yang, *Electroweak and supersymmetric two-loop corrections to lepton anomalous magnetic and electric dipole moments*, *Nucl. Phys.* **B 800** (2008) 221 [arXiv:0805.1122] [INSPIRE].

[56] T.-F. Feng and X.-Y. Yang, *Renormalization and two loop electroweak corrections to lepton anomalous dipole moments in the standard model and beyond (I): Heavy fermion contributions*, *Nucl. Phys.* **B 814** (2009) 101 [arXiv:0901.1686] [INSPIRE].

[57] T.-F. Feng, X.-Q. Li, L. Lin, J. Maalampi and H.-S. Song, *The Two-loop supersymmetric corrections to lepton anomalous magnetic and electric dipole moments*, *Phys. Rev.* **D 73** (2006) 116001 [hep-ph/0604171] [INSPIRE].

[58] S.M. Barr and A. Zee, *Electric Dipole Moment of the Electron and of the Neutron*, *Phys. Rev. Lett.* **65** (1990) 21 [*Erratum ibid.* **65** (1990) 2920] [INSPIRE].

[59] N. Yamanaka, *R-parity violating two-loop level rainbowlike contribution to the fermion electric dipole moment*, arXiv:1212.5800 [INSPIRE].

[60] N. Yamanaka, *Two-loop level rainbow-like supersymmetric contribution to the fermion EDM*, *Phys. Rev.* **D 87** (2013) 011701 [arXiv:1211.1808] [INSPIRE].

[61] A. Denner, H. Eck, O. Hahn and J. Kublbeck, *Feynman rules for fermion number violating interactions*, *Nucl. Phys.* **B 387** (1992) 467 [INSPIRE].

[62] T. Takagi, *Japanese J. Math.* **1** (1927) 83.

[63] T. Fritzsche, S. Heinemeyer, H. Rzehak and C. Schappacher, *Heavy Scalar Top Quark Decays in the Complex MSSM: A Full One-Loop Analysis*, *Phys. Rev.* **D 86** (2012) 035014 [arXiv:1111.7289] [INSPIRE].

[64] T. Fritzsche and W. Hollik, *Complete one loop corrections to the mass spectrum of charginos and neutralinos in the MSSM*, *Eur. Phys. J.* **C 24** (2002) 619 [hep-ph/0203159] [INSPIRE].

[65] W. Hollik and H. Rzehak, *The Sfermion mass spectrum of the MSSM at the one loop level*, *Eur. Phys. J.* **C 32** (2003) 127 [hep-ph/0305328] [INSPIRE].

[66] T. Fritzsche, T. Hahn, S. Heinemeyer, H. Rzehak and C. Schappacher, *The Implementation of the Renormalized Complex MSSM in FeynArts and FormCalc*, arXiv:1309.1692 [INSPIRE].

[67] S. Heinemeyer, H. Rzehak and C. Schappacher, *Proposals for Bottom Quark/Squark Renormalization in the Complex MSSM*, *Phys. Rev.* **D 82** (2010) 075010 [arXiv:1007.0689] [iNSPIRE].

[68] A. Denner, *Techniques for calculation of electroweak radiative corrections at the one loop level and results for W physics at LEP-200*, *Fortsch. Phys.* **41** (1993) 307 [arXiv:0709.1075] [iNSPIRE].

[69] W. Hollik, E. Kraus, M. Roth, C. Rupp, K. Sibold and D. Stöckinger, *Renormalization of the minimal supersymmetric standard model*, *Nucl. Phys.* **B 639** (2002) 3 [hep-ph/0204350] [iNSPIRE].

[70] T. Hahn, *Generating Feynman diagrams and amplitudes with FeynArts 3*, *Comput. Phys. Commun.* **140** (2001) 418 [hep-ph/0012260] [iNSPIRE].

[71] S. Agrawal, T. Hahn and E. Mirabella, *FormCalc 7*, *J. Phys. Conf. Ser.* **368** (2012) 012054 [arXiv:1112.0124] [iNSPIRE].

[72] A. Freitas and D. Stöckinger, *Gauge dependence and renormalization of tan beta in the MSSM*, *Phys. Rev.* **D 66** (2002) 095014 [hep-ph/0205281] [iNSPIRE].

[73] N. Baro, F. Boudjema and A. Semenov, *Automatised full one-loop renormalisation of the MSSM. I. The Higgs sector, the issue of* $\tan\beta$ *and gauge invariance*, *Phys. Rev.* **D 78** (2008) 115003 [arXiv:0807.4668] [iNSPIRE].

[74] M. Frank, T. Hahn, S. Heinemeyer, W. Hollik, H. Rzehak and G. Weiglein, *The Higgs Boson Masses and Mixings of the Complex MSSM in the Feynman-Diagrammatic Approach*, *JHEP* **02** (2007) 047 [hep-ph/0611326] [iNSPIRE].

[75] M. Sperling, D. Stöckinger and A. Voigt, *Renormalization of vacuum expectation values in spontaneously broken gauge theories*, *JHEP* **07** (2013) 132 [arXiv:1305.1548] [iNSPIRE].

[76] M. Sperling, D. Stöckinger and A. Voigt, *Renormalization of vacuum expectation values in spontaneously broken gauge theories: Two-loop results*, *JHEP* **01** (2014) 068 [arXiv:1310.7629] [iNSPIRE].

[77] S. Heinemeyer, F. von der Pahlen and C. Schappacher, *Chargino Decays in the Complex MSSM: A Full One-Loop Analysis*, *Eur. Phys. J.* **C 72** (2012) 1892 [arXiv:1112.0760] [iNSPIRE].

[78] A. Bharucha, S. Heinemeyer, F. von der Pahlen and C. Schappacher, *Neutralino Decays in the Complex MSSM at One-Loop: a Comparison of On-Shell Renormalization Schemes*, *Phys. Rev.* **D 86** (2012) 075023 [arXiv:1208.4106] [iNSPIRE].

[79] A. Chatterjee, M. Drees, S. Kulkarni and Q. Xu, *On the On-Shell Renormalization of the Chargino and Neutralino Masses in the MSSM*, *Phys. Rev.* **D 85** (2012) 075013 [arXiv:1107.5218] [iNSPIRE].

[80] N. Baro and F. Boudjema, *Automatised full one-loop renormalisation of the MSSM II: The chargino-neutralino sector, the sfermion sector and some applications*, *Phys. Rev.* **D 80** (2009) 076010 [arXiv:0906.1665] [iNSPIRE].

[81] G. Weiglein, R. Scharf and M. Böhm, *Reduction of general two loop selfenergies to standard scalar integrals*, *Nucl. Phys.* **B 416** (1994) 606 [hep-ph/9310358] [iNSPIRE].

[82] W. Hollik, J.I. Illana, S. Rigolin and D. Stöckinger, *One loop MSSM contribution to the weak magnetic dipole moments of heavy fermions*, *Phys. Lett.* **B 416** (1998) 345 [hep-ph/9707437] [iNSPIRE].

[83] D. Chang, W.-Y. Keung and A. Pilaftsis, *New two loop contribution to electric dipole moment in supersymmetric theories*, *Phys. Rev. Lett.* **82** (1999) 900 [*Erratum ibid.* **83** (1999) 3972] [`hep-ph/9811202`] [INSPIRE].

[84] A. Pilaftsis, *Higgs boson two loop contributions to electric dipole moments in the MSSM*, *Phys. Lett.* **B 471** (1999) 174 [`hep-ph/9909485`] [INSPIRE].

[85] D. Chang, W.-F. Chang, C.-H. Chou and W.-Y. Keung, *Large two loop contributions to g-2 from a generic pseudoscalar boson*, *Phys. Rev.* **D 63** (2001) 091301 [`hep-ph/0009292`] [INSPIRE].

[86] K.-m. Cheung, C.-H. Chou and O.C. Kong, *Muon anomalous magnetic moment, two Higgs doublet model and supersymmetry*, *Phys. Rev.* **D 64** (2001) 111301 [`hep-ph/0103183`] [INSPIRE].

[87] PARTICLE DATA GROUP collaboration, J. Beringer et al., *Review of Particle Physics (RPP)*, *Phys. Rev.* **D 86** (2012) 010001 [INSPIRE].

[88] B. Allanach et al., *The Snowmass points and slopes: Benchmarks for SUSY searches*, *Eur. Phys. J.* **C 25** (2002) 113 [`hep-ph/0202233`] [INSPIRE].

[89] P. Grothaus, M. Lindner and Y. Takanishi, *Naturalness of Neutralino Dark Matter*, *JHEP* **07** (2013) 094 [`arXiv:1207.4434`] [INSPIRE].

[90] G. Degrassi, S. Heinemeyer, W. Hollik, P. Slavich and G. Weiglein, *Towards high precision predictions for the MSSM Higgs sector*, *Eur. Phys. J.* **C 28** (2003) 133 [`hep-ph/0212020`] [INSPIRE].

[91] S. Heinemeyer, W. Hollik and G. Weiglein, *The Masses of the neutral CP - even Higgs bosons in the MSSM: Accurate analysis at the two loop level*, *Eur. Phys. J.* **C 9** (1999) 343 [`hep-ph/9812472`] [INSPIRE].

[92] S. Heinemeyer, W. Hollik and G. Weiglein, *FeynHiggs: A Program for the calculation of the masses of the neutral CP even Higgs bosons in the MSSM*, *Comput. Phys. Commun.* **124** (2000) 76 [`hep-ph/9812320`] [INSPIRE].

[93] A. Delgado, G.F. Giudice, G. Isidori, M. Pierini and A. Strumia, *The light stop window*, *Eur. Phys. J.* **C 73** (2013) 2370 [`arXiv:1212.6847`] [INSPIRE].

[94] M. Carena, S. Heinemeyer, O. Stal, C. Wagner and G. Weiglein, *MSSM Higgs Boson Searches at the LHC: Benchmark Scenarios after the Discovery of a Higgs-like Particle*, *Eur. Phys. J.* **C 73** (2013) 2552 [`arXiv:1302.7033`] [INSPIRE].

[95] B. Batell, S. Jung and C.E. Wagner, *Very Light Charginos and Higgs Decays*, *JHEP* **12** (2013) 075 [`arXiv:1309.2297`] [INSPIRE].